LIETUVOS SVEIKATOS MOKSLŲ UNIVERSITETAS
MEDICINOS AKADEMIJA

Hermanas Inokaitis

SINUSINIO PRIEŠIRDŽIO MAZGO IR JO INERVACIJOS LYGINAMOJI ANATOMIJA

Daktaro disertacija
Biomedicinos mokslai,
biologija (01B)

Kaunas, 2016

Disertacija rengta 2011–2016 metais Lietuvos sveikatos mokslų universiteto Medicinos akademijoje.

Mokslinė vadovė

prof. dr. Neringa Paužienė (Lietuvos sveikatos mokslų universitetas, biomedicinos mokslai, biologija – 01B)

Disertacija ginama Lietuvos sveikatos mokslų universiteto Medicinos akademijos biologijos mokslo krypties taryboje:

Pirmininkas

prof. dr. Edgaras Stankevičius (Lietuvos sveikatos mokslų universitetas, biomedicina, biologija – 01B)

Nariai:

dr. Regina Mačianskienė (Lietuvos sveikatos mokslų universitetas, biomedicinos mokslai, biologija – 01B)

prof. habil. dr. Zygmunt Mackevič (Valstybinio mokslinių tyrimų instituto Inovatyvios medicinos centras, biomedicinos mokslai, biologija – 01B)

prof. dr. Rimantas Jankauskas (Vilniaus universitetas, biomedicinos mokslai, medicina – 06B)

prof. dr. Andres Arend (Tartu universitetas, biomedicinos mokslai, medicina – 06B)

Disertacija ginama 2016 m. rugpjūčio 25 d. 13 val. viešame biologijos mokslo krypties tarybos posėdyje Lietuvos sveikatos mokslų universiteto prof. J. Žilinsko auditorijoje.

Adresas: A. Mickevičiaus g. 9, LT-44307 Kaunas, Lietuva.

LITHUANIAN UNIVERSITY OF HEALTH SCIENCES
MEDICAL ACADEMY

Hermanas Inokaitis

COMAPARATIVE STUDY OF SINOATRIAL NODE MORPHOLOGY AND INNERVATION

Doctoral Dissertation
Biomedical Sciences,
Biology (01B)

Kaunas, 2016

Dissertation has been prepared at the Institute of Anatomy of Medical Academy of Lithuanian University of Health Sciences during the period of 2011–2016 years.

Scientific Supervisor

Prof. Dr. Neringa Paužienė (Lithuanian University of Health Sciences, Biomedical Sciences, Biology – 01B)

Dissertation is defended at the Biology Research Council of the Lithuanian University of Health Sciences.

Chairman

Prof. Dr. Edgaras Stankevičius (Lithuanian University of Health Sciences, Biomedical Sciences, Biology – 01B)

Members:

Dr. Regina Mačianskienė (Lithuanian University of Health Sciences, Biomedical Sciences, Biology – 01B)

Prof. Dr. Habil. Zygmunt Mackevič (State Research Institute Centre for Innovative Medicine, Biomedical Sciences, Biology – 01B)

Prof. Dr. Rimantas Jankauskas (Vilnius University, Biomedical Sciences, Medicine – 06B)

Prof. Dr. Andres Arend (University of Tartu, Biomedical Sciences, Medicine – 06B)

Dissertation will be defended at the open session of the Biology Research Council at 13:00 on the 25th of August 2016 in the prof. J. Žilinskas Auditorium of Lithuanian University of Health Sciences.

Address: A. Mickevičiaus 9, LT-44307 Kaunas, Lithuania.

TURINYS

SANTRUMPOS

AChE – acetilcholinesterazė
AV – prieširdinis skilvelio
AVN – prieširdinis skilvelio mazgas
AVK – prieširdinis skilvelio kanalas
ChAT – cholino acetiltransferazė
DGV – dešinioji galvinė vena
DP – dešinysis prieširdis
DPV – dešinioji plautinė vena
EkNS – ekstrakardinė nervų sistema
HCN4 – kalio natrio hiperpoliarizacija aktyvinamas, ciklinio nukleotido valdomas kanalo proteinas 4
INS – intrakardinė nervų sistema
IR – imunoreaktyvumas
MA – sinusinio prieširdžio mazgo arterija
MIF – mažos intensyviai florescuojančios ląstelės
NDS – normalus asilo serumas
nNOS – neuroninė azoto oksido sintazė
Ns – nervinės skaidulos
NS – nervų sistema
PBS – fosfatinis fiziologinis tirpalas
PGP 9.5 – proteininis genų produktas 9.5
SP – substancija P
SAN – sinusinis prieširdžio mazgas
ŠLS – širdies laidžioji sistema
ŠNS – širdies nervų sistema
TH – tirozino hidroksilazė
UV – uodeginė vena

ĮVADAS

Autonominė nervų sistema chromotropiškai, dromotropiškai ir inotropiškai reguliuoja širdies laidžiosios sistemos (ŠLS) veiklą [1, 2]. ŠLS laidumo ar inervacijos nepakankamumas ir/arba disbalansas sąlygoja įvairių aritmijų atsiradimą ir neretais atvejais staigią mirtį [3]. Priklausomai nuo sutrikimo pobūdžio ir sunkumo, jie gali būti koreguojami farmakologiniais preparatais, įvairiomis chirurginėmis intervencijomis, širdies stimuliatoriumi, o sunkiais atvejais ir pačios širdies transplantacija [4, 5]. Dėl įvairių taikomų gydymo būdų ir jų komplikacijų yra reikalingi detalūs morfologiniai ir neuromorfologiniai ŠLS ir jos atskirų dalių tyrimai [1, 2, 6–8].

Žinios apie ŠLS ir jos inervaciją yra ribotos dėl tyrimų sudėtingumo ir paprastai apsiriboja šios sistemos mazgų sandara ir topografija [9–12], bei jos imunohistocheminėmis savybėmis. Ankstesniuose tyrimuose didelis dėmesys buvo skiriamas bendrai širdies ir ŠLS inervacijai [13–19]. Šiuose tyrimuose buvo taikomas histocheminis acetilcholintrasferazės (AChE) metodas, kaip cholinerginis neuroninis žymuo, jį derinant su imunohistocheminiais metodais, pažymėti adrenerginius bei juntamuosius neuronus [15–19]. Tačiau AChE nėra tiesioginis ir selektyvus cholinerginės sistemos žymuo [20–23], todėl iki šių dienų nėra aiškus dominuojančios nervų sistemos tipas visoje ŠLS.

Ieškant naujų ar tobulinant jau esamus širdies veiklos sutrikimų gydymo būdus yra naudojami gyvūniniai modeliai. Šių tyrimų efektyvumui didelę reikšmę turi žinios apie tarprūšinius širdies anatominius ir neuroanatominius skirtumus.

Darbo naujumas ir aktualumas

Šiame tyrime buvo ištirta trijų dažnai naudojamų elektrofiziologiniuose tyrimuose gyvūnų SAN sandara ir jos inervacija. Tai yra pirmas detalus pelės, triušio ir kiaulės SAN struktūros ir jos inervacijos ištyrimas ir palyginimas simultaniškai taikant imunohistocheminius laidžiųjų miocitų ir nervinius žymenis viso prieširdžio bei pjūvių preparatuose.

Gauti rezultatai atskleidžia, jog ŠLS inervacija yra kur kas sudėtingesnė negu buvo manoma iki šiol. Šiuo darbu pirmą kartą aprašytos SAN srityje esančių nervinių mazgų neurocheminės ypatybės ir naujas atradimas – nitrerginiai neuronai, kurie pozityvūs vien tik neuroninei azoto oksido sintazei (nNOS).

Darbo tikslas ir uždaviniai

Darbo tikslas: nustatyti sinusinio prieširdžio mazgo ribas ir inervaciją pelės, triušio ir kiaulės širdyse.

Darbo uždaviniai:

1. Nustatyti ritmą generuojančių ląstelių išsidėstymą dešiniajame prieširdyje.
2. Ištirti sinusinio prieširdžio mazgo inervacijos gausumą.
3. Ištirti neuronų kūnų paplitimą sinusiniame prieširdžio mazge.
4. Ištirti prieširdžio sinusinio mazgo neuronų neurochemines ypatybes.
5. Ištirti sinusinio prieširdžio mazgo neuronų morfologines ypatybes.

1. LITERATŪROS APŽVALGA

1.1. Širdies laidžiosios sistemos tyrimų istorija

Širdies tyrimų istorija siekia Elijo Klaudijaus Galeno laikus II a. [24]. Šis graikų gydytojas – filosofas pastebėjo, jog abu skilveliai pulsuoja net tada, kai širdis yra išimta iš krūtinės ląstos. Dėl šios priežasties širdies automatinio susitraukimo kilmė buvo siejama su vidinėmis širdies savybėmis. Galenas savo mokymuose savitai aiškino širdies darbą. Jo raštuose teigiama, jog širdis veikė kaip kalvio dumplės ar kempinė, įsiurbdama kraują į priešširdžius išsiplėsdavo ir pilnai prisipildžiusi trenkdavosi į krūtinės sieną [24]. Šia teorija buvo vadovaujamasi 15 šimtmečių iki 1628 m., kuomet Viljamas Harvey išleido 72 puslapių knygą „On the Motion of the Heart and Blood in Animals“, kuria iš esmės buvo pakeista kardiovaskulinės sistemos funkcijos samprata ir pasiūlyta uždaros kraujotakos teorija, t. y. tiek venomis, tiek arterijomis tas pats kraujas tekėjo ratu [24].

„Aukso amžius“ širdies veiklos tyrimams – tai XIX a. antra pusė ir XX a. pradžia. Šiuo laikotarpiu iškeltos 2 pagrindinės teorijos – nervinė ir miogeninė. Jų pagrindu yra aiškinama širdies veikla iki šių dienų. Šiuo laikotarpiu buvo ištirtos ir aprašytos atskiros ŠLS dalys, kurios vėliau buvo apjungtos į vieną bendrą sistemą [25–32].

Pirmasis ŠLS atradimas – tai 1839 m. čekų fiziologo – anatomo Jano Evangelisto Purkinje (1787–1869) atrastas pilkų „želatininių“ ląstelių tinklas (vėliau pavadintas atradėjo vardu) avies skilveliuose iškart po endokardu. Nors iš pradžių šias ląsteles klaidingai priskyrė kremzliniam audiniui, tačiau po 6 metų jau aprašė kaip raumeninės kilmės ląsteles [30]. Ilgą laiką šios ŠLS dalies funkcija buvo nežinoma ir prireikė beveik šimtmečio jai išsiaiškinti [28, 30].

Didelis indelis tolimesniuose ŠLS tyrimuose yra Valter Gaskel (1847–1914) darbai. Jo tyrimuose aprašyta širdies peristaltinės veiklos samprata yra nepakitusi iki mūsų dienų. Nors V. Gaskel buvo miogeninės širdies veiklos teorijos šalininkas, jis apjungė abi sistemas (raumeninę ir nervinę), priskirdamas joms atskiras – ritmo vedlio ir reguliacijos funkcijas. Jo darbuose aprašoma, jog impulso plitimas prasideda veniniame antyje ir išplinta priešširdžiuose, o vėliau skilveliuose. Priešširdinėje skilvelių jungtyje impulsas prieš išplisdamas į skilvelius yra užlaikomas. Jo nuomone, tokią funkciją atliko diferencijuotas raumeninis audinys. Taip pat savo eksperimentais V. Gaskel įrodė, jog suardžius tam tikras tarppriešširdinės pertvaros zonas ištinka priešširdinė skilvelių blokada [25–27, 29, 31].

Įkvėptas Gaskel darbų Vilhelmas Hisas (1863–1934) pradėjo tyrimus, siekdamas nustatyti impulso plitimą iš prieširdžių į skilvelius. Stebėdamas skirtingas embriogenezės stadijas 1893 m. aprašė raumeninio audinio pluoštą, kuris vėliau buvo pavadintas jo vardu, jungiantį apatines ir viršutines širdies kameras. Jo nuomone, šis pluoštelis tiesiogiai jungė skilvelius su prieširdžiais, bet funkciškai nereguliavo impulso plitimo greičio. Po šių tyrimų fiziologiniais eksperimentais buvo įrodyta, jog skilvelių susitraukimas prasideda sužadinus jų pamatą [27–29].

Viena garsiausių asmenybių, tyrusių ŠLS, yra japonų kilmės gydytojas – anatomas Suano Tavara (1873–1952). Gavęs finansinę paramą, jaunas gydytojas atvyko tęsti studijas į Vokietiją ir vadovaujamas profesoriaus Ludviko Aschoff pradėjo širdies histologinius tyrimus. Savo darbuose Tavara pirmasis suprato, jog Purkinje skaidulos jungiasi su Hiso pluoštu, o impulsas prasidėjęs prieširdžiuose yra užlaikomas prieširdžių skilveliniame mazge. Tokiomis savo įžvalgomis Tavara aprašė prieširdžių skilvelinę laidžiąją sistemą, kuri apjungė visas anksčiau aprašytas dalis į vieną bendrą visumą [27–29].

1906 m. medicinos studentas Martinas Fliakas (1882–1931), vasaros praktikos metu, vadovaujamas Artūro Keito (1866–1955) aptiko unikalią struktūrą, esančią kurmio širdies viršutinės tuščiosios venos ir dešiniojo prieširdžio ausytės jungties srityje. Ši struktūra turėjo ryšį su klajokliu nervu ir simpatiniu kamienu bei atskirą arterinę kraujotaką. Kurį laiką ši struktūra buvo vadinama Keito ir Fliako sinusiniu ausytės mazgu, o vėliau pervadinta sinusiniu prieširdžio mazgu. Po Tomo Luiso fiziologinių eksperimentų 1909 m. sinusinis prieširdžio mazgas buvo pripažintas pagrindiniu ritmo vedliu. Iš esmės atradus SAN, buvo aprašytos visos pagrindinės širdies elektrinės sistemos dalys [3, 9, 12, 23, 25–29, 31, 33].

1910 m. Erlange Vokietijos patologų draugijos susirinkime, remiantis ankstesniais tyrimais, buvo patvirtinti histologiniai kriterijai, kuriuos turi atitikti ŠLS ir jos atskiros dalys:

1. Ląstelės histologiškai skiriasi nuo darbinio miokardo;
2. Jas galima atpažinti skirtinguose serijiniuose pjūviuose;
3. Ląstelės atskirtos nuo aplinkinio darbinio miokardo jungiamuoju audiniu [34].

Nors ne visais atvejais ŠLS ląstelės atitinka visus šiuos kriterijus [35, 36], tačiau jais dažnai yra naudojamasi tiriant ŠLS klasikiniais histologiniais dažymo metodais ir šiuolaikiniuose tyrimuose [37, 38].

1.2. Klasikinė širdies laidžiosios sistemos samprata

ŠLS generuoja elektrinius impulsus, kurie sukelia ritmiškus ir sinchronizuotus miokardo skaidulų susitraukimus prieširdžiuose ir skilveliuose [3, 29, 39, 40]. Laidžiąją sistemą sudaro specializuotas miokardas. Hipotezė, jog ŠLS yra neurogeninės kilmės, nepasitvirtino [3, 41–44]. Aukštesniųjų stuburinių gyvūnų ŠLS yra sudaryta iš sinusinio prieširdžio (SAN) ir prieširdinio skilvelio mazgų (AVN) bei skilvelių „laidų“, kuriems priklauso prieširdinis skilvelio (Hiso) pluoštas, kairioji ir dešinioji Hiso pluošto kojytės ir periferinė skilvelių laidžioji sistema [3, 45]. Nors visų žinduolių ŠLS išlaiko tą pačią struktūrą ir jos komponentai yra gerai išreikšti, tačiau yra aprašomi tarprūšiniai skirtumai. Kanopinių gyvūnų ŠLS yra gerai išsivysčiusi, o graužikų silpnai. Tuo tarpu žmogaus ŠLS yra išsivysčiusi vidutiniškai [45]. Taip pat yra teigiama, jog ŠLS išsivystymas nepriklauso nuo gyvūno dydžio [46].

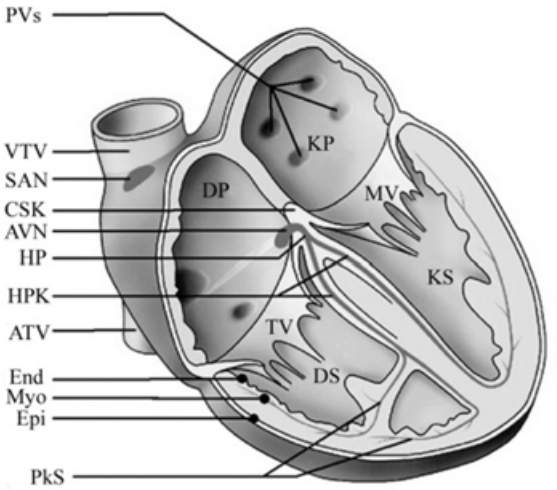

1.2.1 pav. *Klasikinė žmogaus ŠLS schema (modifikuota remiantis [45]).*
ATV – apatinė tuščioji vena; AVN – prieširdinis skilvelių mazgas; CSK – centrinis skaidulinis kūnas; DP – dešinysis prieširdis; DS – dešinysis skilvelis; KS – kairysis skilvelis; End – endokardas; Epi – epikardas; HP – Hiso pluoštas; HPK – Hiso pluošto kojytės; KP – kairysis prieširdis; Myo – miokardas; PkS – Purkinje skaidulos; PVs – plautinės venos; SAN – sinusinis prieširdžio mazgas; VTV – viršutinė tuščioji vena.

SAN atlieka ritmo vedlio funkciją [3, 29, 39, 40]. Iš jo signalas plinta prieširdžių miokardu, kuris laikomas neatsiejama laidžiosios sistemos dalimi, iki AVN. Čia impulsas yra užlaikomas, o vėliau patenka į prieširdinį

skilvelio pluoštą [3, 29, 39, 40]. Toliau impulsas plinta į Hiso pluošto kojytes (angl. *bundle branches* – BB) ir periferinį Purkinje tinklą [3]. Čia signalas dideliu greičiu išplinta visame miokarde, sukeldamas skilvelių susitraukimą nuo viršūnės iki pamato [3, 29, 39, 40].

Bet kurios ŠLS dalies (mazgų ar pluoštelių) nepakankamumas sąlygoja aritmijų atsiradimą, kurios gali būti gydomos implantuojant širdies stimuliatorių [3]. Antra vertus, ektopinis ritmo vedlio ar laidumo aktyvumo sutrikimas sąlygoja aritmijas, kurioms gydyti taikomos chirurginės intervencijos [3].

1.3. Imunohistocheminiai laidžiosios sistemos tyrimai

ŠLS nėra vienalytė sistema sudaryta iš daugiau ar mažiau panašių ląstelių. Kiekvienos ŠLS dalies miocitai atlieka skirtingas funkcijas ir pasižymi skirtinga citomorfologija, molekuliniu fenotipu ir funkcija [3]. Antra vertus visi laidžiosios sistemos miocitai turi panašias savybes, kuriomis skiriasi nuo darbinio miokardo, tokiomis kaip silpniau išreikšti sarkomerai, sarkoplazminis tinklas, mažesnis mitochondrijų kiekis ir t. t. [3, 43, 45]. Šios savybės nesunkiai pastebimos histologiniuose preparatuose [43, 45]. Iš esmės ŠLS sudaro 2 tipų ląstelės, atliekančios skirtingas funkcijas: ritmą generuojančios ir tranzitinės ląstelės [43, 45]. Tarpusavyje šie specializuoti miocitai skiriasi membraninėmis savybėmis [43, 45]. Dėl skirtingų specifinių plyšinių jungčių savybių laidusis miokardas yra atkirtas nuo darbinio, todėl jos atlieka ne tik signalo perdavimo, bet ir izoliacinę funkciją [9, 12, 29, 33, 47].

Molekulinės genetikos tyrimai atskleidė, jog skirtingi reguliaciniai mechanizmai yra atsakingi už vienos ar kitos sistemos dalies vystymąsi [3, 48, 49]. Vystantis širdies kameroms iš širdies vamzdžio dalyvauja daugelis baltymų, kurie nulemia raumeninių ląstelių diferenciaciją į laidžiuosius ar darbinius miocitus. Kardiomiocitų diferenciacijai yra svarbūs baltymai kurie buvo pavadinti T-box (Tbx) transkripcijos veiksniais. Dažniausiai yra aprašomi Tbx2, Tbx3, Tbx5 ir Tbx18 [3, 12, 29, 33, 48, 50, 51]. Kiekvienas jų turi tik jiems būdingą funkciją. Pvz., Tbx18 ekspresija nulemia pirminių SAN ląstelių atsiradimą iš mezenchimos [3]. Tbx3 ir Tbx5 dalyvauja vystantis visai laidžiajai sistemai, tačiau Tbx3 turi didesnę įtaką formuojantis SAN, o Tbx5 – AVN [3, 45, 48, 49]. Tbx2 ekspresija svarbi vystantis AVN ir prieširdžio skilvelių kanalui (AVK) [3, 45, 48, 49]. Taikant imunohistocheminius žymenis galima aptikti šiuos baltymus ir taip atpažinti specializuotas ląsteles [3, 9, 12, 23, 29, 33, 48, 50–52].

Morfologiniuose ŠLS tyrimuose taikoma daugelis imunohistocheminių žymenų, iš kurių dažniausiai naudojami HCN4 ir Cx45 laidiesiems miocitams, Cx43 ir Cx40 darbiniam miokardui žymėti [11, 33, 51, 53, 54].

HCN4 membraninis kanalas yra aptinkamas beveik visose laidžiosios sistemos dalyse, išskyrus periferinę, nuo Hiso pluošto kojyčių. HCN4 kanalai yra pagrindinis impulso generavimo šaltinis. Skirtingos sistemos dalys pasižymi skirtingu HCN4 kanalų kiekiu, todėl jos gali kurti automatinį ritmą skirtingu intensyvumu. Kuo didesnis kanalų kiekis, tuo dažniau atitinkamoje srityje yra sukeliama depoliarizacija. SAN ląstelėse aptinkamas didžiausias HCN4 kanalų kiekis ir dėl šios priežasties mazgas atlieka pagrindinio ritmo vedlio funkciją. Kiek mažiau šių kanalų yra AVN ir dar mažiau Hiso pluošte [11, 29, 33, 51, 53, 54]. Esant SAN blokadai, AVN, Hiso pluoštas ir kitos ŠLS dalys, turinčios HCN4 kanalus, gali perimti ritmo vedlio funkciją [3, 11, 29, 33, 51, 53, 54], o patologiniais atvejais tapti aritmijų priežastimi [3].

1.3.1 lentelė. *Dažniausiai ŠLS tyrimuose naudojami imunohistocheminiai žymenys ir jų paplitimas skirtingose dalyse* [3]

Genas	**SAN**	**AVK**	**AVN**	**HP (a)**	**HP (b)**	**HPk**
Cx40	–	–	–	–	+	+
Cx43	–	–	–	–	–	–
Cx45	+	+	+	–	–	–
HCN4	+	–	+	–	+	–
Tbx3	+	+	+	+	+	+
Tbx2	–	+	+/–	–	–	–
Tbx18	+	–	–	–	–	–
Tbx5	+	+	+	+	+	+

AVK – prieširdinis skilvelių kanalas; AVN – prieširdinis skilvelio mazgas;
HP – Hiso pluoštas; HP (a) – Hiso pluoštas ankstyvoje vystymosi stadijoje;
HPk – Hiso pluošto kojytės; SAN – sinusinis prieširdžio mazgas.

Cx40 ir Cx43 yra greitosios pernašos plyšinių jungčių baltymai, kurie yra atsakingi už greitą impulso pernašą miokarde, todėl jų gausiai sutinkama darbiniame miokarde [55, 56]. Tuo tarpu lėtosios pernašos Cx45 kanalų yra gausu miocituose, esančiuose aplinkui HCN4 pozityvias ląsteles, atsakinguose už impulso užlaikymą [45, 56, 57].

Remiantis imunohistocheminiais eksperimentais buvo patvirtinti ankstesni ŠLS morfologiniai tyrimai, kuriuose teigiama jog, SAN yra dešiniosios galvinės venos (DGV) ir dešiniojo prieširdžio (DP) suaugimo srityje, tačiau visas mazgo ląstelių masyvas apsupa DGV iš priekio, nuo medialinės iki lateralinės dalies ir toliau driekiasi tarp pastarosios venos ir galinės skiauterės, *crista terminalis*, beveik iki uodeginės venos [11, 47, 58]. AV mazgas prasideda dešiniajame prieširdyje tarpprieširdinės pertvaros apačioje, nugarinėje

dalyje prie vainikinio ančio ir užima Koch‘o trikampio viršūnę [33], nusitęsia į priekį ir prieširdiniame skilvelių kanale (AVK) perveria skaidulinį žiedą. Toliau driekiasi viršutine tarpskilvelinės pertvaros dalimi kaip Hiso pluoštas (nusileidžiančioji dalis) ir priekyje išsišakoja į dešiniąją ir kairiąją Hiso pluošto kojytes [12].

Derėtų pabrėžti, jog pradėjus taikyti imunohistocheminius metodus, buvo ir išplėsta ŠLS sąvoka, jai priskiriant užaortinį mazgą ir laidžiuosius žiedus, esančius aukščiau dviburio ir triburio vožtuvų žiočių (1.3.1 pav.) [3, 9, 12, 23, 33, 52]. Be to atrasta ir Hiso pluošto tąsa, kuri driekiasi į priekinį kairiojo skilvelio paviršių, apsupa aortą per dešinę pusę ir ten pasibaigia. Ši struktūra vadinama aortos žiedu [12].

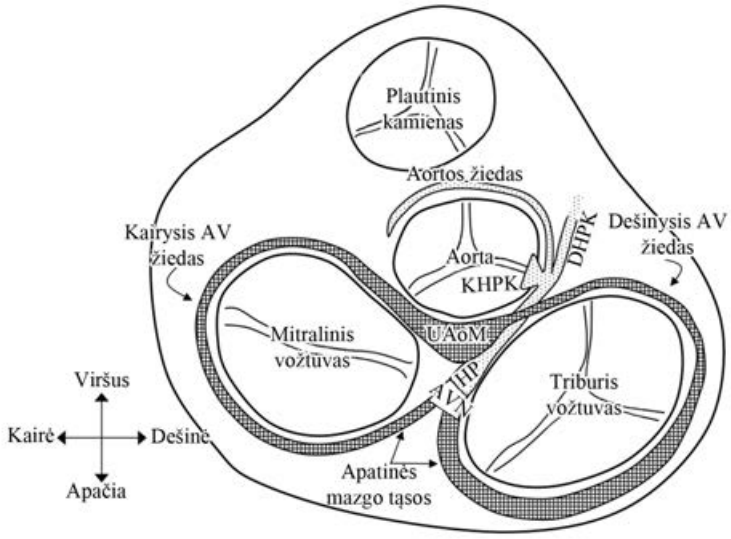

1.3.1 pav. *Laidžiųjų miocitų išsidėstymas aplink mitralinio ir triburio vožtuvų žiotis, remiantis imunohistocheminiais tyrimais (modifikuota remiantis[12]).*

DHPK – dešinioji Hiso pluošto kojytė; HP – Hiso pluoštas;
KHPK – kairioji Hiso pluošto kojytė; UAoM – užaortinis mazgas.

Ląstelių pluoštai, apsupantys dviburio ir triburio vožtuvų žiotis [11], detaliau gali būti tiriami tik taikant imunohistocheminius žymenis, kadangi dažnai nuo aplinkinio darbinio miokardo nėra atskirti jungiamuoju audiniu, o jų diferenciaciją lemia plyšinės jungtys, apsaugančios nuo nepageidaujamos depoliarizacijos [9, 11, 12, 29, 33]. AV žiedai prasideda iš AVN kairiosios ir dešiniosios nugarinių šakų, apsupa mitralinio ir triburio vožtuvų žiotis ir prieširdžio priekyje suformuoja užaortinį mazgą (1.3.1 pav.) [9, 12,

33]. Nusileidžiančioji laidžiosios sistemos dalis (Hiso pluoštas) pereina žemiau užaortinio mazgo ir yra nuo jo atskirtas skaiduliniu žiedu [11, 12].

Taikant HCN4 ir Cx45 žymenis pastebėta, jog kairysis ir dešinysis žiedai skiriasi imunohistocheminėmis savybėmis. Dešiniajame žiede yra daugiau HCN4 imunoreaktyvių (IR) ląstelių, o kairiajame stebimos tik pavienės HCN4 pozityvios ląstelės. Cx45 IR abiejuose AV žieduose nesiskiria [11]. Šiose zonose HCN4 kanalai gali sąlygoti aritmijų atsiradimą esant SAN disfunkcijai [11].

1.4. Širdies nervų sistema

Širdies nervų sistema (ŠNS) atlieka svarbų vaidmenį reguliuojant širdies susitraukimų dažnį, laidumą, miokardo susitraukimo jėgą ir koronarinę kraujotaką [19, 39, 59–62]. Yra žinoma, jog po širdies transplantacijos operacijos, dėl denervacijos pacientai negali jausti pooperacinio krūtinės anginos skausmo [63, 64]. Be to, tokie pacientai dažnai kenčia nuo ortostatinės hipotenzijos [63, 64]. Kita dažna problema, jog nejaučiamas antiaritminių vaistų, kurie tiesiogiai veikia per ŠNS, tokių kaip širdį veikiančių glikozidų ar atropino, poveikis [63, 64].

ŠNS sudaryta iš aferentinių, eferentinių ir įterptinių neuronų [2, 65], kurie yra išsidėstę galvos ir nugaros smegenyse, simpatinio kamieno ir visceraliniuose mazguose ir atlieka išskirtiniai tik jiems būdingą funkciją [1, 2]. ŠNS funkcija yra užtikrinti reikiamą kraujo tėkmę į visas kūno sritis [2]. Ji gali būti apibūdinta kaip lygiagreti ir didžiąja dalimi stochastiška kontūrolės sistema, užtikrinanti stabilų širdies darbą ir pasireiškianti be matomo efekto ir priežasties [2, 65].

Pagal vietą galima išskirti dvi ŠNS dalis. Tai ekstrakardinė (EkNS) ir intrakardinė (INS) nervų sistemos. Struktūriškai ir funkciškai INS nėra paprasta EkNS projekcijų persijungimo vieta [8, 66]. INS atlieka integruoto nervinio rezginio, galinčio priimti ekstrakardinius impulsus ir moduliuoti vidinius širdinius refleksus, funkciją [2, 8, 67, 68].

Tyrimais įrodyta, jog intrakardinė ir ekstrakardinė ŠNS gali veikti priklausomai ir nepriklausomai viena nuo kitos [8, 67, 69]. Šie teiginiai patvirtinti elektrofiziologiniais tyrimais pastebėjus, jog papildomi ekstrakardinės NS impulsai „integruojami“ intrakardinės NS mazgų. Po širdies autotransplantacijos visiškai atskyrus intrakardinę NS nuo ekstrakardinės NS, pagrindines širdies reguliacijos funkcijas perima intrakardinė NS [8, 67, 69].

Ankstesniais tyrimais yra įrodyta, jog simpatinių ir parasimpatinių ekstrakardinės NS komponentų stimuliacija gali sukelti įvairias aritmijas, tokias kaip prieširdžių virpėjimą ar skilvelių tachiaritmiją [70, 71]. Vėlesni kardiofiziologiniai tyrimai parodė, jog veikiant intrakardinius mazgus aukšto

dažnio elektrostimuliacija arba tiesiogiai paveikiant acetilcholinu, gaunamas tas pats efektas [72, 73].

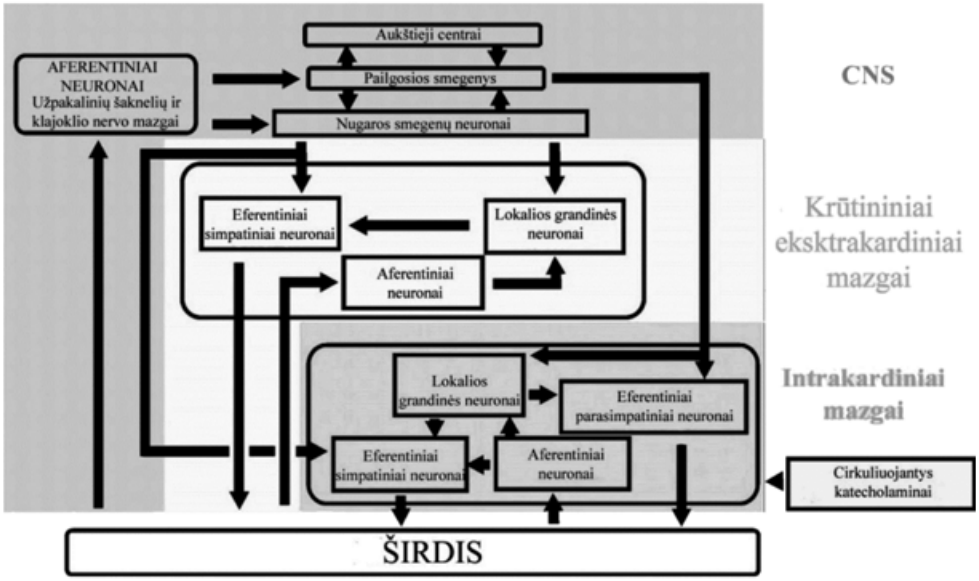

1.4.1 pav. *Hipotetinė širdies reguliacijos schema pagal A. J. Armour (modifikuota remiantis [1, 68]).*

ŠNS neuronai komunikuoja per daugybę receptorių įskaitant angiotenziną II ir beta adrenerginius receptorius. Tokie duomenys rodo, jog farmakologinė terapija gydant širdies ligas gali būti nukreipta į šios ŠNS sinapses. Be to tokiu būdu veikiantys farmakologiniai preparatai gali įtakoti kardiomiocitų darbą ne tik per tiesioginius, bet ir netiesioginius mechanizmus [1, 2].

A. J. Armour pasiūlytoje schemoje (1.4.1 pav.) pabrėžiama, jog aukštesnieji neuronai gali būti pakeisti žemesniųjų. Širdiniai juntamieji signalai perduodami per krūtininius ekstrakardinius ir intrakardinius neuronus. Taip pat šie signalai gali būti perduodami tiesiai į nugaros ir pailgąsias smegenis. Cirkuliuojantys katecholaminai gali veikti širdies motorinį darbą tiesiogiai arba per intrakardinius neuronus [1, 68].

ŠNS tyrimus neuromorfologinius tyrimus galima suklasifikuoti į dvi grupes: vieni nukreipti į EkNS, kiti – į INS dalį [74–92]. Kadangi simpatinė ir parasimpatinė autonominės NS dalys tarpusavyje stipriai skiriasi savo morfologija ir cheminėmis savybėmis [93], EkNS tyrimai dažnai apsiriboja tik vienos iš sistemų analize. Simpatinės NS tyrimai paprastai apsiriboja tik proksimaline arba distaline dalimis, t.y. tiria tik simpatinio kamieno mazgus

ir nugarinius nervus, arba visceralinius nervus išėjusius iš simpatinio kamieno mazgų iki įnervuojamo organo [6, 7, 74–80, 94–100].

Lyginant įvairių gyvūnų ekstrakardinę nervų sistemą bendroji inervacijos schema išlieka panaši. Tačiau lyginant net evoliuciškai artimų žmogbeždžionių autonominę NS yra stebimi simpatinio kamieno skirtumai, kadangi žvaigždinio mazgo struktūros ir kaklinių simpatinio kamieno mazgų morfologija yra nevienoda, o tai nulemia ir skirtingas simpatinių nervų išsidėstymo variacijas [94, 100, 101]. Šie skirtumai yra būdingi tik simpatinei NS, o parasimpatinės inervacijos šakos visais atvejais išlieka tos pačios [94, 100, 101].

Pregangliniai simpatiniai neuronai, reguliuojantys širdies aktyvumą, yra T1–T5 nugaros smegenų segmentuose [93, 102]. Jų aksonai sąveikauja su viršutinio, vidurinio ir apatinio kaklinių ir viršutinio krūtininio simpatinio kamieno mazgų neuronais [6, 7, 102]. Simpatinės NS nervai, sudarantys širdies rezginį arba tiesiogiai pasiekiantys širdį, yra vadinami atitinkamai pagal mazgus, kuriuose prasideda – viršutinis, vidurinis ir apatinis kakliniai ir krūtininis širdiniai nervai [6, 7]. Su pastaraisiais plinta ir juntamosios skaidulos, kurios prasideda C_8–Th_6 nugariniuose mazguose [6, 7]. Preganglinių neuronų neurotransmiteris yra acetilcholinas, o postganglinių – norepinefrinas [93, 103]. Pagrindinis norepinefrino šaltinis yra amino rūgštis tirozinas, kuris fermentų pagalba verčiamas dihidrofenilaninu ir vėliau dopaminu. Toliau dalyvaujat fermentui β hidroksilazei iš dopamino sintetinamas norepinefrinas [104, 105]. Simpatinės nervinės stimuliacijos metu norepinefrinas išskiriamas į sinapses. Be nervinės stimuliacijos šis procesas yra reguliuojamas ir kitais reguliaciniais mechanizmais, kuriuose dalyvauja α2 adrenerginiai receptoriai [104, 105]. Simpatinis aktyvumas didina širdies susitraukimų dažnį ir miokardo susitraukimo jėgą [93, 103–105].

Užmazginiai eferentiniai parasimpatiniai nervai skiriasi nuo simpatinių tuo, jog jie prasideda smegenų kamiene ir sudaro sinapses su užmazginiais neuronais, esančiais inervuojamuose organuose arba šalia jų [93]. Parasimpatiniai širdies rezginio nervai – tai viršutinės ir apatinės klajoklio nervo šakos, atsišakojusios gerklų nervo bei krūtininės klajoklio nervo šakos [6, 7, 94, 100, 101]. Acetilcholinas yra pagrindinis ikimazginių ir užmazginių parasimpatinių neuronų neurotransmiteris [4, 93]. Acetilcholinas sintezuojamas dalyvaujant fermentui cholinacetiltransferazei (ChAT) iš laisvo cholino ir acetyl-koenzimo A [4, 21]. Acetilcholinas kaupiamas vakuolėse, išsiskyręs parasimpatinės stimuliacijos metu aktyvuoja postsinaptinius muskarininius ir preganglinius nikotininius receptorius [106, 107]. Poveikis baigiasi suskilus acetilcholinesterazei [106–108]. Parasimpatiniai pregangliniai cholinerginiai neuronai, sudarantys sinapses su užmazginiais neuronais, esančiais pačioje širdyje, yra galvos smegenų kamieno dvejinio branduolio,

nucleus ambiguus, ventralinėje lateralinėje srityje [109], kiek mažiau nugariniame klajoklio nervo branduolyje, *nucleus dorsalis n. vagi*, ir srityje tarp abiejų šių branduolių [110]. Parasimpatinis aktyvumas mažina širdies susitraukimų dažnį, prieširdžių ir skilvelių miokardo susitraukimo jėgą, bei AVN laidumą [1, 2, 93].

Tiek simpatinis, tiek parasimpatinis širdies poveikis yra reguliuojamas juntamųjų neuronų. Kadangi miokardo išemijos sukeltas skausmas jaučiamas kairėje rankoje ir/arba kairėje krūtinės pusėje, buvo manoma [2], kad juntamieji neuronai yra kairės pusės krūtininiuose nugariniuose mazguose, *ganglion spinale* [111]. Tačiau neuroanatominiais tyrimais įrodyta, jog aferentiniai neuronai įnervuojantys širdį yra abiejuose viršutiniuose klajoklio nervo mazguose, *ganglion nodosum,* ir abiejų pusių C7–T4 nugariniuose mazguose [111]. Taip pat jų juntamųjų neuronų aptinkama pačioje INS [2]. Parasimpatinių centrinių eferentinių neuronų darbas daugiausia priklauso nuo arterinių baroreceptorių funkcijos [2, 8]. Simpatinė eferentinių neuronų veikla priklauso nuo krūtininių refleksų ir yra mažiau priklausoma nuo centrinės kontrolės [1, 2].

Fiziologiniu požiūriu aferentiniai neuronai perneša informaciją apie nuolat kintančią širdies terpę. Dauguma aferentinių neuronų perduoda informaciją apie kintančią mechaninę ir/arba cheminę terpę aplink jų neuritus [2, 93]. Pavyzdžiui ~75 proc. viršutinio klajoklio nervo mazgo neuronų perduoda cheminį, kiek mažiau ~35 proc. mechanosensorinį signalą [112].

Nugarinių mazgų neuronai dažniausiai atlieka multimodalinį signalo pernešimą (mechaninį ir cheminį) [2]. Intrakardiniouse ir ekstrakardiniuose visceraliniuose mazguose esantys juntamieji neuronai taip pat pasižymi multimodalinėmis savybėmis [2]. Dauguma juntamųjų neuronų yra jautrūs adenozinui, kurio didesnis kiekis išsiskiria vystantis miokardo išemijos atveju [113]. Taip pat mechanoreceptorių neuritų gausiai aptinkama ant aortos, kurie reguliuoja jos dinamiką [1, 2].

Tiek EkNS, tiek INS buvo aprašyti įterptiniai neuronai. Ši ląstelių grupė įsiterpusi tarp eferentinių ir aferentinių neuronų. Jų aksonai sudaro projekcijas ne tik nervinių mazgų viduje, bet ir su kitų mazgų neuronais ir tokiu būdu, sujungdami nervinius mazgus atlieka vietinės grandinės funkciją [1, 68]. Manoma, jog šie neuronai išsiskiria savo dideliu kūnu (~30 μm) [2]. Yra tyrimų kuriuose teigiama, jog įterptiniai neuronai yra pozityvūs katecholaminų žymenims [114–116].

1.5. Intrakardinio nervinio rezginio morfologija

Nervai ir nervinės skaidulos iš ekstrakardinio nervinio rezginio perėję širdies vartus sudaro intrakardinį rezginį, iš kurio toliau tęsiasi nervai ir nervinės skaidulos, inervuojančios prieširdžių ir skilvelių miokardą [7, 81, 85, 90, 103]. Nervinės skaidulos išplinta nuo širdies pamato iki viršūnės, jų didžiausias tankis yra prieširdžiuose, kiek mažesnis – prieširdžių skilvelinėje vagoje ir mažiausias – širdies viršūnėje [7, 103].

Pagrindinis vidinis širdies inervacijos šaltinis yra prieširdžių epikardinis rezginys, kuris susiformuoja iškart nervams perėjus širdies vartus [81, 84, 88, 89, 91]. Intrakardinis rezginys gali būti suskirstytas į smulkesnius subrezginius. Pagrindinės širdinių subrezginių vietos yra skirstomos pagal jų funkcinę reikšmę arba anatominę vietą.

Daugelio žinduolių epikardinis rezginys išlaiko panašią struktūrą, todėl kardiofiziologiniuose tyrimuose puikiai tinka eksperimentinių gyvūnų modeliai [81–83, 86, 89, 117]. Tačiau yra aprašoma ir nemažai tarprūšinių anatominių skirtumų [62, 81–83, 85–87, 89, 118–121]. Paprastai evoliuciškai žemesnių gyvūnų epikardinis nervinis rezginys sudarytas iš mažiau subrezginių, geriau išsivysčiusių gyvūnų epikardinio nervinio rezginio morfologija panašesnė į žmogaus, tačiau dažnai skiriasi inervuojamos zonos plotas, mazgų dydis, neuronų skaičius ir t. t. [62, 81–83, 86, 89, 118–121].

Remiantis tyrimais yra sudaromos intrakardinio nervinio rezginio schemos, jį dalinant į mažesnius subrezginius. Tokie „širdilapiai“ gali skirtis priklausomai nuo autorių. Pvz., J. A. Armour ir bendraautorių yra siūloma 10 ganglinių subrezginių schema, iš kurių 5 išsidėstę prieširdžiuose, o kiti 5 aplinkui skilvelius esančiuose riebaluose [121]. Lietuvoje paprastai naudojama schema, kurioje prieširdžių nervinis rezginys suskirstas į 7 subrezginius:

- kairįjį vainikinį;
- dešinįjį vainikinį;
- ventralinį dešiniojo prieširdžio;
- ventralinį kairio prieširdžio;
- kairįjį dorsalinį;
- vidurinį dorsalinį;
- dešinįjį dorsalinį [89].

Žmogaus širdies dešinįjį prieširdį paprastai inervuoja 2 – ventralinis ir dorsalinis dešiniojo prieširdžio – epikardiniai rezginiai. Kairįjį prieširdį 3 – ventralinis kairiojo prieširdžio, vidurinis dorsalinis, kairysis dorsalinis subrezginiai. Dešinįjį skilvelį inervuoja 1 – dešinysis vainikinis subrezginys, kairįjį skilvelį taip pat vienas – kairysis vainikinis subrezginys [89].

XX a. antroje pusėje imta domėtis intrakardinių mazgų anatomija ir funkcija [97, 122–125]. Daugiausia intrakardinio rezginio mazgų aptinkama epikardiniuose riebaluose už aortos, aplink prieširdžių skilvelinę vagą ir didžiąsias (plautines) širdies venas [62, 118–120]. Poveikis širdies funkcijai priklauso nuo išorinių šaltinių, tačiau yra reguliuojamas vidinių nervinių mazgų, kurie turi savo atskiras širdies inervacijos zonas [62]. Yra aprašomi vidiniai juntamieji aferentiniai keliai, kurie tiesiogiai įtakoja intrakardines simpatines ir parasimpatines reakcijas [93].

Taip pat domėtasi INS nervų ir mazgų imunohistocheminės ypatybėmis pelės, žiurkės, jūros kiaulytės bei primatų širdyse [83, 125–127]. Šiais tyrimais parodyta, jog intrakardiniuose mazguose esančios ląstelės pasižymi gausia imunohistochemine įvairove. Dažniausia yra analizuojami cholinerginiai ir adrenerginiai neuronai bei MIF ląstelės. Šiuose tyrimuose buvo aprašyti bifenotipiniai neuronai pasižymintys ChAT ir TH IR, kurie yra aptinkami tik INS ir ekrinėnėse prakaito liaukose [126]. Bifenotipiniai ChAT ir nNOS neuronai buvo aprašyti žiurkės, jūros kiaulytės ir triušio INS [84, 125, 127]. Šiuose tyrimuose teigiama, jog visi nNOS pozityvūs neuronai buvo pozityvūs ChAT, tačiau ne visos ChAT nervinės ląstelės pasižymėjo nNOS IR [84, 125, 127]. Be visų minėtų nervinių ląstelių grupių, jūros kiaulytės INS dar buvo aprašyti SP IR neuronai [122].

1.6. Širdies laidžiosios sistemos inervacijos tyrimai

Daugelyje ankstesnių tyrimų, siekiant nustatyti laidžiosios sistemos inervaciją, taikyti imunohistocheminiai metodai, skirti parodyti andrenergines nervines skaidulas ir nervus bei histocheminė AChE reakcija – cholinerginius komponentus [13–15, 17, 19, 60]. Šiais tyrimais nustatyta, jog ŠLS yra kur kas gausiau inervuota nei aplinkinis – darbinis miokardas [13–15, 17–19, 60, 128]. ŠLS gausus smulkių nervinių skaidulų tinklas yra suformuotas iš nervų įėjusių pro širdies vartus ir plintančių iš intrakardinių mazgų [13].

Daugumos gyvūnų SAN nervai pasiekia panašiai. Nervai apsupa DGV iš pilvinės, šoninės ir nugarinės pusių. Pačioje SAN srityje dauguma nervų išsišakoja į smulkų Ns tinklą. Nervai, pasiekiantys SAN priekinėje DGV dalyje, suformuoja keletą šakų, kurios įsilieja į gausų sinusinio mazgo nervinių skaidulų tinklą, o patys toliau driekiasi per visą mazgo ilgį lygiagrečiai ribinei širdies vagai, *sulcus terminalis*, iki uodeginės venos (UV) ir ją apjuosia. Šie nervai taip pat suformuoja šakas, kurios įsilieja į SAN Ns tinklą visame savo kelyje. Kiek plonesni nervai medialiau DGV taip pat leidžiasi link UV ir su anksčiau minėtais nervais sudaro žiedą aplink pastarąją [13, 14]. Nugarinėje DGV dalyje aukščiau dešiniosios plautinės venos

SAN sritį pasiekia keletas stambių nervų, kurie šakojasi ir įsilieja į gausų nervinių skaidulų tinklą sinusinio mazgo kūne ir uodegoje. Dalis jų jungiasi su nervais, einančiais lygiagrečiai ribinei širdies vagai [13, 14].

Lyginant atskiras ŠLS dalis ir mazgus tarpusavyje nustatyti tam tikri tarprūšiniai panašumai ir skirtumai. Pvz., žmogaus ŠLS stebimas inervacijos mažėjimas pereinant nuo SAN iki Hiso pluošto ir jo kojyčių [17, 19]. Kitų gyvūnų, kaip pvz., jūros kiaulytės, žiurkės ar triušio inervacijos tankis SAN ir AVN nesiskiria [15, 16]. Tačiau daugumos gyvūnų ŠLS inervacija ženkliai sumažėja Hiso pluošto kojytėms perėjus į Purkinje skaidulas ir dažnai tankiu nesiskiria nuo aplinkinio darbinio skilvelių miokardo[13–19, 60, 128].

Tiriant žmogaus SAN inervaciją pastebėta, jog centrinė SAN dalis yra gausiau inervuota nei periferinė [17, 19]. Be to nervinių skaidulų tankis žmogaus ŠLS kinta priklausomai ir nuo individo amžiaus – didžiausias yra stebimas vaikystėje, o vėliau mažėja [17].

1.7. Nervų ir nervinių skaidulų cheminis tipas širdies laidžiojoje sistemoje

Kiekybiniais tyrimais buvo siekiama išsiaiškinti dominuojantį nervinių skaidulų tipą jaučio, jūros kiaulytės, kiaulės, šuns ir žmogaus širdies laidžiojoje sistemoje. Juose stebėta, jog AChE Ns sudarė 60–80 proc. visų skaidulų, todėl buvo teigiama, jog ŠLS didžiausią veiklos įtaką turi cholinerginė inervacija. Kitas gausus inervacijos šaltinis – tai TH IR Ns [15–19, 60]. Be šių dviejų gausių Ns grupių stebėtos ir juntamosios skaidulos, pasižyminčios CGRP ir SP IR [15, 17–19, 60, 128]. Nemažas dėmesys ŠNS tyrimuose yra skiriamas nNOS nervinėm skaidulom, tačiau pastarųjų kiekis ŠLS nebuvo vertintas [84, 129].

Nors AChE metodas yra taikomas iki šiol kaip cholinerginės inervacijos indikatorius, tačiau yra nemažai tyrimų, kritikuojančių šio metodo tinkamumą [23, 108, 130], kadangi AChE yra aptinkama adreneginiuose ir juntamuosiuose neuronuose [130]. Be to taikant AChE metodą buvo pastebėta, jog nervai išskirtinai pasižymintys TH IR, buvo pozityvūs AChE ir ne visi AChE pozytivios skaidulos pozityvios – ChAT [87, 131]. Acetilcholiną (ACh) cholinerginiuose neuronuose sintetina cholinacetiltransferazė (ChAT) [21], šis fermentas yra siūlomas kaip tikslesnis cholinerginių neuronų žymuo [22, 23]. Tačiau tyrimų, taikančių būtent šį žymenį ne tik ŠLS, bet ir visos širdies inervacijai yra tik keletas [23, 88, 127, 132–134].

2. MEDŽIAGA IR TYRIMO METODAI

Tyrimui panaudota 25 suaugusių C57BL/6J-linijos pelių, 22 Naujosios Zelandijos triušių (4–6 savaičių amžiaus; 420–940 g svorio) ir 21 negyvų gimusių arba neišgyvenusių pirmąją gimimo dieną paršelių ir 3 jaunų kiaulių (3–4 mėnesių, 25–40 kg) širdys. Pelės ir triušiai gauti iš Lietuvos sveikatos mokslų universiteto Veterinarijos akademijos vivariumo. Gyvūnams buvo atlikta eutanazija taikant stuburo kaklinės dalies dislokaciją. Paršiukai gauti iš ūkininko A. Banionio gyvulininkystės ūkio.

Tyrimai atlikti gavus Valstybinės maisto ir veterinarinės tarnybos leidimą Nr. 0206 bei laikantis geros laboratorinės praktikos reikalavimų.

2.1. Tiriamos širdies paruošimas

Po gyvūno (pelės, triušio) eutanazijos krūtinės ląsta buvo atveriama perpjaunant šonkaulines kremzles. Pelės širdis, iki išsiplaus kraujas, perfuzuojama fosfatiniu fiziologiniu tirpalu (PBS), įvedus kateterį į kairįjį skilvelį. Triušių ir paršelių širdys perfuzuojamos jas išėmus iš krūtinės ląstos, retrogradiniu būdu įvedus katerį į aortą ir ją užspaudus aukščiau kateterio įvedimo vietos. Po perfuzijos atliekama prefiksacija tokiu pat būdu sušvirkščiant 20–40 ml 4 proc. paraformaldehido PBS tirpalo (pH–7,4).

2.2. Viso prieširdžio preparatai

Po pirminės fiksacijos prieširdžiai atskiriami nuo skilvelių. Tokia prieširdžių „kepurė“ adatėlėmis pritvirtinama prie specialaus silikoninio pado. Nuo jos pašalinami perikardo likučiai. Tuomet preparatas apverčiamas endokardu į viršų, nuo jo atsargiai nukerpama tarpprieširdinė pertvara. Siekiant išgauti kuo plonesnį preparatą, dalis šukinių raumenų ir galinė skiauterė nukerpama. Toks preparatas apverčiamas epikardu į viršų, ištempiamas. Dėl audinių storio kiaulės prieširdžio preparatas ruošiamas kitaip – DGV perkerpama medialinėje dalyje ir tik tada preparatas ištempiamas. Po šių procedūrų preparatai buvo fiksuojami 40 min. 4 proc. paraformaldehido PBS tirpale (pH – 7,4). Vėliau atliekamos imunohistocheminės reakcijos pažymėti laidžiuosius miocitus (HCN4), cholinerginius (ChAT), adrenerginius (TH), nitrierginius (nNOS) ir juntamuosius (SP) nervinius komponentus (antikūnų sąrašas pateikiamas 2.2.1 lentelėje), pagal 2.2.2 lentelėje aprašytus protokolus. Dažniausia naudotos antikūnų kombinacijos buvo HCN4+ +PGP9.5, HCN4+ChAT, ChAT+nNOS, ChAT+TH ir SP+PGP9.5.

2.2.1 lentelė. *Tyrime naudotų antikūnų sąrašas*

Antigenas	Šeimininkas	Skiedimas	Gamintojas	Katalogo nr.
Pirminiai:				
ChAT	Ožka	1:100	Chemicon[1]	AB144P
TH	Triušis	1:500	Chemicon[1]	AB152
TH	Pelė	1:200	Chemicon[1]	MAB-318
TH	Avis	1:800	Chemicon[1]	AB1542
SP	Jūros kiaulytė	1:1000	Abcam[2]	AB1053
SP	Triušis	1:800	ImmunoStar[3]	20064
PGP 9.5	Pelė	1:200	ABD Serotec[4]	7863-1004
PGP 9.5	Triušis	1:500	ABD Serotec[4]	7869-0504
HCN4	Pelė	1:200	StressMarq Biosciences[5]	SMC-320D
HCN4	Triušis	1:100	Chemicon[1]	AB5808
nNOS	Pelė	1:500	Santa Cruz Biotechonology[6]	SC-5302
Antriniai:				
Ožka ^{Cy3}	Asilas	1:300	Chemicon[1]	AP180C
Pelė ^{Cy3}	Asilas	1:300	Chemicon[1]	AP192C
Pelė $^{DyLight\ ®488}$	Asilas	1:300	Abcam[3]	AB96875
Pelė ^{FITC}	Asilas	1:100	Jackson Immunoresearch[7]	715-095-151
Avis ^{FITC}	Asilas	1:100	Chemicon[1]	AP184F
Jūros kiaulytė ^{FITC}	Asilas	1:100	Chemicon[1]	AP193F
Triušis ^{Cy3}	Asilas	1:300	Chemicon[1]	AP182C
Triušis ^{FITC}	Asilas	1:100	Chemicon[1]	AP182F

[1]Chemicon International, Temecula, California, USA.
[2]Abcam, Cambridge, UK.
[3]ImmunoStar Incorporation, Wisconsin, USA.
[4]AbD Serotec, Kidlington, UK.
[5]StressMarq Biosciences Incorporation, Cadboro Bay, Victoria, Canada.
[6]Santa Cruz Biotechnology, Dallas, TX, USA.
[7]Jackson Immunoresearch, West Grove, PA, USA.

2.2.2 lentelė. *Imunohistocheminių reakcijų protokolai*

Etapas	Viso prieširdžio preparatai			Pjūviai
	Pelė	**Triušis**	**Kiaulė**	
Išplovimas PBS buferiu	3 × 10 min.			3 × 5 min
Audinių dehidratavimas	Dehidratuojama 30°, 50°, 70°, 90°, 96° koncentracijos spiritu po 10 min. kiekviename ir 100° 3 × 10 min.			Neatliekama
Audinių pralaidumo didinimas	Audiniai inkubuojami 2–3 val. Dent'o tirpalu (1 dalis DMSO: 4 dalys 100° etanolio)			Neatliekama
Balinimas	Audiniai per naktį (6–12 val.) inkubuojami 30% H_2O_2 (1dalis) ir Dent'o (4 dalys) tirpalu.			Neatliekama
Rehidratavimas	Audiniai rehidratuojami 70°, 50°, 30° spiritu po 10 min. kiekviename			Neatliekama
Išplovimas PBS Triton X-100 tirpale	Konc. 0,5%, 3 × 10 min.	Konc. 1%, 3 × 10 min.		Konc. 0,5%, 3 × 10 min.
Nespecifinių antikūnų blokavimas	2 val. 5% NDS ir PBS ir 0,5% Triton X-100 tirpalu	2–3 val. 5% NDS ir PBS ir 1% Triton X-100 tirpalu.		40 min. 5% NDS ir PBS ir 0,5% Triton X-100 tirpalu
Inkubavimas pirminiais antikūnais	18–48 val. pirminių antikūnų (pagal gamintojo rekomendaciją) ir PBS su 0,5% Triton X-100 mišiniu	48–72 val. pirminių antikūnų (pagal gamintojo rekomendaciją 2.2.1 lentelė) ir PBS su 0,5% Triton X-100 mišiniu		8–12 val. pirminių antikūnų (pagal gamintojo rekomendaciją) ir PBS su 0,5% Triton X-100 mišiniu
Audinių išplovimas PBS	3 × 10 min.			3 x 5 min.
Audinių inkubavimas antriniais antikūnais	4–6 val. PBS ir antrinių antikūnų tirpalu			1–2 val. PBS ir antrinių antikūnų tirpalu
Audinių išplovimas PBS	3 × 10 min.			3 × 5 min.
Audinių dengimas	Audiniai ištempiami ant objektinio stikliuko ir uždengiami dengiamuoju stikliuku naudojant terpę Vectashield H-1000 arba H-1200 (Vector Laboratories, JAV). Dengiamojo stiklelio kraštai užhermetizuoti bespalviu nagų laku			

DMSO – dimetilsulfoksidas $(CH_3)_2SO_2$; H_2O_2 – vandenilio peroksidas;
NDS – normalus asilo serumas, PBS – fosfatinis fiziologinis tirpalas.

2.3. Sinusinio prieširdžio mazgo pjūvių preparatai

Siekiant patikslinti HCN4 ląstelių išsidėstymą prieširdžio sienoje, pjūvių preparatams buvo atkerpami DP gabaliukai iš trijų vietų aplink DGV, paliekant nedidelę venos dalį ir ribinę skiauterę. Vienas gabaliukas iškerpamas priekinėje dešiniosios venos dalyje, antras – šoninėje DGV dalyje ir trečias – tarp nugarinės DGV dalies iki uodeginės venos. Paruošti mėginiai fiksuoti 40 min. 4 proc. paraformaldehido PBS tirpale (pH – 7,4).

Pasibaigus fiksacijai audiniai 3 kartus po 10 minučių plauti PBS tirpale. Po plovimo, siekiant užtikrinti krioprotekciją, kuri apsaugo nuo šaldymo metu sukeliamo ląstelių suardymo, audiniai pamerkti į 20 proc. sacharozės PBS tirpalą kol paskęs (4–12 valandų, priklausomai nuo audinių storio). Audiniai užšaldyti, naudojat greitojo šaldymo terpę (Triangle Biomedical Sciences, USA), suorientuoti taip, kad matytųsi visas SAN skerspjūvis ir visi prieširdžio sienos sluoksniai (epikardas, miokardas ir endokardas). Kriotomu HM 560 (Microm, Vokietija) –22 °C temperatūroje atpjauti 20 µm storio pjūviai, elektrostatiniu būdu pritvirtinti prie objektinių stikliukų Superfrost Plus (Menzel Glaser, Vokietija), po 3–5 pjūvius ant kiekvieno ir išdžiovinti kambario temperatūroje. Toliau atliekamos imunohistocheminės reakcijos pagal 2.2.2 lentelėje pateiktą protokolą.

2.4. Kiekybinė ir statistinė analizė

Tik tie preparatai, kuriuose imunohistocheminės reakcijos buvo ryškios ir kontrastingos, buvo naudoti tolimesnei analizei. Nervinės struktūros tirtos ir fotografuotos konfokaliniu mikroskopu LSM 700 (Carl Zeiss, Jena, Vokietija). Vaizdai analizuoti laisvos prieigos programa FIJI, naudojant automatinius skaičiavimus, prieš tai apdorojant vaizdą, iš jo pašalinant triukšmą ir foną. Nervinių skaidulų užimamas plotas matuotas SAN galvoje, kūne ir uodegoje, lyginant zonas tarpusavyje ir su aplinkiniu darbiniu miokardu. Skaidulų ploto vertinimui rankiniu būdu buvo parenkamas plotas, tokiu būdu išvengiant tuščių laukų. Skaidulų plotas išreikštas procentais, kurį užėmė parinktame plote. Užimamam plotui įvertinti buvo panaudota po 3 kiekvienos rūšies gyvūno širdis. Nervinių skaidulų užimamas plotas buvo matuotas kiekvienai zonai ir žymeniui atskirai parinktuose 95–135 pjūviuose (po 30–45 iš kiekvieno gyvūno).

Neuronų kūnai skaičiuoti ir matuoti tik viso prieširdžio preparatuose. Neuronų diametras išreikštas trumposios ir ilgosios ašių aritmetiniu vidurkiu. Duomenų analizei naudotas dviejų nepriklausomų imčių t testas, naudojant IBM SPSS 20 programą. Duomenys laikyti patikimais parinkus 95 proc. pasikliovimo lygmenį ($p<0,05$).

3. REZULTATAI IR JŲ APTARIMAS

3.1. HCN4 pozityvių ląstelių išsidėstymas

Visų tirtų gyvūnų viso prieširdžio preparatuose HCN4 pozityvios ląstelės buvo išsidėstę panašiai (3.1.1 pav.). SAN stebėtas DGV ir DP jungties srityje. Mazgas prasidėjo DGV priekinėje dalyje, toliau tęsėsi šonine venos dalimi per ribinę širdies vagą ir beveik pasiekė uodeginę veną (UV). Viso prieširdžio preparatuose stebėta, jog pelės SAN HCN4 ląstelių užimamas plotas buvo 3,1±0,1 mm^2, triušio 18,0±2,4 mm^2 ir kiaulės 52±5,2 mm^2. Dėl didelio HCN4 ląstelių užimamo ploto SAN sritis buvo padalinta į tris dalis: galvą – priekinėje dešiniosios venos dalyje, kūną – šoninėje dešiniosios venos dalyje ir uodegą nugarinėje dešiniosios venos dalyje iki uodeginės venos (3.1.1 pav.). Šios dalys viena į kitą perėjo be aiškių ribų.

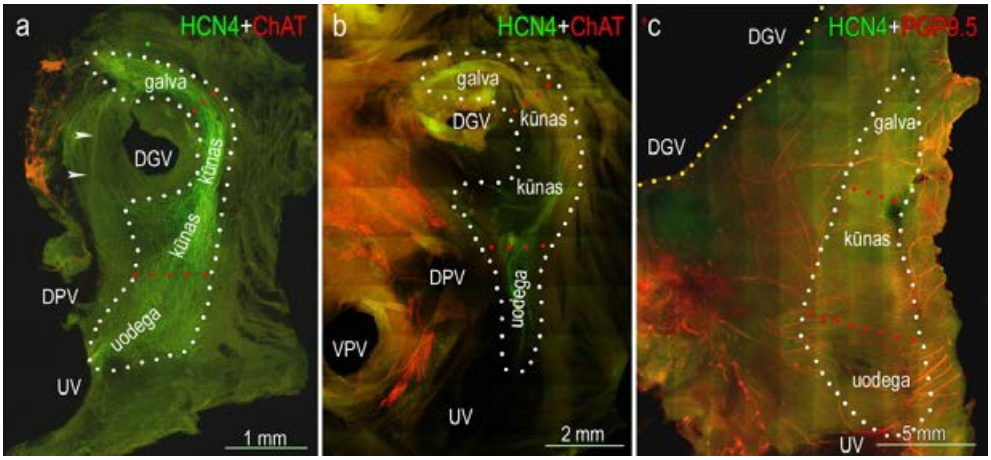

3.1.1 pav. *HCN4 ląstelių išsidėstymas aplink dešiniąją galvinę veną (DGV), (a) pelės, (b) triušio ir (c) kiaulės viso prieširdžio preparatuose.*
Žalia spalva pažymėtos HCN4 pozityvios ląstelės. Raudona ChAT (a, b) ir PGP9.5 (c) pozityvios nervinės struktūros. Balta punktyrine linija apibrėžtas plotas, kuriame stebėtas didžiausias HCN4 pozityvių ląstelių masyvas. Raudona punktyrinė linija skiria zonas (galvą, kūną, uodegą) SAN srityje. (a) strėlių galai žymi siaurą HCN4 ląstelių pluoštą apsupantį DGV iš medialinės pusės. (c) geltonu punktyru pažymėtos dešiniosios DGV žiotys. DGV – dešinioji galvinė vena; DPV – dešinioji plautinė vena; UV – uodeginė vena; VPV – vidurinioji plautinė vena.

Nors SAN išlaikė panašų ląstelių išsidėstymą visų tirtų gyvūnų prieširdžiuose, tačiau viso SAN preparatuose buvo nustatyti tarprūšiniai skirtumai. Pelės SAN HCN4 ląstelės taip pat stebėtos vidinėje DGV dalyje

(3.1.1 pav. (a) – strėlių galai). Čia jos sudarė siaurą pluoštelį. Triušio ir kiaulės prieširdžiuose, vidinėje DGV dalyje, HCN4 ląstelių aptikta nebuvo. Dėl šio pluoštelio, pelės SAN forma buvo panaši į pasagą (3.1.1 pav. a), kuri DGV apsupo iš vidinės, pilvinės ir šoninės pusių (žr. 67 psl. 2 pav. ir 77 psl. 3 pav.). Triušio (3.1.1 pav. b, taip pat žr. 57 psl. 1 pav.) ir kiaulės (3.1.1 pav. c) SAN – kablio formos, kurio pradžia pilvinėje DGV dalyje, o kūnas nusitęsė per šoninę DGV dalį beveik iki uodeginės venos. Derėtų pabrėžti, jog kiaulės DGV buvo perkirpta medialinėje dalyje, todėl mazgas atrodo kaip pailga struktūra (3.1.1 pav. c). Visų tirtų gyvūnų širdyse HCN4 ląstelių masyvas stipriai išplatėjo mazgo kūne, nugarinėje DGV dalyje.

Viso prieširdžio preparatai atskleidė, jog SAN yra vientisa struktūra, sudaryta iš daugybės ląstelių. Tačiau juose buvo galima išskirti centrinę – „kompaktiškąją“ – ir periferinę SAN dalis. Centrinę dalį sudarė pagrindinis HCN4 ląstelių masyvas (3.1.1 pav. balta punktyrinė linija), kuriame ląstelės buvo išsidėsčiusios tankiai bei keliais sluoksniais. Periferinę dalį sudarė HCN4 pozityvių ląstelių „rankovės“, kurios nuo pagrindinio ląstelių masyvo nusitęsė tolyn į dešiniojo prieširdžio miokardą (žr. 57 psl., 1 pav. b–e). Priekinėje DGV dalyje jos beveik pasiekė užaortinį mazgą, o šonuose – vainikinę vagą. Prieširdžio pjūviuose mazgo centrą sudarė kompaktiškai išsidėsčiusios HCN4 pozityvios ląstelės, o „rankovės“ atrodė kaip pavieniai miocitai, įsiterpę į darbinį miokardą. Šios struktūros buvo būdingos visoms tirtoms rūšims. Ankstesniais morfologiniais tyrimais taip pat aprašyta centrinė ir periferinė SAN dalys, tačiau juose buvo teigiama, kad dalys yra atskiros ir izoliuotos viena nuo kitos [33, 135, 136].

Kadangi HCN4 „rankovės“ nepasiekė tarpprieširdinės vagos ir AV tranzitinės zonos [137–144], funkciniu požiūriu jos tėra periferinės mazgo dalys, galinčios atlikti ritmo vedlio funkciją šiose srityse. Įdomu tai, kad toks HCN4 ląstelių išsidėstymas papildo elektrofiziologinius eksperimentus, kuriais nustatyta, jog pirminį impulsą gali generuoti ne tik SAN centrinė dalis, bet ir stipriai nutolusios periferinės mazgo dalys [145].

Pjūvių preparatuose mazgo centre gerai matėsi SAN arterija. Triušio ir kiaulės SAN ji sudarė 2–3 šakas. Šių kraujagyslių vieta nebuvo pastovi (3.1.2 pav. b, c). Pelės SAN arterija šakų nesudarė ir paprastai buvo pačiame mazgo centre (3.1.2 pav. a).

SAN pjūvių preparatuose visos HCN4 pozityvios ląstelės atitiko klasikinius laidžiųjų ŠLS miocitų požymius t. y. buvo apsuptos jungiamuoju audiniu ir jas buvo galima stebėti gretimuose pjūviuose [34]. Prieširdžio sienos atžvilgiu, HCN4 ląstelės skirtingose mazgo zonose buvo išsidėstę nevienodai. SAN galvoje jos sudarė platų prieširdžio paviršiaus, tačiau miokardo sienos atžvilgiu ploną sluoksnį, esantį iškart po epikardu. Kūne ląstelių masyvas išplatėjo ir užėmė visą prieširdžio sienos skerspjūvio plotą, o kūnui

pereinant į uodegą, šis masyvas siaurėjo ir uodegoje sudarė siaurą pluoštelį, esantį iškart po endokardu (žr. 58 psl., 2 pav. a–c).

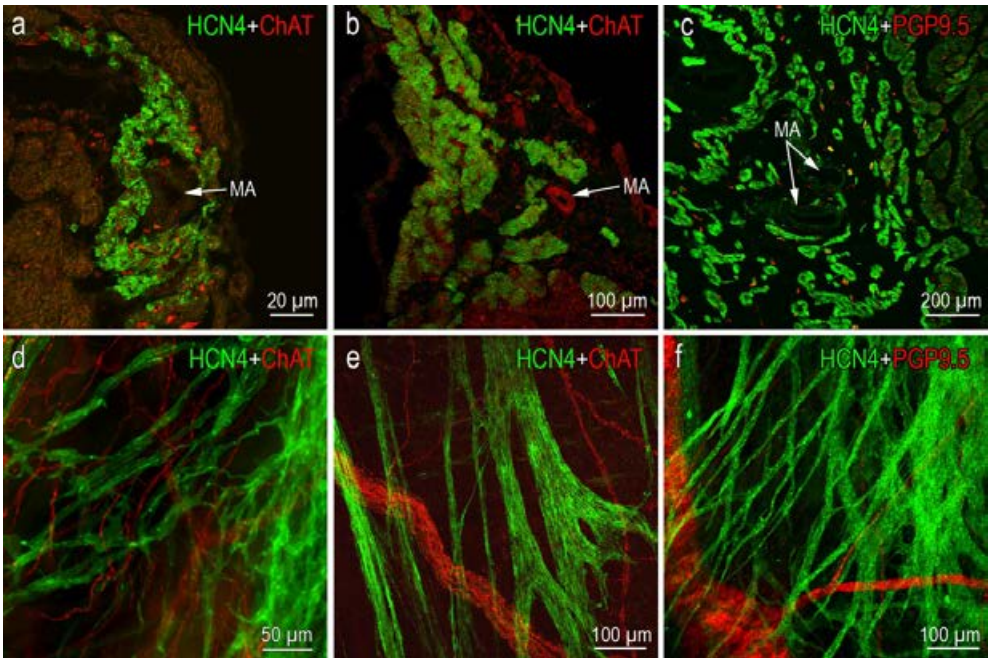

3.1.2 pav. *HCN4 ląstelių išsidėstymas aplink mazginę arteriją (a) pelės, (b) triušio, (c) kiaulės SAN pjūvių preparatuose ir HCN4 „rankovės“ viso prieširdžio preparatuose (d) pelės, (e) triušio, (f) kiaulės SAN periferinėse dalyse.*

Žalia spalva pažymėtos HCN4 ląstelės, raudona – (a, b, d, e) ChAT ir (c, f) PGP9.5 pozityvios nervinės struktūros. MA – prieširdžių sinusinio mazgo arterija.

Panašus specializuotų ląstelių išsidėstymas parodytas ir ankstesniuose tyrimuose atliekat 3D rekonstrukcijas iš SAN pjūvių [37, 135]. Tačiau dėl padriko HCN4 ląstelių išsidėstymo mazgo periferinėje dalyje buvo rekonstruojama tik centrinė mazgo dalis [9, 11, 37, 52, 54, 58, 146].

3.2. Sinusinio prieširdžio mazgo inervacijos šaltiniai ir nervinių skaidulų užimamas plotas

Visoms tirtoms rūšims buvo būdinga panaši į SAN sritį plintančių nervų schema. Dalis ekstrakardinių nervų, patekę pro širdies vartus veninėje dalyje, sudarė šakas, kurios apjuosė DGV iš priekinės ir šoninės pusių. Kiti nervai nusidriekė iki intrakardinių mazgų esančių greta SAN (žr. 59 psl., 3 pav.;

61 psl. 7 pav.; 71 psl., 6 pav.; 80 psl., 6 pav.; 81 psl., 7 pav.). Iš jų nervai per nugarinę DGV dalį aukščiau DPV pasiekė SAN kūną ir tarp DPV bei UV – uodegą. Keletas smulkių nervų sudarė kilpą aplink UV nugarinę dalį. Panašus nervinių komponentų išsidėstymas stebėtas ankstesniuose tyrimuose taikant histocheminius ir imunohistocheminius metodus [13, 14, 81–83, 88, 147].

Nervai, pasiekę SAN, šakojosi ir sudarė gausų nervinių skaidulų tinklą, kuris atitiko HCN4 pozityvių ląstelių užimamą sritį. Visais atvejais SAN Ns kiekis buvo didesnis negu darbiniame miokarde. Pjūvių preparatuose gausi inervacija stebėta aplik HCN4 pozityvias ląsteles, lyginant su darbiniu miokardu. Didelis Ns kiekis taip pat aprašytas ir ankstesniuose tyrimuose taikant kitas metodikas viso prieširdžio preparatuose, pvz., laidžiuosius miocitus nudažius Alciano mėliu, o nervus – histochemine AChE reakcija [14].

Kiekybinė analizė parodė, jog Ns skaidulų tankis skirtingose SAN zonose yra nevienodas. Pelės (žr. 72 psl., 2 lentelė) ir triušio (3.2.1 lentelė) SAN didžiausias nervinių skaidulų tankis buvo stebėtas galvoje ir mažiausias uodegoje. Kiaulės didžiausias Ns tankis stebėtas kūne, o mažiausias uodegoje (3.2.2 lentelė).

3.2.1 lentelė. *Skirtingų cheminių tipų Ns užimami plotai (vidurkis ± standartinė paklaida μm^2) triušio SAN skirtingose zonose ir prieširdžių darbiniame miokarde*

Sritis	PGP9.5	TH	ChAT	nNOS	SP
Galva	3,41±0,05*	1,90±0,03‡	1,47±0,04*‡	0,34±0,03*	0,19±0,01
Kūnas	3,25±0,04*	1,84±0,03‡	1,24±0,03*‡	0,66±0,03*	0,19±0,01
Uodega	2,23±0,04*	1,22±0,04*‡	0,95±0,02*‡	0,59±0,02*	0,21±0,01
SAN bendrai	2,96±0,04†	1,69±0,02†‡	1,29±0,02†‡	0,55±0,02†	0,20±0,00†
Darbinis miokardas	0,70±0,02†	0,31±0,01†	0,30±0,01†	0,15±0,01†	0,04±0,00†

*Statistiškai reikšmingas skirtumas lyginant to paties neurocheminio fenotipo Ns užimamą plotą skirtingose mazgo zonose ($p<0,05$).
†Statistiškai reikšmingas skirtumas lyginant Ns užimamą plotą SAN bendrai su darbiniu miokardu ($p<0,05$).
‡Statistiškai reikšmingas skirtumas lyginant TH ir ChAT Ns užimamą plotą ($p<0,05$).

Nervinių skaidulų pasiskirstymo analizė skirtingose mazgo zonose atlikta pirmą kartą. Ankstesniuose tyrimuose Ns tankis vertintas ŠLS mazguose, Hiso pluošte ir Hiso pluošto kojytėse [15–19, 60, 128]. Šiuose tyrimuose aprašomi tam tikri tarprūšinai skirtumai. Pvz. jūros kiaulytės SAN ir AVN Ns tankis yra toks pats, o žmogaus SAN didesnis negu AVN. Antra vertus dažniausiai tokiuose tyrimuose yra stebėtas laipsninis Ns mažėjimas perei-

nant iš vieno mazgo į kitą ir t. t. Be to daugumai rūšių yra būdinga, jog Hiso pluoštui perėjus į kojytes, o šioms į Purkinje skaidulas, inervacija ženkliai mažėja ir beveik nesiskiria nuo aplinkinio darbinio miokardo [15–19, 60, 128].

3.2.2 lentelė. *Skirtingų cheminių tipų Ns užimami plotai (vidurkis ± standartinė paklaida μm^2) kiaulės SAN skirtingose zonose ir prieširdžių darbiniame miokarde.*

Sritis	PGP9.5	TH	ChAT	nNOS	SP
Galva	2,89±0,08*	1,55±0,04*‡	1,15±0,04*‡	0,18±0,01*	0,22±0,01
Kūnas	3,15±0,11*	1,88±0,05*‡	1,36±0,06*‡	0,16±0,01	0,22±0,01
Uodega	1,85±0,07*	1,01±0,04*‡	0,73±0,03*‡	0,15±0,01*	0,22 ± 0,01
SAN Bendrai	2,68±0,06†	1,49±0,03†‡	1,08±0,03†‡	0,16±0,00†	0,22±0,00†
Darbinis miokardas	0,70±0,02†	0,23±0,01†	0,13±0,00†	0,06±0,00†	0,09±0,00†

*Statistiškai reikšmingas skirtumas lyginant to paties neurocheminio fenotipo Ns užimamą plotą skirtingose mazgo zonose ($p<0,05$).
†Statistiškai reikšmingas skirtumas lyginant Ns užimamą plotą SAN bendrai su darbiniu miokardu ($p<0,05$).
‡Statistiškai reikšmingas skirtumas lyginant TH ir ChAT Ns užimamą plotą ($p<0,05$).

Detaliau buvo analizuoti Ns užimami plotai triušio (3.2.1 lentelė) ir kiaulės SAN (3.2.2 lentelė). Triušio SAN bendras Ns užimamas plotas buvo didesnis negu kiaulės. Lyginant skirtingo cheminio tipo Ns užimamus plotus stebėta, kad triušio SAN TH, ChAT ir nNOS Ns buvo daugiau, o SP mažiau negu kiaulės SAN. Abiejų gyvūnų SAN vyravo TH pozityvios Ns. Triušio SAN mažiausiai buvo SP Ns, o kiaulės – nNOS.

Didžiausias TH Ns užimamas plotas triušio SAN buvo stebėtas galvoje ir mažiausias uodegoje. Kiaulės TH Ns daugiausiai buvo kūne ir mažiausiai uodegoje.

Kita didelė grupė – tai ChAT pozityvios Ns. Triušio SAN jų taip pat buvo daugiausiai galvoje ir mažiausiai kūne, o kiaulės daugiausiai kūne ir mažiausiai uodegoje. Abiejų rūšių SAN SP nervinės skaidulos visose mazgo zonose buvo pasiskirsčiusios vienodai. Kiaulės SAN nNOS Ns daugiausiai buvo galvoje ir mažiausiai kūne, o triušio daugiausiai kūne ir mažiausiai galvoje.

Gauti rezultatai prieštarauja ankstesnių tyrimų duomenims, kadangi juose buvo teigiama, jog SAN dominuoja cholinerginės Ns [15, 17–19, 60, 128]. Toks rezultatų skirtumas galėjo būti gautas dėl skirtingų tyrimų metodų. Šiam tyrimui buvo pasirinktas cholinacetiltransferazės (ChAT) imunohistocheminis žymuo, kadangi acetilcholinas cholinerginiuose neuronuose yra

sintetinamas veikiant šiam fermentui [21]. Be to tyrimais įrodyta, kad ChAT yra tikslus cholinerginių neuronų ir Ns požymis [22, 23]. Ankstesniuose kiekybiniuose tyrimuose cholinerginėm nervinėm struktūrom žymėti buvo taikomas AChE histocheminis metodas. Visos AChE pozityvios nervinės struktūros buvo priskiriamos cholinerginėm [15, 17–19, 60]. Tačiau AChE metodas nėra tiesioginis cholinerginės NS žymuo, šio fermento taip pat yra aptinkama adrenerginiuose ir juntamuosiuose neuronuose [130]. Taip pat neuroanatominiuose tyrimuose buvo pastebėta, jog nervai sudaryti iš vien TH pozityvių Ns yra pozityvūs AChE, bet nepozityvūs ChAT [87, 131].

3.3. Sinusinio prieširdžio mazgo neuronai ir nerviniai mazgai

Lyginant SAN inervacijos sandarą stebėti ženklūs tarprūšiniai skirtumai, kadangi triušio ir kiaulės SAN buvo rasti neuronai ir nerviniai mazgai, išsibarstę po visą SAN plotą (3.3.1, 3.4.1 ir 3.4.2 pav.). Pelės SAN neuronų kūnų nebuvo rasta.

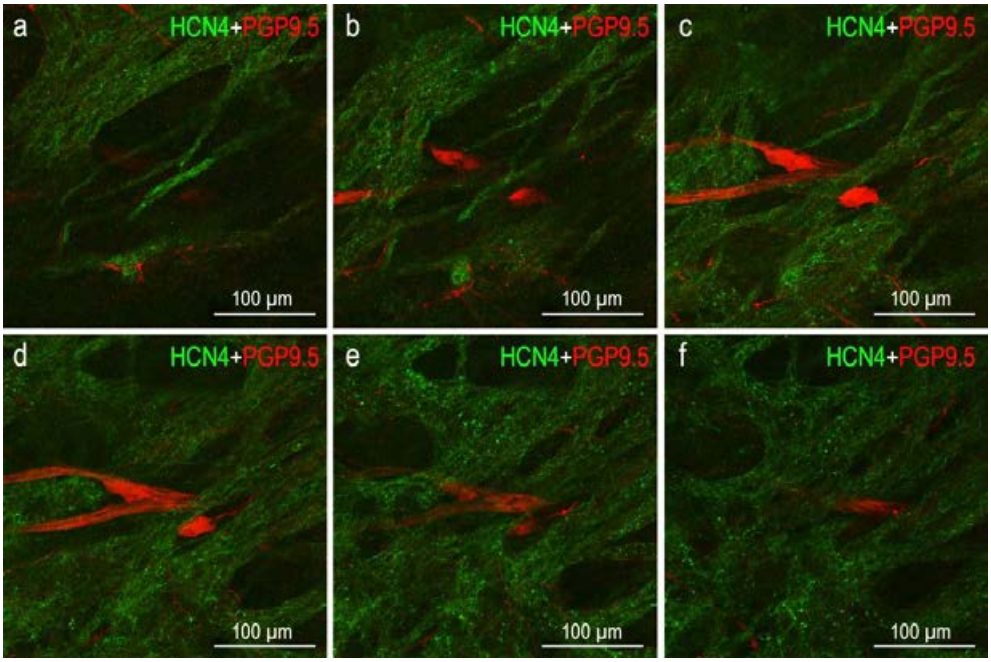

3.3.1 pav. *Nervai ir nedideli nerviniai mazgai (raudona) kiaulės SAN įsiterpę tarp HCN4 (žalia) pozityvių ląstelių klosčių.*
(a–f) SAN optiniai pjūviai skirtingame gylyje, nuo epikardo (a) gilyn link endokardo (f). Nuotraukose c ir d matomi neuronai įsiterpę tarp miokardo ląstelių.

Tiek kiaulės, tiek triušio SAN pjūvių preparatuose neuronai buvo stebėti tik atsitiktiniuose pjūviuose, todėl neuronų skaičius, pasiskirstymas, ir neurocheminis fenotipas buvo tirti tik viso prieširdžio preparatuose.

Nervų atžvilgiu neuronai ir nerviniai mazgai triušio ir kiaulės SAN buvo išsidėstę panašiai. Nerviniai mazgai apsupo nervą, taip pat ląstelės stebėtos šalia nervo ar įsiterpusios tarp pastarojo nervinių skaidulų. Tačiau mazgų ir nervų išsidėstymas miokardo atžvilgiu skyrėsi, kadangi triušio SAN jie buvo stebėti epikarde. Kiaulės SAN šios struktūros stebėtos ne tik epikarde, bet ir įsiterpusios tarp HCN4 pozityvių miocitų klosčių (3.3.1 pav.).

Triušio SAN būdingi maži nerviniai mazgai ir pavienės nervinės ląstelės. Suskaičiavus 5 triušių SAN esančius neuronus (n=288) nustatyta, jog vidutiniškai triušio SAN buvo 57,2±10 (nuo 41 iki 93) nervinių ląstelių. Triušio SAN nervinį mazgą sudarė 3,6±0,3 neuronai. Didžiausias nervinis mazgas triušio SAN buvo sudarytas iš 14 neuronų. Vidutiniškai triušio SAN buvo rasti 12,4±1,2 (nuo 8 iki 15) nerviniai mazgai. Viso mazguose buvo išsidėstę 78,6±6,0 proc. neuronų. Dominavo labai maži mazgai, kuriuose buvo iki 4 neuronų, ir tik nedidelė magų grupė buvo sudaryta iš 5 ir daugiau neuronų (3.3.2 pav.). Vidutinis pavienių neuronų skaičius siekė 12,0±3 (nuo 4 iki 19) ir sudarė 21,4±6,0 proc. nuo visų stebėtų nervinių ląstelių SAN zonoje (3.3.2 pav.).

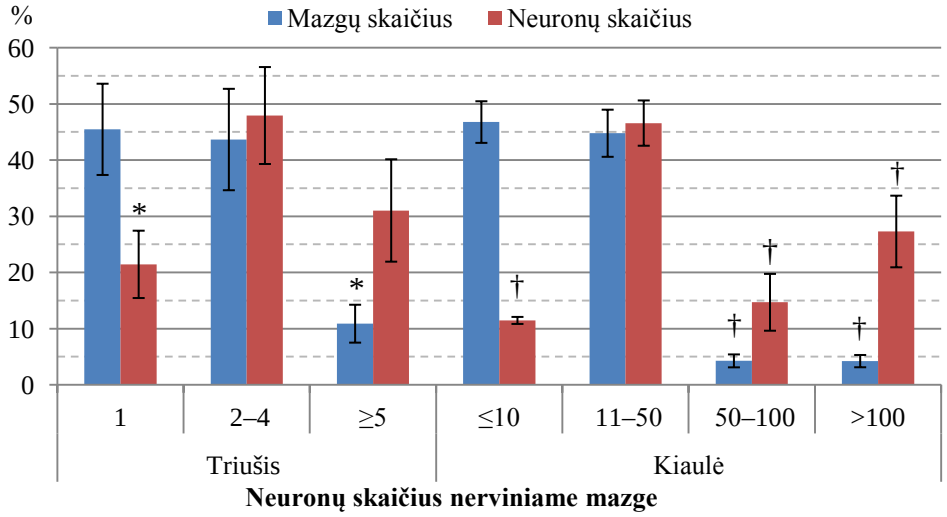

3.3.2 pav. *Nervinių mazgų ir neuronų skaičiaus pasiskirstymas triušio ir kiaulės SAN.*

*Statistiškai reikšmingas skirtumas lyginant su mazgais sudarytais iš 2–4 neuronų triušio SAN ($p<0,05$).

†Statistiškai reikšmingas skirtumais lyginant su mazgais sudarytais iš 11–50 neuronų kiaulės SAN ($p<0,05$).

Kiaulės SAN buvo gausu nervinių mazgų, kurie pasižymėjo dideliu neuronų skaičiumi. Dėl šios priežasties kiaulės SAN vertintas vidutinis mazgų skaičius ir vidutinis neuronų skaičius nerviniame mazge. Šiai analizei panaudoti 4 kiaulės SAN preparatai. Vidutinis mazgų skaičius buvo 97,5±10,1 (nuo 75 iki 120). Taip pat rasta ir pavienių neuronų, tačiau jų skaičius labai mažas (<10 neuronų visame SAN plote). Įvertinus 163 atsitiktinai pasirinktus mazgus nustatyta, jog juos vidutiniškai sudarė 21,3±2,4 (nuo 2 iki 187) neuronai. Taigi vidutiniškai kiaulės SAN srityje buvo išsidėstę virš 2000 neuronų ir tai yra ~35 kartais daugiau negu triušio SAN. Antra vertus kiaulės SAN plotas yra 3 kartus didesnis nei triušio, todėl 1 mm^2 tenka 41 neuronas, o triušio 3 (~10 kartų mažiau). Dėl šios priežasties galima daryti prielaidą, kad SAN nervinių ląstelių kiekis nėra priklausomas tik nuo gyvūno dydžio.

Pagal neuronų skaičių kiaulės SAN mazgai buvo suskirstyti į grupes:

- maži (≤10 neuronų),
- vidutiniai (11–50 neuronų),
- dideli (51–100),
- labai dideli (>100 neuronų).

Kiaulės SAN daugiausiai buvo mažų ir vidutinių nervinių mazgų. Tačiau atsižvelgiant į bendrą neuronų skaičių, daugiausiai neuronų buvo susitelkę vidutinio dydžio mazguose, o mažuose mažiausiai (3.3.2 pav.). Nerviniai mazgai ir neuronai SAN srityje taip pat buvo paminėti ankstesniuose darbuose, tiriant triušio, kiaulės ir šuns širdis [14, 81, 148], tačiau šiuose tyrimuose detali SAN nervinių komponentų analizė nebuvo atliekama. Kitose kiaulės INS rezginio mazguose buvo aprašomi, kiek didesni nerviniai mazgai, vidutiniškai sudaryti iš ~31 neurono, nei SAN srityje [81].

Kiaulės ir triušio SAN mazgai skyrėsi ne tik neuronų skaičiumi, bet ir pačių nervinių ląstelių dydžiu. Vidutinis neurono diametras kiaulės SAN buvo statistiškai reikšmingai didesnis (19,2±0,3 μm) negu triušio (16,5±0,2 μm). Neuronai, esantys triušio SAN, buvo mažesni už esančius kitose prieširdžių (23,1±02 μm) ir skilvelių (24,8±0,2 μm) nerviniuose mazguose [132]. Neuronai, esantys triušio SAN nerviniuose mazguose buvo mažesni (16,2±0,3 μm) už pavienius (17,2±0,6 μm), šis skirtumas buvo statistiškai reikšmingas. Pavieniai ir mazguose esantys neuronai, rasti triušio skilveliuose, tarpusavyje dydžiu nesiskyrė [132]. Dėl to galima daryti prielaidą, jog nervinių ląstelių dydis yra priklausomas nuo intrakardinio subrezginio.

3.4. Neuronų įvairovė sinusiniame prieširdžio mazge

Ankstesniuose tyrimuose SAN esatys neuronai nebuvo analizuoti imunohistocheminiais metodais [13, 14]. Šis tyrimas yra pirma detali SAN srityje esančių neuronų imunohistocheminė analizė triušio ir kiaulės širdyse.

Atsižvelgiant į neuronų neurochemines ypatybes, stebėti ženklūs tarprūšiniai skirtumai. Triušio SAN buvo rasti 3 skirtingų tipų neuronai (3.4.1 pav.), kurie pasižymėjo ChAT, nNOS ir bifenotipiniu (ChAT+nNOS) imunoreaktyvumu (IR). Kiaulės SAN (3.4.2 pav.) be šių 3 tipų nervinių ląstelių, stebėti TH ir bifenotipiniai (CHAT+TH) neuronai. Be to, kiaulės SAN buvo būdingos ir mažos intensyviai florescuojančios ląstelės (MIF), pasižyminčios TH IR. Nors bifenotipinių ChAT+TH, TH pozityvių neuronų triušio SAN neaptikta, tačiau šios ląstelės stebėtos prieširdžių intrakardiniuose mazguose, iš kurių išeinantys nervai inervuoja SAN [84]. Taip pat MIF ląstelių buvo rasta triušio skilveliuose [132].

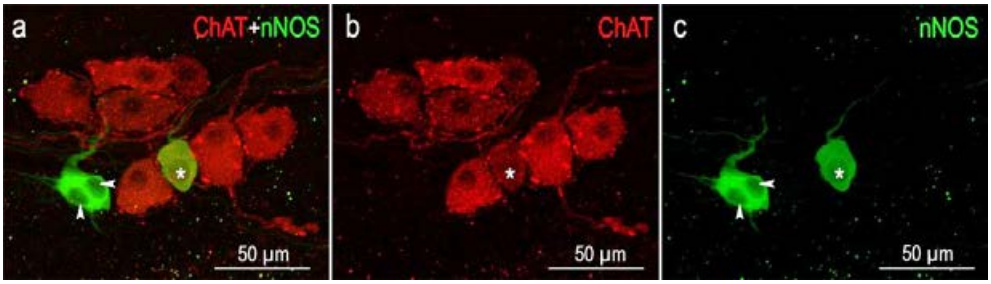

3.4.1 pav. *ChAT, nNOS ir bifenotipiniai neuronai triušio SAN.*
Raudona spalva žymi ChAT, žalia nNOS pozityvius neuronus. Žvaigždute pažymėtas bifenotipinis neuronas (a–c). Rodyklėmis pažymėti vien nNOS pozityvūs neuronai (a, c).

ChAT, TH ir bifenotipiniai ChAT+nNOS bei TH+nNOS neuronai buvo aprašyti kitų žinduolių INS mazguose [61, 83, 88, 124, 126, 134], tačiau būtina pabrėžti, jog šiame tyrime pirmą kartą aprašyti neuronų kūnai, pasižymintys vien nNOS (3.4.1 c ir 3.4.2 d pav., baltos rodyklės) IR. Anksčiau aprašytiems nNOS IR neuronams buvo būdingas bifenotipiškumas su ChAT IR [23, 125, 126]. Šis atradimas gali būti grindžiamas posnataliniu INS vystymusi, kadangi yra žinoma, jog šiuo laikotarpiu kai kurių rūšių žinduolių nervinės ląstelės geba keisti neurochemines savybes [149]. Antra vertus, tiek kiaulės, tiek triušio SAN neuronai nebuvo tyrinėti imunohistocheminiais metodais, todėl vien nNOS pozityvios ląstelės gali būti išskirtinai būdingos tik šių rūšių SAN inervacijai, panašiai kaip ChAT+TH

bifenotipiniai neuronai, kurie yra būdingi išskirtinai tik INS ir prakaito liaukoms [126].

Jūros kiaulyčių širdyse buvo aprašyti SP IR neuronai [122], tačiau tiriant triušio ir kiaulės SAN buvo stebėtos tik SP IR skaidulos.

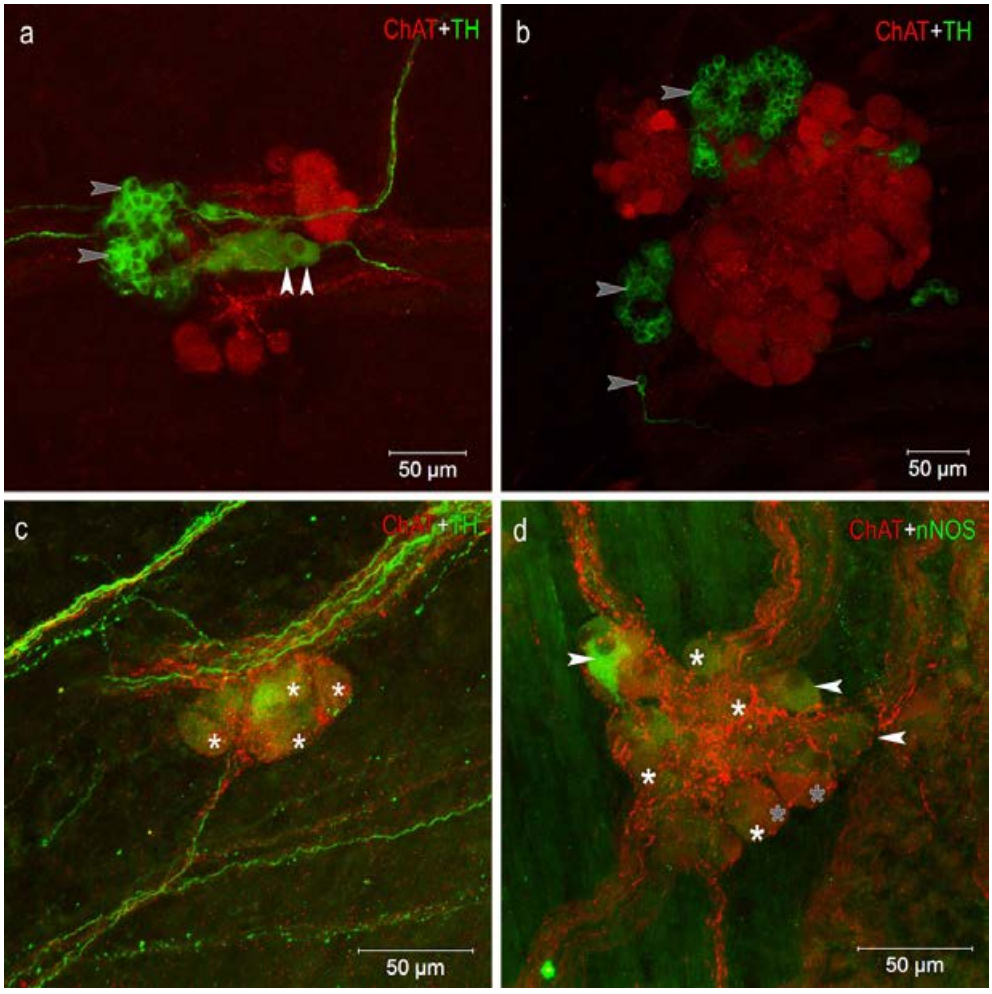

3.4.2 pav. *Nervinių mazgų ir neuronų įvairovė kiaulės SAN.*
Baltos rodyklės nurodo vien TH pozityvius neuronus (a), pilkos – MIF ląsteles (a, b). Baltomis žvaigždėmis pažymėtos bifenotipines ChAT+TH nervines ląsteles (c). (d) iliustruoja ChAT ir nNOS nervines ląstelės, baltos rodyklės žymi vien nNOS pozityvius neuronus, baltos žvaigždės bifenotipines ChAT+nNOS, o pilkos vien ChAT pozityvias nervines ląsteles.

Įvertinus 5 viso prieširdžio preparatus (286 neuronus) nustatyta, kad bendrai triušio SAN dominavo ChAT pozityvios ląstelės. Jos sudarė 50,3±4,9 proc. šioje srityje stebėtų ląstelių. Kita didelė ląstelių grupė, tai bifenotipiniai (ChAT+nNOS) neuronai, kurie sudarė 35,5±4,2 proc. Mažiausia grupė 14,2±1,7 proc. – tai grynai nNOS pozityvios ląstelės (3.4.3 pav.). Skirtumai tarp skirtingo neurocheminio fenotipo ląstelių grupių buvo statistiškai reikšmingi (3.4.3 pav.).

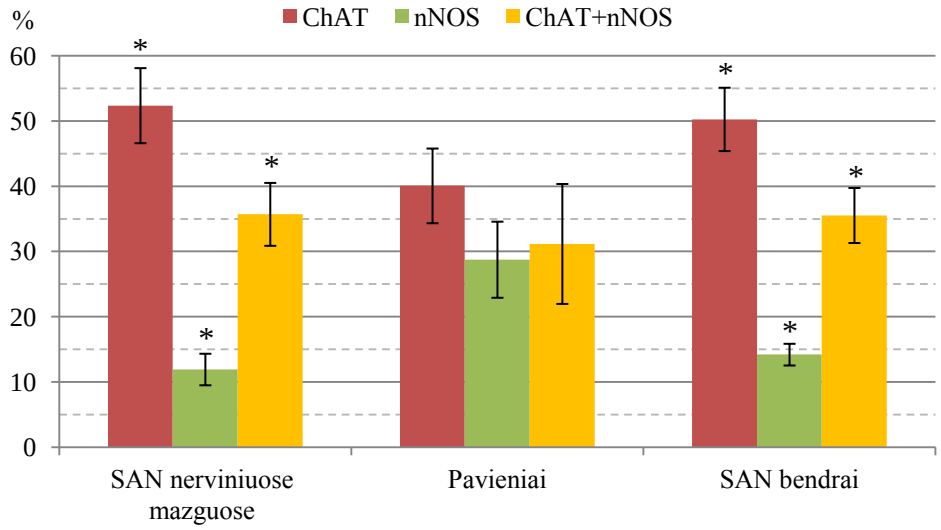

3.4.3 pav. *Triušio SAN dominuojantis neuronų fenotipas priklausomai nuo išsidėstymo.*

*Statistiškai reikšmingas skirtumas lyginant skirtingo fenotipo nervinių ląstelių grupes ($p<0,05$).

Pavienių ChAT, nNOS ir bifenotipinių neuronų skaičius buvo panašus. SAN nerviniuose mazguose statistiškai reikšmingai dominavo vien ChAT pozityvios ląstelės, o mažiausias skaičius buvo vien nNOS IR neuronų (3.4.3 pav.).

Kadangi viso prieširdžio preparatuose metodiškai buvo galima atlikti tik dvigubą imunohistocheminį žymėjimą, kiaulės SAN nervinių mazgų ir neuronų analizė buvo atliekama preparatuose, kuriuose taikytas ChAT+nNOS ir ChAT+TH žymėjimai.

Įvertinus 79 mazgus (1293 neuronus) esančius keturių paršelių viso prieširdžio preparatuose, kurioje taikytas dvigubas ChAT+nNOS žymėjimas, nustatyta, jog dominavo vien ChAT pozityvios (65,5±4,4 proc.) nervinės ląstelės, kiek mažesnę grupę (21,6±3,5 proc.) sudarė bifenotipinės ir

mažiausią (12,9±2,6 proc.) grynai nNOS IR neuronai. Skirtumai tarp skirtingo imonohistocheminio neuronų tipo grupių buvo statistiškai reikšmingi (3.4.4 pav.).

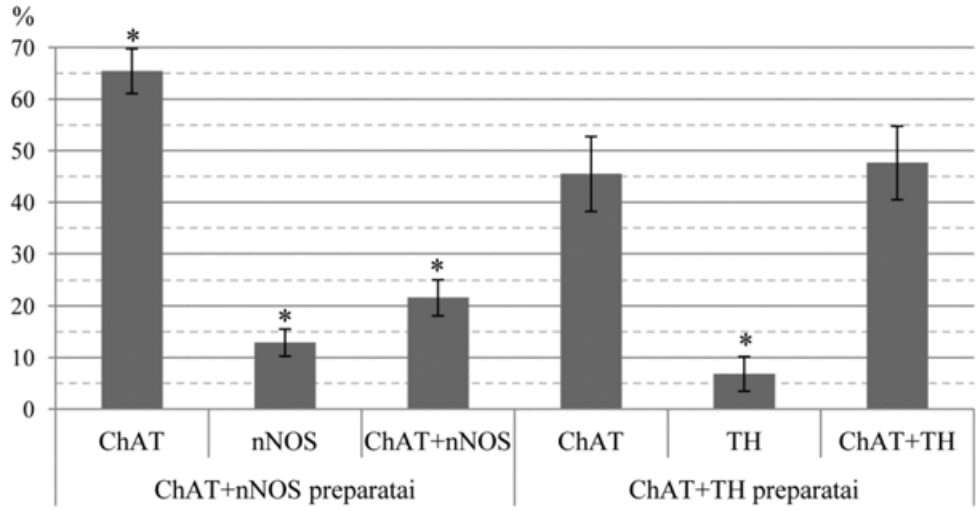

3.4.4 pav. *Skirtingo fenotipo neuronų pasiskirstymas kiaulės SAN nerviniuose mazguose.*

*Statistiškai reikšmingas skirtumas lyginant skirtingo fenotipo neuronų grupes ($p<0,05$).

Grupėje, kurioje taikytas dvigubas ChAT+TH imunohistocheminis žymėjimas, buvo įvertinti 43 nerviniai mazgai (902 neuronai), esantys 4 viso prieširdžio preparatuose. Čia stebėtos dvi stambios, savo dydžiu statistiškai reikšmingai nesiskiriančios grupės. Tai bifenotipiniai (47,6±7,1 proc.) ir ChAT IR (45,5±7,3 proc.) neuronai. Šiuose preparatuose mažiausiai buvo grynai TH IR (6,9±3,3 proc.) neuronų (3.4.4 pav.).

Tyrime stebėta neuronų dydžio priklausomybė nuo imunohistocheminio tipo (3.4.1 ir 3.4.2 lentelės). Triušio SAN mažiausi buvo ChAT IR neuronai, bei didžiausi bifenotipiniai (3.4.1 lentelė). Kiaulės SAN didžiausi neuronai buvo ChAT IR (3.4.2 lentelė). Kiek mažesni buvo bifenotipiniai neuronai ir mažiausi nNOS. Neuronų dydžio priklausomybė nuo imunohistocheminio tipo yra aprašyta ir pelės INS prieširdžių mazguose ir triušio skilveliuose [83, 132]. Žinios apie ląstelių dydžio skirtumus gali būti naudingos atliekant elektroninės mikroskopijos eksperimentus interpretuojant nervinių ląstelių cheminę sudėtį.

3.4.1 lentelė. *Nervinių ląstelių dydžio parametrų (vidurkis ± standartinė paklaida µm) priklausomybė nuo neurocheminio fenotipo triušio SAN.*

Neuronų grupė	**Nervinis žymuo**	**n**	**Diametras**	**Trumpoji ašis**	**Ilgoji ašis**
Pavieniai neuronai	ChAT	22	15,78±0,77†	12,02±0,62	19,54±0,81*
	nNOS	15	17,81±1,41	13,17±0,87	22,44±2,10
	ChAT+nNOS	23	18,02±0,96†	13,04±0,60	23,00±1,13*†
	Bendrai	60	17,16±0,59*	12,70±0,39	21,61±0,76*
SAN mazgų neuronai	ChAT	121	14,92±0,31†	12,42±0,30	17,41±0,41*
	nNOS	25	17,20±0,72†	14,20±0,83†	20,21±0,86†
	ChAT+nNOS	80	17,47±0,45†	13,9±0,44†	20,97±0,55*†
	Bendrai	226	16,23±0,26*	13,27±0,25	19,20±0,33*

*Statistiškai reikšmingas skirtumas lyginant pavienius ir SAN nervinių mazgų neuronus ($p<0,05$).

†Statistiškai reikšmingas skirtumas lyginant nNOS ir bifenotipinius neuronus su ChAT pozityviomis ląstelėmis toje pačioje grupėje ($p<0,05$).

3.4.2 lentelė. *Nervinių ląstelių dydžių parametrų (vidurkis ± standartinė paklaida µm) priklausomybė nuo neurocheminio fenotipo kiaulės SAN.*

Preparato tipas	**Nervinis žymuo**	**n**	**Diametras**	**Trumpoji ašis**	**Ilgoji ašis**
ChAT + TH	ChAT	34	21,21±0,59*	18,34±0,62*	24,09±0,72*
	TH	25	18,38±0,86†	15,12±0,83†	21,64±1,20†
	ChAT+TH	33	19,43±0,57	16,32±0,48	22,54±0,68
ChAT + nNOS	ChAT	32	20,64±0,75†	17,87±0,88†	23,40±1,00
	nNOS	32	16,12±0,63*†	13,32±0,58*†	18,92±0,88*†
	ChAT+nNOS	33	19,12±0,81	15,96±0,93	22,27±1,08

*Statistiškai reikšmingas skirtumas lyginant su ChAT pozityviais neuronais toje pačioje preparatų grupėje ($p<0,05$).

†Statistiškai reikšmingas skirtumas lyginant TH neuronus su ląstelėmis stebėtomis ChAT+nNOS preparatuose ($p<0,05$).

IŠVADOS

1. Ritmą generuojančios ląstelės pelės, triušio ir kiaulės prieširdžiuose yra išsidėsčiusios panašiai:
   a) Užima beveik trečdalį dešiniojo prieširdžio ploto;
   b) Suformuoja kompaktišką centrinę mazgo dalį;
   c) Sinusinio prieširdžio mazgo kraštuose formuoja „rankoves“, kurios nusidriekia tolyn į prieširdžio miokardą.
2. Visų tirtų gyvūnų sinusinio prieširdžio mazgo sritis nepriklausomai nuo vietos ir nervinių skaidulų tipo gausiau inervuota negu aplinkinis darbinis miokardas. TH pozityvios nervinės skaidulos buvo dominuojančios. Mažiau buvo ChAT pozityvių nervinių skaidulų. SP ir nNOS nervinių skaidulų buvo mažiausiai.
3. Pelės SAN nervinių mazgų ar pavienių neuronų neaptikta. Triušio SAN išsidėstę nedaug pavienių neuronų ir mažų nervinių mazgų. O kiaulės SAN būdingi dideli nervinai mazgai sudaryti iš daug neuronų.
4. SAN buvo nustatyti skirtingo cheminio tipo neuronai:
   a) Triušio SAN buvo rasti 3 tipų neuronai: grynai pozityvūs ChAT, nNOS ir bifenotipiniai ChAT+nNOS;
   b) Kiaulės SAN neuronai buvo 5 tipų: grynai pozityvūs ChAT, TH ir nNOS bei bifenotipiniai ChAT+nNOS ir ChAT+TH.
5. Neuronų dydis priklauso nuo ląstelės neurocheminio fenotipo ir gyvūno rūšies.

LITERATŪROS SĄRAŠAS

[1] Armour JA. Cardiac neuronal hierarchy in health and disease. American Journal of Physiology Regulatory, Integrative and Comparative Physiology 2004;287:R262–71.

[2] Armour JA. The little brain on the heart. Cleveland Clinic Journal of Medicine 2007;74:48–51.

[3] Christoffels VM, Moorman AFM. Development of the cardiac conduction system: why are some regions of the heart more arrhythmogenic than others? Circulation Arrhythmia and Electrophysiology 2009;2:195–207.

[4] Coote JH. Myths and realities of the cardiac vagus. The Journal of Physiology 2013;591:4073–85.

[5] Vanoli E, De Ferrari GM, Stramba-Badiale M, Hull SS, Foreman RD, Schwartz PJ. Vagal stimulation and prevention of sudden death in conscious dogs with a healed myocardial infarction. Circulation Research 1991;68:1471–81.

[6] Kawashima T. Anatomy of the cardiac nervous system with clinical and comparative morphological implications. Anatomical Science International 2011;86:30–49.

[7] Kawashima T. The autonomic nervous system of the human heart with special reference to its origin, course, and peripheral distribution. Anatomy and Embryology 2005;209:425–38.

[8] Po SS, Yu L, Scherlag BJ. Cardiac autonomic nervous system: A tug of war between the big brain and little brain friends or foes? Heart Rhythm 2009;6:1780–1.

[9] Atkinson AJ, Logantha SJRJ, Hao G, Yanni J, Fedorenko O, Sinha A, et al. Functional, anatomical, and molecular investigation of the cardiac conduction system and arrhythmogenic atrioventricular ring tissue in the rat heart. Journal of the American Heart Association 2013;2:1–25.

[10] Bharati S, Levine M. The conduction system of the swine heart. CHEST 1991:207–12.

[11] Yamamoto M, Dobrzynski H, Tellez J, Niwa R, Billeter R, Honjo H, et al. Extended atrial conduction system characterised by the expression of the HCN4 channel and connexin45. Cardiovascular Research 2006;72:271–81.

[12] Yanni J, Boyett MR, Anderson RH, Dobrzynski H. The extent of the specialized atrioventricular ring tissues. Heart Rhythm 2009;6:672–80.

[13] Roberts LA. The sinoatrial ring bundle: a cardiac neural communication system? The American Journal of Anatomy 1991;191:250–60.
[14] Roberts LA, Slocum GR, Riley DA. Morphological study of the innervation pattern of the rabbit sinoatrial node. The American Journal of Anatomy 1989;185:74–88.
[15] Anderson RH. The disposition, morphology and innervation of cardiac specialized tissue in the guinea-pig. Journal of Anatomy 1972;111: 453–68.
[16] Anderson RH. The disposition and innervation of atrioventricular ring specialized tissue in rats and rabbits. Journal of Anatomy 1972;113: 197–211.
[17] Chow LT, Chow SS, Anderson RH, Gosling J a. Autonomic innervation of the human cardiac conduction system: changes from infancy to senility. An immunohistochemical and histochemical analysis. The Anatomical Record 2001;264:169–82.
[18] Crick SJ, Sheppard MN, Anderson RH, Polak JM, Wharton J. A quantitative assessment of innervation in the conduction system of the calf heart. The Anatomical Record 1996;245:685–98.
[19] Crick SJ, Wharton J, Sheppard MN, Royston D, Yacoub MH, Anderson RH, et al. Innervation of the human cardiac conduction system. A quantitative immunohistochemical and histochemical study. Circulation 1994;89:1697–708.
[20] Koelle GB. The histochemical identification of acetylcholinesterase in cholinergic, adrenergic and sensory neurons. The Journal of Pharmacology and Experimental Therapeutics 1955;114:167–84.
[21] Nachmansohn D, John HM, Berman M. Studies on choline acetylase; the formation of acetylcholine in the nerve axon. The Journal of Biological Chemistry 1946;163:475–80.
[22] Arvidsson U, Riedl M, Elde R, Meister B. Vesicular acetylcholine transporter (VAChT) protein: a novel and unique marker for cholinergic neurons in the central and peripheral nervous systems. The Journal of Comparative Neurology 1997;378:454–67.
[23] Hoover DB, Ganote CE, Ferguson SM, Blakely RD, Parsons RL. Localization of cholinergic innervation in guinea pig heart by immunohistochemistry for high-affinity choline transporters. Cardiovascular Research 2004;62:112–21.
[24] Aird WC. Discovery of the cardiovascular system: From Galen to William Harvey. Journal of Thrombosis and Haemostasis 2011;9:118–29.

[25] Gaskell WH. On the innervation of the heart, with special reference to the heart of the tortoise. J Physiol. 1883;4:43–127.
[26] Silverman ME, Upshaw CB. Walter Gaskell and the understanding of atrioventricular conduction and block. Journal of the American College of Cardiology 2002;39:1574–80.
[27] Silverman ME, Grove D, Upshaw CB. Why does the heart beat? The discovery of the electrical system of the heart. Circulation 2006;113: 2775–81.
[28] Akiyama T. Sunao Tawara: Discoverer of the atrioventricular conduction system of the heart. Cardiology Journal 2010;17:428–33.
[29] Boyett MR. "And the beat goes on." The cardiac conduction system: the wiring system of the heart. Experimental Physiology 2009;94: 1035–49.
[30] Schweitzer P. Jan Evangelista Purkinje. Ceskoslovenska Epidemiologie, Mikrobiologie, Imunologie 1987;36:129–31.
[31] Fye WB. The origin of the heart beat: a tale of frogs, jellyfish, and turtles. Circulation 1987;76:493–500.
[32] Silverman ME, Hollman A. Discovery of the sinus node by Keith and Flack: on the centennial of their 1907 publication. Heart 2007;93: 1184–7.
[33] Anderson RH, Yanni J, Boyett MR, Chandler NJ, Dobrzynski H. The anatomy of the cardiac conduction system. Clinical Anatomy New York NY 2009;22:99–113.
[34] Mazgalev TN, Ho SY, Anderson RH. Anatomic-Electrophysiological Correlations Concerning the Pathways for Atrioventricular Conduction. Circulation 2001;103:2660–7.
[35] Sánchez-Quintana D, Cabrera J a, Farré J, Climent V, Anderson RH, Ho SY. Sinus node revisited in the era of electroanatomical mapping and catheter ablation. Heart 2005;91:189–94.
[36] Sánchez-Quintana D, Yen Ho S. Anatomy of cardiac nodes and atrioventricular specialized conduction system. Revista Española de Cardiología 2003;56:1085–92.
[37] Dobrzynski H, Li J, Tellez J, Greener ID, Nikolski VP, Wright SE, et al. Computer three-dimensional reconstruction of the sinoatrial node. Circulation 2005;111:846–54.
[38] Duan D, Yu S, Cui Y. Morphological study of the sinus node and its artery in yak. The Anatomical Record 2012;295:2045–56.
[39] Kember G, Armour JA, Zamir M. Neural control of heart rate: the role of neuronal networking. Journal of Theoretical Biology 2011;277: 41–7.

[40] Schwartz PJ, Vanoli E. From exercise training to sudden death prevention via adrenergic receptors. American Journal of Physiology Heart and Circulatory Physiology 2007;293: 631–3.
[41] Cheng G, Litchenberg WH, Cole GJ, Mikawa T, Thompson RP, Gourdie RG. Development of the cardiac conduction system involves recruitment within a multipotent cardiomyogenic lineage. Development 1999;126:5041–9.
[42] Gourdie RG, Mima T, Thompson RP, Mikawa T. Terminal diversification of the myocyte lineage generates Purkinje fibers of the cardiac conduction system. Development 1995;121:1423–31.
[43] Dehaan RL. Differentiation of the atrioventricular conducting system of the heart. Circulation 1961;24:458–70.
[44] Virágh S, Challice CE. The development of the conduction system in the mouse embryo heart. I. The first embryonic AV conduction pathway. Developmental Biology 1977;56:382–96.
[45] Moorman AFM, Christoffels VM. Cardiac chamber formation: development, genes, and evolution. Physiological Reviews 2003;83: 1223–67.
[46] Sedmera D, Gourdie RG. Why do we have Purkinje fibers deep in our heart? Physiological Research 2014;63:9–18.
[47] Viswanathan S, Burch JBE, Fishman GI, Moskowitz IP, Benson DW. Characterization of sinoatrial node in four conduction system marker mice. Journal of Molecular and Cellular Cardiology 2007;42:946–53.
[48] Bakker ML, Boukens BJ, Mommersteeg MTM, Brons JF, Wakker V, Moorman AFM, et al. Transcription factor Tbx3 is required for the specification of the atrioventricular conduction system. Circulation Research 2008;102:1340–9.
[49] Hoogaars WMH, Engel A, Brons JF, Verkerk AO, de Lange FJ, Wong LYE, et al. Tbx3 controls the sinoatrial node gene program and imposes pacemaker function on the atria. Genes & Development 2007; 21:1098–112.
[50] Dobrzynski H, Boyett MR, Anderson RH. New insights into pacemaker activity: promoting understanding of sick sinus syndrome. Circulation 2007;115:1921–32.
[51] Atkinson A, Inada S, Li J, Tellez JO, Yanni J, Sleiman R, et al. Anatomical and molecular mapping of the left and right ventricular His-Purkinje conduction networks. Journal of Molecular and Cellular Cardiology 2011;51:689–701.
[52] Pauza DH, Saburkina I, Rysevaite K, Inokaitis H, Jokubauskas M, Jalife J, et al. Neuroanatomy of the murine cardiac conduction system: A combined stereomicroscopic and fluorescence immunohistoche-

mical study. Autonomic Neuroscience: Basic & Clinical 2013;176:32–47.
[53] Dobrzynski H, Nikolski VP, Sambelashvili AT, Greener ID, Yamamoto M, Boyett MR, et al. Site of origin and molecular substrate of atrioventricular junctional rhythm in the rabbit heart. Circulation Research 2003;93:1102–10.
[54] Tellez JO, Dobrzynski H, Greener ID, Graham GM, Laing E, Honjo H, et al. Differential expression of ion channel transcripts in atrial muscle and sinoatrial node in rabbit. Circulation Research 2006;99: 1384–93.
[55] Papadatos GA, Wallerstein PMR, Head CEG, Ratcliff R, Brady PA, Benndorf K, et al. Slowed conduction and ventricular tachycardia after targeted disruption of the cardiac sodium channel gene Scn5a. Proceedings of the National Academy of Sciences of the United States of America 2002;99:6210–5.
[56] Kreuzberg MM, Willecke K, Bukauskas FF. Connexin-Mediated Cardiac Impulse Propagation: Connexin 30.2 Slows Atrioventricular Conduction in Mouse Heart. Trends in Cardiovascular Medicine 2006; 16:266–72.
[57] Jong F, Opthof T, Wilde AA, Janse MJ, Charles R, Lamers WH, et al. Persisting zones of slow impulse conduction in developing chicken hearts. Circulation Research 1992;71:240–50.
[58] Liu J, Dobrzynski H, Yanni J, Boyett MR, Lei M. Organisation of the mouse sinoatrial node: structure and expression of HCN channels. Cardiovascular Research 2007;73:729–38.
[59] Crick SJ, Anderson RH, Ho SY, Sheppard MN. Localisation and quantitation of autonomic innervation in the porcine heart II: endocardium, myocardium and epicardium. Journal of Anatomy 1999;195 (Pt3):359–73.
[60] Crick SJ, Sheppard MN, Ho SY, Anderson RH. Localisation and quantitation of autonomic innervation in the porcine heart I: conduction system. Journal of Anatomy 1999;195 (Pt3):341–57.
[61] Hasan W. Autonomic cardiac innervation: development and adult plasticity. Organogenesis 2013;9:176–93.
[62] Lachman N, Syed FF, Habib A, Kapa S, Bisco SE, Venkatachalam KL, et al. Correlative anatomy for the electrophysiologist, part II: Cardiac ganglia, phrenic nerve, coronary venous system. Journal of Cardiovascular Electrophysiology 2011;22:104–10.
[63] Raczak G, La Rovere MT, Mortara A, Assandri J, Prpa A, Pinna GD, et al. Arterial baroreflex modulation of heart rate in patients early after heart transplantation: lack of parasympathetic reinnervation. The

Journal of Heart and Lung Transplantation: The Official Publication of the International Society for Heart Transplantation 1999;18:399–406.
[64] Bengel FM, Ueberfuhr P, Schiepel N, Nekolla SG, Reichart B, Schwaiger M, et al. Effect of sympathetic reinnervation on cardiac performance after heart transplantation. The New England Journal of Medicine 2001;345:731–8.
[65] Waldmann M, Thompson GW, Kember GC, Ardell JL, Armour JA. Stochastic behavior of atrial and ventricular intrinsic cardiac neurons. Journal of Applied Physiology 2006;101:413–9.
[66] Gray AL, Johnson TA, Ardell JL, Massari VJ. Parasympathetic control of the heart II. A novel interganglionic intrinsic cardiac circuit mediates neural control of heart rate. Journal of Applied Physiology 2004;96:2273–8.
[67] Hou Y, Scherlag BJ, Lin J, Zhang Y, Lu Z, Truong K, et al. Ganglionated plexi modulate extrinsic cardiac autonomic nerve input: effects on sinus rate, atrioventricular conduction, refractoriness, and inducibility of atrial fibrillation. Journal of the American College of Cardiology 2007;50:61–8.
[68] Armour JA. Potential clinical relevance of the “little brain” on the mammalian heart. Experimental Physiology 2008;93:165–76.
[69] Chiou CW, Eble JN, Zipes DP. Efferent Vagal Innervation of the Canine Atria and Sinus and Atrioventricular Nodes: The Third Fat Pad. Circulation 1997;95:2573–84.
[70] Hoff HE, Geddes LA. Cholinergic factor in auricular fibrillation. Journal of Applied Physiology 1955;8:177–92.
[71] Schwartz PJ, Stone HL, Brown AM. Effects of unilateral stellate ganglion blockade on the arrhythmias associated with coronary occlusion. American Heart Journal 1976;92:589–99.
[72] Po SS, Scherlag BJ, Yamanashi WS, Edwards J, Zhou J, Wu R, et al. Experimental model for paroxysmal atrial fibrillation arising at the pulmonary vein-atrial junctions. Heart Rhythm 2006;3:201–8.
[73] Zhang Y, Scherlag BJ, Lu Z, Niu GD, Yamanashi WS, Hogan C, et al. Comparison of atrial fibrillation inducibility by electrical stimulation of either the extrinsic or the intrinsic autonomic nervous systems. Journal of Interventional Cardiac Electrophysiology : An International Journal of Arrhythmias and Pacing 2009;24:5–10.
[74] Becker RF, Grunt JA. The cervical sympathetic ganglia. The Anatomical Record 1957;127:1–14.
[75] Axford M. Some Observations on the Cervical Sympathetic in Man. Journal of Anatomy 1928;62:301–18.

[76] Harman B, Cantab MB, Eng FRCS. The anterior limit of the cervicothoracic visceral efferent nerves in man. J Anat Physiol 1900;34.
[77] Hoffman HH. An Analysis of the Sympathetic Trunk and Rami in the Cervical and Upper Thoracic Regions in Man. Annals of Surgery 1957;145:94–103.
[78] Jamieson DW, Smith DB, Anson JB. The cervical sympathetic ganglia: an anatomical study of 100 cervicothoracic dissections. Quarterly Bulletin Northwestern University (Evanston, III) Medical School 1952;26:219–27.
[79] Pick J, Sheehan D. Sympathetic rami in man. Journal of Anatomy 1946;80:12–20.
[80] Wrete M. The anatomy of the sympathetic trunks in Man. Journal of Anatomy 1959;93:448–59.
[81] Batulevicius D, Skripka V, Pauziene N, Pauza DH. Topography of the porcine epicardiac nerve plexus as revealed by histochemistry for acetylcholinesterase. Autonomic Neuroscience: Basic & Clinical 2008;138:64–75.
[82] Saburkina I, Gukauskiene L, Rysevaite K, Brack KE, Pauza AG, Pauziene N, et al. Morphological pattern of intrinsic nerve plexus distributed on the rabbit heart and interatrial septum. Journal of Anatomy 2014;224:583–93.
[83] Rysevaite K, Saburkina I, Pauziene N, Vaitkevicius R, Noujaim SF, Jalife J, et al. Immunohistochemical characterization of the intrinsic cardiac neural plexus in whole-mount mouse heart preparations. Heart Rhythm 2011;8:731–8.
[84] Brack KE. The heart's "little brain" controlling cardiac function in the rabbit. Experimental Physiology 2014;0:1–6.
[85] Pauza DH, Skripka V, Pauziene N, Stropus R. Anatomical study of the neural ganglionated plexus in the canine right atrium: Implications for selective denervation and electrophysiology of the sinoatrial node in dog. Anatomical Record 1999;255:271–94.
[86] Batulevicius D, Pauziene N, Pauza DH. Key anatomic data for the use of rat heart in electrophysiological studies of the intracardiac nervous system. Medicina 2004;40:253–9.
[87] Saburkina I, Rysevaite K, Pauziene N, Mischke K, Schauerte P, Jalife J, et al. Epicardial neural ganglionated plexus of ovine heart: anatomic basis for experimental cardiac electrophysiology and nerve protective cardiac surgery. Heart Rhythm 2010;7:942–50.
[88] Rysevaite K, Saburkina I, Pauziene N, Noujaim SF, Jalife J, Pauza DH. Morphologic pattern of the intrinsic ganglionated nerve plexus in mouse heart. Heart Rhythm 2011;8:448–54.

[89] Pauza DH, Skripka V, Pauziene N, Stropus R. Morphology, distribution, and variability of the epicardiac neural ganglionated subplexuses in the human heart. The Anatomical Record 2000;259: 353–82.
[90] Batulevicius D, Pauziene N, Pauza DH. Topographic morphology and age-related analysis of the neuronal number of the rat intracardiac nerve plexus. Annals of Anatomy 2003;185:449–59.
[91] Batulevicius D, Pauziene N, Pauza DH. Architecture and age-related analysis of the neuronal number of the guinea pig intrinsic cardiac nerve plexus. Annals of Anatomy 2005;187:225–43.
[92] Vaitkevicius R, Saburkina I, Rysevaite K, Vaitkeviciene I, Pauziene N, Zaliunas R, et al. Nerve Supply of the Human Pulmonary Veins: An Anatomical Study. Heart Rhythm 2009;6:221–8.
[93] Hildreth V, Anderson RH, Henderson DJ. Autonomic innervation of the developing heart: Origins and function. Clinical Anatomy 2009;22:36–46.
[94] Kawashima T, Thorington RW, Kunimatsu Y, Whatton JF. Systematic morphology and evolutionary anatomy of the autonomic cardiac nervous system in the lesser apes, gibbons (Hylobatidae). Anatomical Record 2008;291:939–59.
[95] Ellison JP, Williams TH. Sympathetic nerve pathways to the human heart, and their variations. American Journal of Anatomy 1969;124: 149–62.
[96] Fukuyama U. Macroscopic anatomy of the nerves innervating the human heart. Kaibogaku zasshi Journal of anatomy 1982;57:357–80.
[97] Janes RD, Brandys JC, Hopkins DA, Johnstone DE, Murphy DA, Armour JA. Anatomy of human extrinsic cardiac nerves and ganglia. The American Journal of Cardiology 1986;57:299–309.
[98] Tanaka A, Tanaka S, Miyamoto K, Yi SQ, Nakatani T. Gross anatomical study of the sympathetic cardiac nerves in the house musk shrew (Suncus murinus). Anatomical Record 2007;290:468–76.
[99] Mizeres NJ. The cardiac plexus in man. American Journal of Anatomy 1963;112:141–51.
[100] Kawashima T, Sato K, Akita K, Sasaki H. Comparative anatomical study of the autonomic cardiac nervous system in macaque monkeys. Journal of Morphology 2005;266:112–24.
[101] Kawashima T, Thorington RW, Whatton JF. Comparative anatomy and evolution of the cardiac innervation in new world monkeys. The Anatomical Record 2009;292:670–91.

[102] Norris JE, Lippincott D, Wurster RD. Responses of canine endocardium to stimulation of the upper thoracic roots. The American Journal of Physiology 1977;233:H655–9.
[103] Angelakos ET, King MP, Millard RW. Regional distribution of catecholamines in the hearts of various species. Annals of the New York Academy of Sciences 1969;156:219–40.
[104] Francis GS. Modulation of peripheral sympathetic nerve transmission. Journal of the American College of Cardiology 1988;12:250–4.
[105] Dickson DW, Lund DD, Subieta AR, Prall JL, Schmid PG, Roskoski R. Regional distribution of tyrosine hydroxylase and dopamine beta-hydroxylase activities in guinea pig heart. Journal of the Autonomic Nervous System 1981;4:319–26.
[106] Jones DL, Tuomi JM, Chidiac P. Role of cholinergic innervation and RGS2 in atrial arrhythmia. Frontiers in Physiology 2012;3 Jun:1–12.
[107] Sharpey-Schafer E. Vagal control of myocardial contractility in humans. Experimental Physiology. British Medical Journal 1933;86.6: 817:823.
[108] Koelle GB, Massoulié J, Eugène D, Melone M a, Boulla G. Distributions of molecular forms of acetylcholinesterase and butyrylcholinesterase in nervous tissue of the cat. Proceedings of the National Academy of Sciences of the United States of America 1987;84:7749–52.
[109] McAllen RM, Spyer KM. The location of cardiac vagal preganglionic motoneurones in the medulla of the cat. The Journal of Physiology 1976;258:187–204.
[110] Hopkins DA, Armour JA. Localization of sympathetic postganglionic and parasympathetic preganglionic neurons which innervate different regions of the dog heart. The Journal of Comparative Neurology 1984;229:186–98.
[111] Vance WH, Bowker RC. Spinal origins of cardiac afferents from the region of the left anterior descending artery. Brain Research 1983; 258:96–100.
[112] Thoren P. Role of cardiac vagal C-fibers in cardiovascular control. Reviews of Physiology, Biochemistry and Pharmacology 1979;86:1–94.
[113] Rubio R, Berne RM, Katori M. Release of adenosine in reactive hyperemia of the dog heart. The American Journal of Physiology 1969;216:56–62.
[114] Darvesh S, Nance DM, Hopkins DA, Armour JA. Distribution of neuropeptide-like immunoreactivity in intact and chronically decentralized middle cervical and stellate ganglia of dogs. Journal of the

Autonomic Nervous System 1987;21:167–80.
[115] Horackova M, Armour JA, Byczko Z. Distribution of intrinsic cardiac neurons in whole-mount guinea pig atria identified by multiple neurochemical coding. A confocal microscope study. Cell and Tissue Research 1999;297:409–21.
[116] Singh S, Johnson PI, Javed A, Gray TS, Lonchyna VA, Wurster RD. Monoamine and histamine synthesizing enzymes and neurotransmitters within neurons of adult human cardiac ganglia. Circulation 1999;99:411–9.
[117] Kaese S, Verheule S. Cardiac electrophysiology in mice: a matter of size. Frontiers in Physiology 2012;3:345.
[118] Asirvatham SJ, Kapa S. Sleep Apnea and Atrial Fibrillation. The Autonomic Link. Journal of the American College of Cardiology 2009;54:2084–6.
[119] Ghias M, Scherlag BJ, Lu Z, Niu G, Moers A, Jackman WM, et al. The Role of Ganglionated Plexi in Apnea-Related Atrial Fibrillation. Journal of the American College of Cardiology 2009;54:2075–83.
[120] Niu G, Scherlag BJ, Lu Z, Ghias M, Zhang Y, Patterson E, et al. An acute experimental model demonstrating 2 different forms of sustained atrial tachyarrhythmias. Circulation: Arrhythmia and Electrophysiology 2009;2:384–92.
[121] Armour JA, Murphy DA., Yuan BX, Macdonald S, Hopkins DA. Gross and microscopic anatomy of the human intrinsic cardiac nervous system. The Anatomical Record 1997;247:289–98.
[122] Baluk P, Gabella G. Some intrinsic neurons of the guinea-pig heart contain substance P. Neuroscience Letters 1989;104:269–73.
[123] Davies F, Francis ETB, King TS. Neurological studies of the cardiac ventricles of mammals. Journal of Anatomy 1952;86:130–43.
[124] Gu J, Polak JM, Allen JM, Huang WM, Sheppard MN, Tatemoto K, et al. High concentrations of a novel peptide, neuropeptide Y, in the innervation of mouse and rat heart. Journal of Histochemistry & Cytochemistry 1984;32:467–72.
[125] Mawe GM, Talmage EK, Lee KP, Parsons RL. Expression of choline acetyltransferase immunoreactivity in guinea pig cardiac ganglia. Cell and Tissue Research 1996;285:281–6.
[126] Weihe E, Schütz B, Hartschuh W, Anlauf M, Schäfer MK, Eiden LE. Coexpression of cholinergic and noradrenergic phenotypes in human and nonhuman autonomic nervous system. The Journal of Comparative Neurology 2005;492:370–9.

[127] Richardson RJ, Grkovic I, Anderson CR. Immunohistochemical analysis of intracardiac ganglia of the rat heart. Cell and Tissue Research 2003;314:337–50.
[128] Kent KM, Epstein SE, Cooper T, Jacobowitz DM. Cholinergic Innervation of the Canine and Human Ventricular Conducting System: Anatomic and Electrophysiologic Correlations. Circulation 1974;50: 948–55.
[129] Klimaschewski L, Kummer W, Mayer B, Couraud JY, Preissler U, Philippin B, et al. Nitric Oxide Synthase in Cardiac Nerve Fibers and Neurons of Rat and Guinea Pig Heart. Circulation Research 1992: 1533–7.
[130] Koelle GB. The histochemical identification of acetylcholinesterase in cholinergic, adrenergic and sensory neurons. The Journal of Pharmacology and Experimental Therapeutics 1955;114:167–84.
[131] Pauza DH, Rysevaite-Kyguoliene K, Vismantaite J, Brack KE, Inokaitis H, Pauza AG, et al. A combined acetylcholinesterase and immunohistochemical method for precise anatomical analysis of intrinsic cardiac neural structures. Annals of Anatomy 2014;196:430–40.
[132] Pauziene N, Alaburda P, Rysevaite-Kyguoliene K, Pauza AG, Inokaitis H, Masaityte A, et al. Innervation of the rabbit cardiac ventricles. Journal of Anatomy 2015;228:26–46.
[133] Calupca MA, Vizzard MA, Parsons RL. Origin of neuronal nitric oxide synthase (NOS) immunoreactive fibers in guinea pig parasympathetic cardiac ganglia. The Journal of Comparative Neurology 2000; 426:493–504.
[134] Yasuhara O, Matsuo A, Bellier JP, Aimi Y. Demonstration of choline acetyltransferase of a peripheral type in the rat heart. The Journal of Histochemistry and Cytochemistry 2007;55:287–99.
[135] Chandler N, Aslanidi O, Buckley D, Inada S, Birchall S, Atkinson A, et al. Computer Three–Dimensional Anatomical Reconstruction of the Human Sinus Node and a Novel Paranodal Area. Anatomical Record 2011;294:970–9.
[136] Monfredi O, Dobrzynski H, Mondal T, Boyett MR, Morris GM. The anatomy and physiology of the sinoatrial node-a contemporary review. Pacing and Clinical Electrophysiology: PACE 2010;33:1392–406.
[137] Anderson RH, Ho SY. The architecture of the sinus node, the atrioventricular conduction axis, and the internodal atrial myocardium. Journal of Cardiovascular Electrophysiology 1998;9:1233–48.

[138] James TN. The internodal pathways of the human heart. Progress in Cardiovascular Diseases 2001;43:495–535.
[139] Racker DK. The AV junction region of the heart: A comprehensive study correlating gross anatomy and direct three-dimensional analysis. Part I. Architecture and topography. Anatomical Record 1999;256:49–63.
[140] Sherf L, James TN. Fine structure of cells and their histologic organization within internodal pathways of the heart: clinical and electrocardiographic implications. The American Journal of Cardiology 1979;44:345–69.
[141] Benvenuti LA, Aiello VD, Higuchi M de L, Palomino SA. Immunohistochemical expression of atrial natriuretic peptide (ANP) in the conducting system and internodal atrial myocardium of human hearts. Acta Histochemica 1997;99:187–93.
[142] Kafer CJ. Internodal pathways in the human atria: a model study. Computers and Biomedical Research 1991;24:549–63.
[143] Ayettey AS, Navaratnam V, Yates RD. Ultrastructure of the internodal myocardium in the rat. Journal of Anatomy 1988;158:77–90.
[144] Thompson DR. Specialized internodal pathways. International Journal of Cardiology 1983;4:393–6.
[145] Fedorov VV, Hucker WJ, Dobrzynski H, Rosenshtraukh LV, Efimov IR. Postganglionic nerve stimulation induces temporal inhibition of excitability in rabbit sinoatrial node. American Journal of Physiology Heart and Circulatory Physiology 2006;291:H612–23.
[146] Pauza DH, Rysevaite K, Inokaitis H, Jokubauskas M, Pauza AG, Brack KE, et al. Innervation of sinoatrial nodal cardiomyocytes in mouse. A combined approach using immunofluorescent and electron microscopy. Journal of Molecular and Cellular Cardiology 2014;75C: 188–97.
[147] Roberts LA. Morphological innervation pattern of the developing rabbit heart. The American Journal of Anatomy 1991;190:370–84.
[148] Pauza DH, Skripka V, Pauziene N. Morphology of the intrinsic cardiac nervous system in the dog: A whole-mount study employing histochemical staining with acetylcholinesterase. Cells Tissues Organs 2002;172:297–320.
[149] Horackova M, Slavikova J, Byczko Z. Postnatal development of the rat intrinsic cardiac nervous system: a confocal laser scanning microscopy study in whole-mount atria. Tissue & Cell 2000;32:377–88.

MOKSLINĖS PUBLIKACIJOS

Mokslinės publikacijos leidiniuose, referuojamuose duomenų bazėje „Thomson Reuters Web of Knowledge“ ir turinčiuose citavimo rodiklį

Susijusios su disertacijos tema

1. **Inokaitis H**, Paužiene N, Rysevaite-Kyguolienė K, Pauža DH. *Innervation of sinoatrial nodal cells in the rabbit.* Annals of Anatomy 2016;205:113–21.
2. Pauža DH, Rysevaitė K, **Inokaitis H**, Jokubauskas M, Pauža AG, Brack KE, et al. *Innervation of sinoatrial nodal cardiomyocytes in mouse. A combined approach using immunofluorescent and electron microscopy*. Journal of molecular and cellular cardiology 2014;75C:188-197.
3. Pauža DH, Saburkina I, Rysevaitė K, **Inokaitis H**, Jokubauskas M, Jalife J, et al. *Neuroanatomy of the murine cardiac conduction system: A combined stereomicroscopic and fluorescence immunohistochemical study.* Autonomic Neuroscience: Basic & Clinical 2013 Jun;176(1–2):32–47.

Nesusijusios su disertacijos tema

1. Pauža DH, Rysevaitė-Kyguolienė K, Vismantaitė J, Brack KE, **Inokaitis H**, Pauža AG, et al. A combined acetylcholinesterase and immunohistochemical method for precise anatomical analysis of intrinsic cardiac neural structures. Annals of Anatomy 2014;196:430–40.
2. Paužienė N, Alaburda P, Rysevaitė-Kyguolienė K, Pauža AG, **Inokaitis H**, Masaitytė A, et al. Innervation of the rabbit cardiac ventricles. Journal of Anatomy 2015;228:26–46.

Kitos publikacijos

Susijusios su disertacijos tema

1. **Inokaitis H**, Rysevaitė-Kyguolienė, K, Pauža, DH. *Comparative neuroanatomy of sinoatrial node*. The 8th Baltic Morthology Scientific Conference: Interdisciplinary Nature of Contemporary Morthology: (the

12–14th of November, 2015, Vilnius, Lithuania), Lithuanian Academy of Sciences and Facu p. 45.

2. **Inokaitis H**, Rysevaitė-Kyguolienė, K, Paužienė, N, Pauža, DH. *Širdies prieširdžių sinusinio mazgo sandaros ir inervacijos immunohistocheminės ypatybės pelės, triušio ir kiaulės širdyse.* VIII nacionalinė doktorantų mokslinė konferencija „Mokslas – sveikatai“: konferencijos pranešimų tezės. Skirta pasaulinei sveikatos dienai paminėti, kuri minima balandžio 7-ąją. Ši p. 15–16.
3. **Inokaitis H**, Paužienė N, Pauža DH. *Immunohistochemical analysis of neurons located in cardiac conductive system.* 6th Conference of Lithuanian Neuroscience Association: Program and abstracts: 5 December, 2014, Vilnius, Lithuanian Neuroscience Association; p. 29, no. P17
4. **Inokaitis H**, Rysevaitė K, Paužienė N, Pauža, DH. *Peculiarities of cardiac conductive system and innervation in rabbit and pig.* Evoliucinė medicina: sveikatos sampratos ir ligų suvokimo perspektyvos: tarptautinė konferencija: 2014 m. gegužės mėn. 27–30 d., Vilniaus universitetas, Lietuva. Evolutionary medicine: p. 60.
5. **Inokaitis H**, Rysevaitė K, Paužienė N, Pauža DH, *Neuroimmunohistochemistry of the rabbit cardiac conductive system.* Fifth conference of Lithuanian Neuroscience Association: program and abstracts: 6–7 December, 2013, Vilnius, Lithuania, Lithuanian Neuroscience Association. p. 31.
6. **Inokaitis H**, Rysevaitė K, Paužienė N, Pauža DH. *The Neuroanatomy of cardiac conductive system in rabbit.* Baltic Morphology VII Scientific Conference „Morphological Sciences in the Experimental and Clinical Medicine“: November 7–9, 2013, Rīga, Latvia: abstract book. Rīga Stradiņš University (RS) p. 39.
7. Pauža DH, Jokūbauskas M, Rysevaitė K, Saburkina I, **Inokaitis H**, Paužienė N. *Occurrence of nerve fibers facilitates discrimination of cardiac conductive myocytes on the level of electron microscope* Anatomische Gesellschaft 108th Annual Meeting of the Anatomical Society: 22–25 March, 2013, Magdeburg, Germany: Lectures and Posters. Anatomical Society. p. 54.

Nesusijusios su disertacijos tema

1. Pauža AG, **Inokaitis H**, Rysevaitė-Kyguolienė K, Pauža DH, Paužienė N. *Distribution, quantity and immunohistochemistry of neuronal cells on pig cardiac ventricles.* Autonomic neuroscience: basic & clinical: ISAN

2015 „Bringing the latest in autonomic neuroscience from around the world“: 9th Meeting of the International Society for Autonomic Neuroscience. I p. 71–72, P5.7.

2. Rysevaitė-Kyguolienė K, Pauža AG, Alaburda P, **Inokaitis H**, Pauža, DH, Paužienė N. *Innervation of cardiac ventricles in the pig. Immunohistochemical study.* The 8th Baltic Morthology Scientific Conference: Interdisciplinary Nature of Contemporary Morthology: (the 12–14th of November, 2015, Vilnius, Lithuania) Lithuanian Academy of Sciences and Facu p. 62.
3. Saburkina I, Paužienė N, Alaburda P, Rysevaitė-Kyguolienė K, **Inokaitis H**, Pauža DH. *A Comparative study of the morphological patterns of the porcine and ovine epicardiac ventricular ganglionated nerve plexuses*. The 8th Baltic Morthology Scientific Conference: Interdisciplinary Nature of Contemporary Morthology: (the 12–14th of November, 2015, Vilnius, Lithuania) Lithuanian Academy of Sciences and Facu p. 63.
4. Alaburda P, Paužienė N, Rysevaitė K, **Inokaitis H**, Pauža, DH. *Innervation of rabbit heart ventricles: an immunohistochemical approach.* 6th Conference of Lithuanian Neuroscience Association: Program and abstracts: 5 December, 2014, Vilnius, Lithuanian Neuroscience Association p. 27, no. P15.
5. Paužienė N, Rysevaitė K, Saburkina I, **Inokaitis H**, Alaburda P, Pauža DH, *Neuroanatomy and immunohistochemistry of cardiac ventricles in rabbit*. The FASEB Journal: Experimental Biology 2014 „Transforming the Future through Science“: San Diego, CA April 26–30, 2014: An Annual Meeting of Professional Research Scientists: Abstract no. 543.2.
6. Rysevaitė K, Saburkina I, **Inokaitis H**, Alaburda P, Paužienė N, Pauža DH. *Innervation of cardiac ventricles in rabbit.* Baltic Morphology VII Scientific Conference „Morphological Sciences in the Experimental and Clinical Medicin“: November 7–9, 2013, Rīga, Latvia: abstract book. Rīga Stradiņš University p. 12.

Publikuoti straipsniai

Annals of Anatomy 205 (2016) 113–121

Contents lists available at ScienceDirect

Annals of Anatomy

journal homepage: www.elsevier.com/locate/aanat

Research article

Innervation of sinoatrial nodal cells in the rabbit

Hermanas Inokaitis, Neringa Pauziene, Kristina Rysevaite-Kyguoliene, Dainius H. Pauza*

Institute of Anatomy, Faculty of Medicine, Lithuanian University of Health Sciences, Kaunas, Lithuania

ARTICLE INFO

Article history:
Received 2 June 2015
Received in revised form 12 February 2016
Accepted 21 March 2016

Keywords:
Sinoatrial nodal cells
Innervation
Cardiac neurons
Immunohistochemistry
Anatomy
Rabbit

ABSTRACT

In spite of the fact that the rabbit is being widely used as a laboratory animal in experimental neurocardiology, neural control of SAN cells in the rabbit heart has been insufficiently examined thus far. This study analyzes the distribution of SAN cells and their innervation pattern employing fluorescent immunohistochemistry on rabbit whole mount atrial preparations. A dense network of adrenergic (positive for TH), cholinergic (positive for ChAT), nitrergic (positive for nNOS) and possibly sensory (positive for SP) NFs together with numerous neuronal somata were identified on the RRCV where the main mass of SAN cells positive for HCN4 were distributed as well. In general, the area occupied by SAN cells comprised nearly the entire RRCV and possessed a three to four times denser network of NFs compared with adjacent atrial walls. Adrenergic NFs predominated noticeably in-between SAN cells. Solitary neuronal somata or somata gathered into small clusters were positive solely for ChAT or nNOS, respectively or simultaneously for both neuronal markers (ChAT and nNOS). Neuronal somata positive for nNOS were more frequent than those positive for ChAT. In conclusion, findings of the present study demonstrate a dense and complex ganglionated neural network of both autonomic and sensory NFs, closely related to SAN cells which spread widely on the RRCV and extend as sleeves of these cells toward the walls of the rabbit RA.

1. Introduction

SAN cells send electrical signals to heart muscle, initiating its contraction. These cells have been an object of investigation in many pathological cases as SAN cells may be a trigger of sudden cardiac death (Christoffels and Moorman, 2009). Employing histological and immunohistochemical techniques, specialized cardiac cells of different functions were observed in the SAN area: pacemaker, transitional myocardial and insulation cells (Atkinson et al., 2013; Bharati and Levine, 1991; Liu et al., 2007; Tellez et al., 2006). HCN4 has been considered as a specific protein of pacemaker cells, allowing a reliable morphological identification of SAN cells (Atkinson et al., 2013; Liu et al., 2007; Tellez et al., 2006).

Physiological studies have shown that acetylcholine and noradrenaline can modulate the rate of SAN myocytes and action potential duration of atrial myocytes over a wide range (Verkerk et al., 2012). This effect may be explained by G protein regulation that suppresses muscarinic sensitivity and parasympathetic tone. It may prove to be a target for the treatment of SAN bradycardia or tachycardia (Verkerk et al., 2012). Moreover, stimulation of postganglionic NFs results in complex changes of pacemaker excitability in SAN cells (Fedorov et al., 2006). Such physiological findings correspond to neuroanatomical observations that the SAN possesses a considerably higher density of NFs relative to the adjacent myocardium (Crick et al., 1999, 1996, 1994; Pauza et al., 2013, 2014a,b; Roberts et al., 1989; Roberts, 1991a) and that two RA neural subplexuses (the dorsal and ventral ones) supply the SAN neural network in various mammalian species and the human (Batulevicius et al., 2005, 2003; Brack, 2014; Pauza et al., 2000, 1999; Rysevaite et al., 2011; Saburkina et al., 2014, 2010). Densities of cholinergic, adrenergic, and peptidergic (sensory) NFs differ significantly among the animal species (Chow et al., 2001; Crick et al., 1999, 1996, 1994). Many previous studies aiming to identify the distribution of nerve fibers in the heart were based on histochemical staining for acetylcholinesterase (AChE) which was considered a trustworthy marker of cholinergic nerve fibers (Crick et al., 1994, 1996, 1999; Chow et al., 2001). However, AChE was also abundantly identified among sensory and sympathetic nerve fibers (Koelle, 1955; Saburkina et al., 2010; Pauza et al., 2014a,b) and, therefore, AChE histochemical staining was altered to an

Abbreviations: AChE, acetylcholinesterase; ChAT, choline acetyltransferase; HCN4, hyperpolarization activated cyclic nucleotide-gated potassium channel 4; NFs, nerve fibers; nNOS, neuronal oxide synthase; RA, right atrial or right atrium; RRCV, root of the right cranial vein (superior vena cava); SAN, sinoatrial nodal or sinoatrial node; SP, substance P; TH, tyrosine hydroxylase.

* Corresponding author at: Institute of Anatomy, Faculty of Medicine, Lithuanian University of Health Sciences, A. Mickeviciaus Street 9, Kaunas LT-44307, Lithuania. Tel.: +370 37 327313; fax: +370 37 220733; mobile: +370 682 39366.
E-mail address: dainius.pauza@lsmuni.lt (D.H. Pauza).

http://dx.doi.org/10.1016/j.aanat.2016.03.007
0940-9602/

Table 1
Primary and secondary antisera used in the study.

Antigens	Host	Dilution	Company	Catalog number
Primary				
CHAT	Goat	1:100	Chemicon[a]	AB144P
TH	Mouse	1:400	Chemicon[a]	MAB318
TH	Sheep	1:800	Chemicon[a]	AB1542
CGRP	Mouse	1:800	Abcam[b]	AB5920
SP	Guinea pig	1:1000	Abcam[b]	AB1053
PGP 9.5	Mouse	1:200	ABD Serotec[c]	7863-1004
nNOS	Mouse	1:500	Santa Cruz Biotechonology[d]	SC-5302
HCN4	Mouse	1:200	StressMarq Biosciences[e]	SMC-320D
Secondary				
Goat^{Cy3}	Donkey	1:300	Chemicon[a]	AP180C
Mouse^{Cy3}	Donkey	1:300	Chemicon[a]	AP192C
Mouse$^{DyLight\ 0488}$	Donkey	1:300	Abcam[b]	AB96875
Mouse^{FITC}	Donkey	1:100	Jackson Immunoresearch[f]	715-095-151
Sheep^{FITC}	Donkey	1:100	Chemicon[a]	AP184F
Guinea pig^{FITC}	Donkey	1:100	Chemicon[a]	AP193F

[a] Chemicon International, Temecula, CA, USA.
[b] Abcam, Cambridge, UK.
[c] AbD Serotec, Kidlington, UK.
[d] Santa Cruz Biotechnology, Dallas, TX, USA.
[e] StressMarq Biosciences Inc., Cadboro Bay, Victoria, Canada.
[f] Jackson Immunoresearch, West Grove, PA, USA.

immunohistochemical method for choline acetyltransferase (ChAT) which is the crucial enzyme in acetylcholine synthesis (Nachmansohn et al., 1946). Recently, immunohistochemical labeling for ChAT has been approved as the most reliable cholinergic marker for parasympathetic nerve fibers (Arvidsson et al., 1997; Hoover et al., 2004; Saburkina et al., 2010; Pauza et al., 2014a,b). Therefore, this study was designed to simultaneously determine the distribution of SAN cells and their innervation in whole mount preparations of the rabbit heart employing immunohistochemical methods for reliable determination of autonomic innervation and SAN cells in order to compare their morphologic patterns with those in other mammalian hearts examined previously (Crick et al., 1994, 1996, 1999; Pauza et al., 2013, 2014a,b; Roberts, 1991a,b; Roberts et al., 1989; Yamamoto et al., 2006).

2. Material and methods

2.1. Study material

Twenty two young (4–6 week old) New Zealand rabbits of either gender weighing 420–940 g were used in accordance with local and state guidelines for the care and use of laboratory animals (Permission No. 0206). Nineteen hearts were used for whole mounts and three hearts for transverse section preparations.

2.2. Whole-mount preparations

Following animal euthanasia, hearts were dissected from the chest, cleaned with 0.01 M phosphate buffer saline (PBS) and the coronary vessels were retrogradely perfused with PBS. Afterwards, the atria were dissected from the ventricles and the interatrial septum. Then, the atria were flattened and pinned in a Petri dish with a silicone bottom. The flattened specimen was fixed for 40 min at 4 °C in 4% paraformaldehyde solution in 0.01 M phosphate buffer (pH = 7.4). In order to decrease background light for laser scanning microscopic examination, tissues were bleached using a dimethyl sulfoxide and hydrogen peroxide solution, and dehydrated as reported previously (Dickie et al., 2006). Subsequently, whole-mount preparations were rehydrated through a graded ethanol series (in each for 10 min), washed 3× 10 min in 0.01 M PBS containing 0.5% Triton X-100 (Serva, Heidelberg, Germany). Non-specific binding was blocked for 2 h in PBS containing 5% normal donkey serum (Jackson ImmunoResearch Laboratories, West Grove, PA, USA). Afterwards, the specimens were incubated with an appropriate combination of primary antisera for 48–72 h at 4 °C (Table 1). Afterwards, whole-mounts were washed 3 times for 10 min in 0.01 M PBS and incubated with an appropriate combination of secondary antisera for 4 h at room temperature (Table 1). Four combinations of antisera were used in this study in order to identify: (1) the SA nodal cells and cholinergic neural components (HCN4 + ChAT), (2) the biphenotypic neuronal somata and nerve fibers (ChAT + nNOS and ChAT + TH) and (3) general distribution of nerves, nerve fibers and neuronal somata as well as adrenergic neural structures and small intensively fluorescent (SIF) cells (PGP9.5 + TH).

During the last stage, specimens were washed 3 times for 10 min in 0.01 M PBS, mounted with Vectashield Mounting Medium (Vector Laboratories, Inc., Burlingame, CA, USA), cover slipped and sealed with clear nail polish.

2.3. Sectioned tissue preparations

In order to obtain transverse sections of walls of the rabbit RA and RRCV, three rabbit hearts were dissected, perfused and prefixed as described above. In order to compare the densities of NFs distributed between cardiac cells positive for HNC4 from distinct localities on RRCV, the SAN region was comparatively divided into three parts as described previously (Pauza et al., 2013, 2014a,b). SAN cells were categorized into three groups: SAN cells distributed on the medial part of the RRCV were considered to be the head of the SAN, the lateral ones that extended along the terminal groove to be the body, and their dorsal portion allocated toward the RRCV as the SAN tail (Fig. 1a). Following 40 min fixation at 4 °C in 4% paraformaldehyde solution in 0.01 M phosphate buffer (pH = 7.4), tissues were washed 3× 10 min in PBS and cryoprotected by immersion in PBS containing 20–25% sucrose until their complete sinking (4 °C, 24 h). Following cryoprotection, the tissues were frozen using a tissue-freezing medium (Triangle Biomedical Sciences, USA) for sectioning. The pieces of the sampled tissues were orientated on a cryomicrotome stage so that the slice cutting plane would be perpendicular to the interatrial septum, right atrial wall and the terminal groove and all layers (epicardium, myocardium and endocardium) could be well discernible in the slice. Tissues were sectioned into 20 μm slices using a cryomicrotome HM

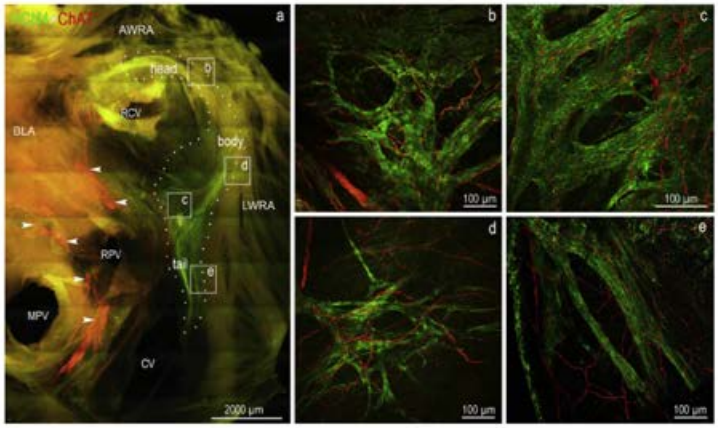

Fig. 1. Distribution of SAN cells positive for HCN4 (in green), neuronal somata (arrowheads) and NFs positive for ChAT (in red) in the rabbit whole-mount atrial preparation. Note the abundant neuronal somata positive for ChAT (arrowheads) on the base of the left atrium (BLA) in panel a. (a) General view of the distribution of cells positive for HCN4 and NFs positive for ChAT. The dotted line approximately outlines the region on the RRCV with the largest concentration of cells positive for HCN4. The boxed areas b–e in panel a are correspondingly enlarged as the left side panels b–e. SAN cells are strongly positive for HCN4 both in the head (b), body (d) and tail (e) of the SAN area and on the dorsal side of the RRCV (c). Other abbreviations: RCV – orifice of the right cranial vein; RPV and MPV – orifices of the right and middle pulmonary veins; CV – orifice of the caudal vein; AWRA – anterior wall of RA; LWRA – lateral wall of RA. (For interpretation of the references to color in this figure legend, the reader is referred to the web version of the article.)

560 (Microm, Germany) at −22 °C and sections were mounted onto Superfrost Plus microscope slides (Menzel Glaser, Germany). Afterwards, immunohistochemical procedures were performed as earlier described applying an appropriate combination of primary and secondary antisera (Table 1). Finally, specimens were washed 3 times for 5–8 min in 0.01 M PBS and mounted with Vectashield Mounting Medium (Vector Laboratories, Inc., Burlingame, CA, USA) and cover slipped. Both positive and negative controls were used.

2.4. Quantitative and statistical analysis

Both whole-mount preparations and RA wall transverse sections, in which immunohistochemical reactions showed the most well defined contrast were used for quantitative analysis. Neural structures were examined and digital images were acquired using a microscope LSM 700 (Carl Zeiss, Jena, Germany).

Intrinsic ganglia and neuronal somata were morphometrically analyzed in five whole mount preparations labeled simultaneously for ChAT and nNOS. The size of clearly visible neuronal somata was measured on digital images and expressed as the mean of their long and short axes. The densities of NFs within distinct portions of the SAN area (head, body and tail) were evaluated in transverse sections of the walls of the RRCV and RA from three rabbits double labeled for HCN4/PGP9.5, HCN4/ChAT, and HCN4/TH. In order to randomize the sampling, the same immunohistochemical reactions were repeated twice on the neighboring serial sections obtained at an interval of 500–800 µm. Digital images were randomly taken from the whole SAN area occupied by HCN4-positive cells and the adjacent myocardium of the RA wall which was free of HCN4-positive cells. NFs were analyzed within all portions of the SAN region in comparison to the adjacent RA myocardium. The density of NFs was expressed in percentage of the area occupied by NFs.

Data in tables are presented as absolute numbers (n), means (M) and standard errors (SE). Statistical analysis for density of NFs and the number of NFs within distinct regions of SAN and atrial areas was performed using the two-sample independent *t*-test with the aid of IBM SPSS software (package 20, IBM). Differences were considered significant when $p < 0.05$.

3. Results

3.1. Distribution of HCN4-positive cells

In whole mount preparations, HCN4-positive cells were widely distributed on the RRCV. The uninterrupted mass of these cells surrounded the RRCV from the anterior, lateral and dorsal sides and extended along the terminal groove toward the root of the caudal vein. The pattern of the distribution of the main mass of these cells was reminiscent of a hook shape hanging on the RRCV. In the dorsal part of the RRCV, these cells expanded medially and almost reached the interatrial groove (Fig. 1a). When SAN cells positive for HCN4 were homogenously distributed on the anterior side of the RRCV and alongside the terminal groove (Fig. 1b and c), these cells were patchily arranged in the SAN tail (Fig. 1e). The transition zones from head to tail of the SAN gradually transformed from one to the other without clear limits. In addition, the HCN4-positive cells spread as "cellular sleeves" from their main mass to the anterior and lateral sides of the RRCV toward the right auricle and lateral RA wall (Fig. 1d and e).

In contrast to whole mount preparations, transversal sections of the RRCV demonstrate a specific distribution of HCN4 positive cells within the myocardial wall in different SAN regions. In the SAN head, these cells were located near the epicardium as a thin cellular rim (Fig. 2a). Rarely, solitary HCN4-positive cells penetrating deeper into the wall of the RRCV may be seen as well. In the SAN body, HCN4-positive cells were widely and densely disseminated between the epicardium and endocardium, and commonly occupied the whole wall of the RRCV (Fig. 2b). In general, the mentioned "sleeves" of the HCN4-positive cells expanded from the SAN body toward the epicardium and endocardium of the lateral RA (Fig. 2b). HCN4-positive cells occupied the mid-myocardium and appeared as a bundle of these cells in the SAN tail (Fig. 2c). Normally,

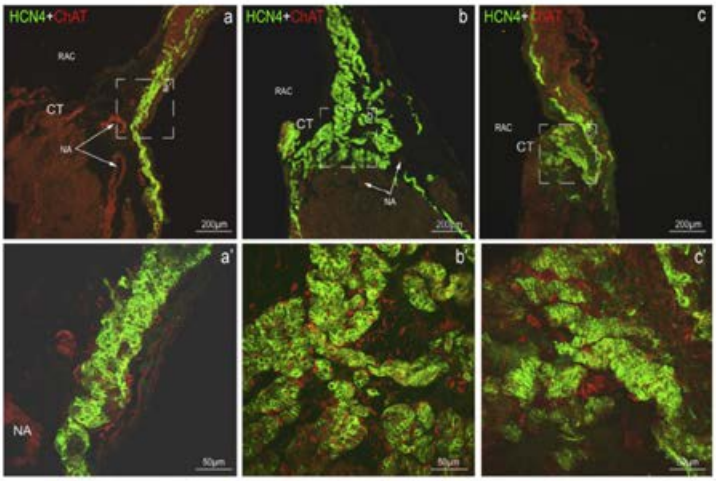

Fig. 2. Distribution of SAN cells positive for HCN4 (in green) and NFs positive for ChAT (in red) in transverse sections of the wall of the rabbit RA at different parts of the SAN area: head (a), body (b) and tail (c). The boxed areas in panels a–c are correspondingly enlarged as panels a'–c'. Abbreviations: NA – SAN artery; RAC – right atrial chamber; CT – crista terminalis. (For interpretation of the references to color in this figure legend, the reader is referred to the web version of the article.)

some profiles of detached HCN4-positive cells could be widely seen within the walls of the RA and the RRCV (Fig. 2c).

3.2. Neural pathways to the SAN region

The distribution of nerves proceeding to the RRCV and the RA, where the highest density of HCN4-positive cells was identified, is seen in whole mount preparations (Fig. 3a). Compared with adjacent RA regions, the RRCV with the wide distribution of HCN4-positive cells contained an obviously denser meshwork of NFs (Fig. 1c and d vs. 1e). Topographically, the area with the highest density of NFs corresponded to the "hooked" distribution of SAN cells positive for HCN4 (Figs. 3a vs. 1a).

The morphologic pattern of nerves supplying the area on the RRCV with SAN cells was similar in every examined heart. Commonly, several epicardial nerves from the intrinsic neuronal cluster that was regularly localized along the interatrial groove on the base of the left atrium extended toward the wide SAN region on the RRCV and the lateral wall of the RA, including the right auricle (Fig. 3a).

3.3. Distribution and density of NFs in the SAN region

Transverse sections of RCCV demonstrated that the thickest nerves at the SA nodal cells were distributed in the epicardium. Some larger nerves were also observed in adventitia of nodal artery, endocardium and near SA nodal cells. However, SA nodal cells positive for HCN4 were mainly accompanied by a dense meshwork of nerve fibers (Fig. 2).

Based on calculations of NFs in transverse sections of the RRCV and the adjacent RA areas, the mean density of NFs within the rabbit SAN region was fourfold compared with the neighboring RA myocardium (Table 2). Moreover, the density of NFs positive for TH was fivefold between SAN cells in respect to the adjacent contractile RA myocardium.

Distribution of NFs was different in various parts of the SAN area. The highest density of NFs positive for PGP9.5, TH and ChAT was identified at the head, while the lowest one – in the tail of the SAN area (Figs. 3 and 4; Table 2). Contrarily, NFs positive for SP and nNOS were the most plentiful in the tail and the body of the SAN area, correspondingly (Table 2). Noteworthy, the coexistence of two neurotransmitters in the same NF was usual for NFs positive for ChAT and nNOS, but it was not characteristic for NFs positive for TH and SP distributed within the rabbit SAN area (Fig. 5).

3.4. Neuronal somata within the SAN region

In addition to nerves and NFs, intrinsic neuronal somata were abundantly revealed in the rabbit SAN region (Table 3). In this region, the rabbit heart contained 57.2 ± 10.1 nerve cell bodies that were scattered solitarily or clustered into small ganglia with 3.6 ± 0.3 nerve cells. The solitary nerve cells and ganglionic cells were distributed unevenly within the SAN area, but $78.6 \pm 6.0\%$ of neuronal somata were identified in the ganglia (Table 3).

Neuronal somata found within the SAN area were either positive for ChAT ($50.3 \pm 4.9\%$), nNOS ($14.2 \pm 1.7\%$) or were biphenotypic; i.e. positive simultaneously for ChAT and nNOS ($35.5 \pm 4.2\%$; Table 3). The neuronal somata solely positive for nNOS were mainly distributed solitarily while the ChAT positive and biphenotypic nerve cells were more common in ganglia (Table 3). No cell bodies positive for TH were found in the rabbit SAN region on the RRCV. Most of nerve terminals observed around neuronal somata were positive for ChAT (Fig. 6).

The sizes of intrinsic neuronal somata were dependent on their distribution and chemical phenotype. Neuronal somata located at the SAN region were smaller than ganglionic nerve cells distributed on the base of the left atrium (Fig. 3a, Table 4). Mostly, solitary neuronal somata were larger than ones located within the ganglia, but the size differences between neuronal somata positive for distinct neuronal markers were statistically significant only between ChAT positive neuronal somata in comparison with nNOS positive and biphenotypic ones (Table 4).

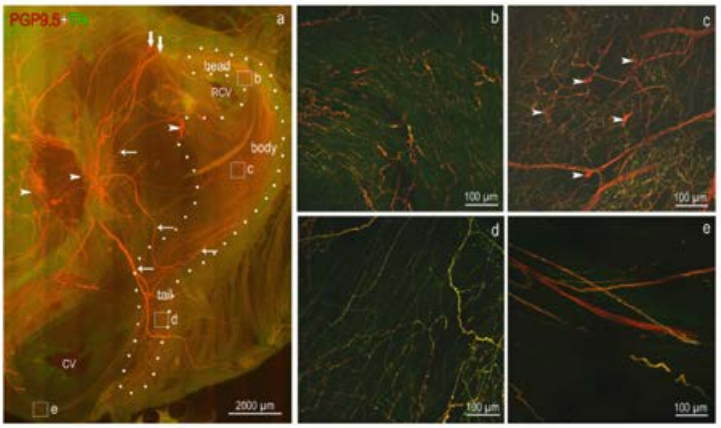

Fig. 3. Whole-mount preparation of the rabbit atria to demonstrate the distribution of ganglionated nerves and NFs positive for PGP9.5 (in red) and for TH (in green) in various parts of the SAN. The dotted line in panel a approximately outlines the region on the RRCV with the largest density of myocardial NFs positive for ChAT and TH. The boxed areas in panel **a** are correspondingly enlarged as panels b–e. Panel b demonstrates the meshwork of NFs in the SAN head, c – in the body, and d – in the SAN tail. Panel e demonstrates some nerves around the CV. Arrowheads in panel a point to clusters of neuronal somata on the base of the left atrium (BLA) and to solitary neuronal somata located at the body part of the SAN area in panel c. Solid arrows in panel a show accessing cardiac nerves that proceed to neuronal clusters (arrowheads) on the base of the left atrium, while the small arrows indicate the epicardial nerves extending from neuronal clusters toward the SAN area. Other abbreviations: RCV – orifice of the right cranial vein; RPV – site of the root of right pulmonary vein; CV – orifice of the caudal vein; AWRA – anterior wall of RA; LWRA – lateral wall of RA. (For interpretation of the references to color in this figure legend, the reader is referred to the web version of the article.)

Table 2
Comparison of densities of nerve fibers (NFs) between three parts of the SA nodal (SAN) region (head, body, and tail) and right atrial myocardium. The density is expressed in percent of the area occupied by NFs within the manually selected equal in size areas.

Region	PGP9.5	TH	ChAT	nNOS	SP
Head	3.41 ± 0.05*	1.90 ± 0.03†	1.47 ± 0.04*,†	0.34 ± 0.03*	0.19 ± 0.01
Body	3.25 ± 0.04*	1.84 ± 0.03†	1.24 ± 0.03*,†	0.66 ± 0.03*	0.19 ± 0.01
Tail	2.23 ± 0.04*	1.22 ± 0.04*,†	0.95 ± 0.02*,†	0.59 ± 0.02*	0.21 ± 0.01
Overall in SAN	2.96 ± 0.04†	1.67 ± 0.02†,‡	1.29 ± 0.02†,‡	0.55 ± 0.02†	0.20 ± 0.01†
Atrial myocardium	0.70 ± 0.02†	0.31 ± 0.01†	0.30 ± 0.01†	0.15 ± 0.01†	0.04 ± 0.01†

* Densities of the same immunohistochemical type NFs type in head, body and tail of SAN were statistically different at $p < 0.05$.
† Differences between the area of NFs in atria myocardium and SAN in general (statistical significant at $p < .0.05$).
‡ Differences between the density of NFs positive for ChAT and TH were statistically significant at $p < 0.05$.

Comparing the size of ganglionic neuronal somata from the SAN area and the base of left atrium, somata of any chemical phenotype from the SAN region were significantly smaller than those that were observed on the base of left atrium (Table 4). Solitary biphenotypic neuronal somata were significantly larger compared with ones positive for ChAT (Table 4).

4. Discussion

This study is the first demonstration of the simultaneous distribution of SAN cells positive for HCN4 and the innervation of these cells in both whole-mount preparations and transverse sections of the rabbit RA and RRCV, utilizing methods of fluorescent

Table 3
The number and percentages of solitary and ganglionic neuronal somata of different chemical phenotype identified in the rabbit SAN area.

Category	Chemical phenotype	Number per animal		Percentage in category		Overall percentage	
		Mean	Range	Mean	Range	Mean	Range
Solitary	ChAT	4.4 ± 1.2	2–9	40.1 ± 5.7	22.2–50.0	8.7 ± 3.1	4.3–20.9
	nNOS	3.0 ± 0.5	1–4	28.8 ± 5.8	15.8–50.0	5.4 ± 0.9	2.3–7.3
	Biphenotypic	4.6 ± 1.9	0–10	31.2 ± 9.2	0–55.6	7.4 ± 2.9	0–16.3
	In general	12.0 ± 3.0	3–19	–	–	21.4 ± 6.0	9.3–44.2
Ganglionic	ChAT	24.2 ± 6.5	11–49	52.4 ± 5.8	34.0–65.3	41.6 ± 6.3	25.6–53.7
	nNOS	5.0 ± 0.9	3–7	11.9 ± 2.4	7.7–20.8	8.8 ± 1.0	7.0–11.6
	Biphenotypic	16.0 ± 3.6	8–28	35.7 ± 4.8	25.3–52.8	28.1 ± 4.5	18.6–42.4
	In general	45.2 ± 8.8	24–75	–	–	78.6 ± 6.0	55.8–90.7

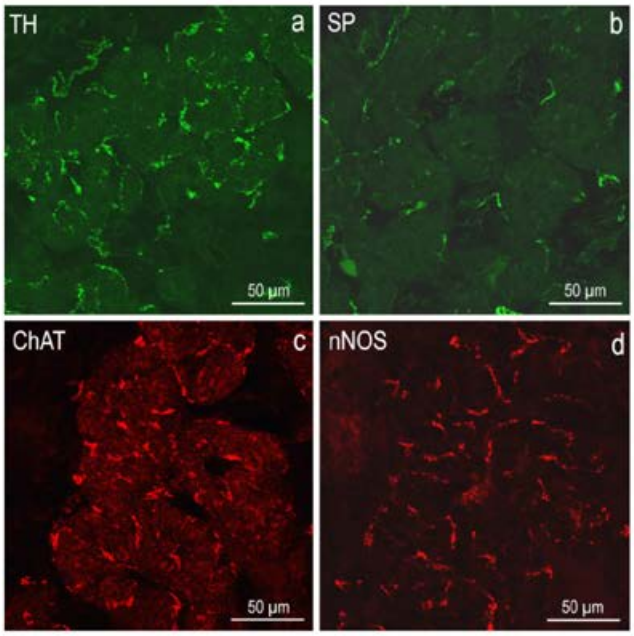

Fig. 4. Different density of NFs positive for TH (a), SP (b), ChAT (c), and nNOS (d) in transverse sections of the wall of the RRCV at the body portion of the SAN region.

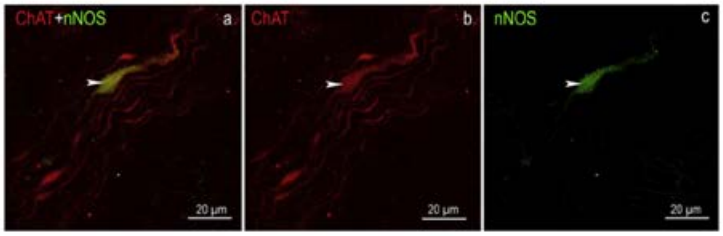

Fig. 5. Coexistence of neuronal proteins ChAT (in red) and nNOS (in green) in a varicosity (arrowhead) of the same NF identified beside the body portion of the SAN in the whole-mount preparation of the rabbit atria. The image in panel a is a merged image of two split images demonstrating the immunoreactivity for ChAT (panel b) and for nNOS (panel c). (For interpretation of the references to color in this figure legend, the reader is referred to the web version of the article.)

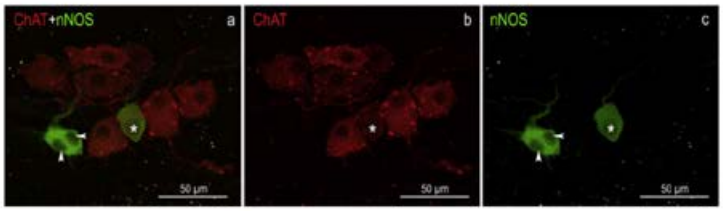

Fig. 6. Several neuronal somata positive for ChAT (in red), nNOS (in green), and simultaneously for both neuronal markers (biphenotypic neuronal soma is marked with asterisk) in the body part of the SA nodal region (image in the panels a are the merged one from the subsequent two images). Arrowheads points to purely nNOS positive neurons. (For interpretation of the references to color in this figure legend, the reader is referred to the web version of the article.)

Table 4
Size (in μm^2) and measurements (in μm) of long and short axis of neuronal somata revealed in the SAN area compared with ganglionic neuronal somata distributed on the base of left atrium.

Category and location	Chemical phenotype	n	Mean size	Long axis		Short axis	
				Mean	Range	Mean	Range
Solitary neuronal somata in SAN region	ChAT	22	15.8 ± 0.8‡	19.5 ± 0.8*,‡	13.8–28.8	12.0 ± 0.6‡	7.6–21.5
	nNOS	15	17.8 ± 1.4‡	22.4 ± 2.1‡	13.5–40.1	13.2 ± 0.9‡	8.1–20.4
	Biphenotypic	23	18.0 ± 1.0†,‡	23.0 ± 1.1*,†,‡	16.4–37.4	13.0 ± 0.6‡	9.8–21.9
	In general	60	17.2 ± 0.6*,‡	21.6 ± 0.8*,‡	13.5–40.1	12.7 ± 0.4‡	7.6–21.9
Ganglionic neuronal somata in SAN region	ChAT	121	14.9 ± 0.3‡	17.4 ± 0.4*,‡	8.5–31.7	12.4 ± 0.3‡	6.9–23.0
	nNOS	25	17.2 ± 0.7†,‡	20.2 ± 0.9†,‡	11.9–29.5	14.2 ± 0.8†,‡	7.5–24.7
	Biphenotypic	80	17.5 ± 0.5†,‡	21.0 ± 0.6*,†,‡	12.6–38.5	14.0 ± 0.4†,‡	6.5–25.9
	In general	226	16.2 ± 0.3*,‡	19.2 ± 0.3*,‡	8.5–38.5	13.3 ± 0.3‡	6.5–25.9
Ganglionic neuronal somata on the base of left atrium	ChAT	130	23.9 ± 0.4‡	28.4 ± 0.4‡	19.1–37.6	19.4 ± 0.4‡	9.6–30.5
	nNOS	136	21.3 ± 0.4‡	25.7 ± 0.5‡	13.3–41.2	16.8 ± 0.3‡	10.3–28.2
	Biphenotypic	128	24.3 ± 0.4‡	28.7 ± 0.5‡	20.5–44.9	20.0 ± 0.4‡	12.2–32.1
	In general	394	23.1 ± 0.2‡	27.6 ± 0.3‡	13.3–44.9	18.7 ± 0.2‡	9.6–32.1

* Statistically significant difference between ganglionic and solitary neuronal somata in the SAN area.
† Significant difference between neuronal somata positive for ChAT in comparison with nNOS positive and biphenotypic ones in distinct categories.
‡ Significant difference between neuronal somata from distinct categories and locations.

immunohistochemistry. The present findings prove that there is a much wider distribution of SAN cells positive for HCN4 on the RRCV and adjacent RA walls than has been previously considered (Atkinson et al., 2013; Liu et al., 2007; Tellez et al., 2006). The demonstrated area of distribution of HCN4-positive cells (Fig. 7) corresponds only in part with the localization of SAN cells identified earlier in the mouse, rat and rabbit (Atkinson et al., 2013; Dobrzynski et al., 2005; Yamamoto et al., 2006; Liu et al., 2007; Pauza et al., 2013, 2014a,b; Tellez et al., 2006). Interestingly, the region of the main mass of these cells overlaps the leading pacemaker sides identified in cardiac electrophysiological studies (Fedorov et al., 2006). Based on the study by Fedorov et al. (2006), it may be implied that the leading pacemaker side is the SAN body and, in some cases, the SAN head. The revealed "sleeves" of HCN4-positive cells at the edges of their massive dissemination may be reminiscent of the

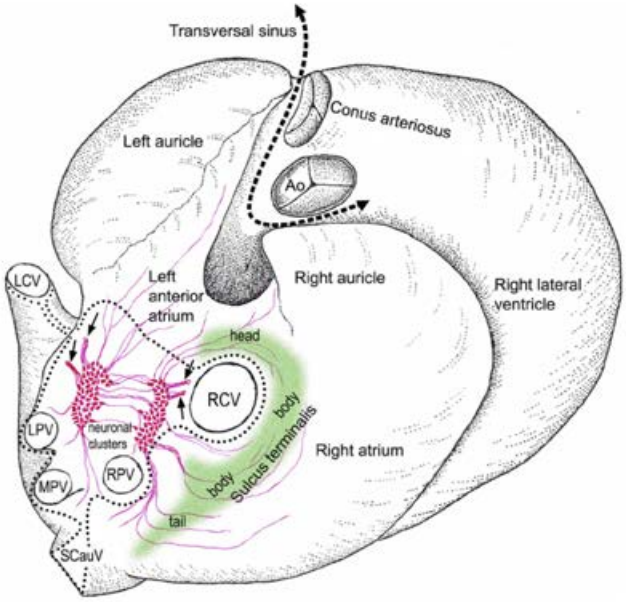

Fig. 7. Schematic drawing summarizing the present findings on the localization and distribution of the SAN (pacemaker) cells positive for HCN4 (green area), neuronal clusters (red triangles) and from them outspreading the main epicardial nerves (in red) that supply the SAN area in the rabbit heart. The dotted line demarcates the limits of the heart hilum. Arrows indicate extrinsic nerves accessing the rabbit heart on the medial side of the RRCV and at the bifurcation of the pulmonary trunk. Abbreviations: RCV – orifice of the right cranial vein; RPV, MPV, and LPV – orifices of the right, middle and left pulmonary veins; SCauV – sinus of the caudal vein; Ao – orifice of aorta. (For interpretation of the references to color in this figure legend, the reader is referred to the web version of the article.)

possible internodal pathways of the cardiac conductive system acknowledged earlier in a number of papers (Anderson and Ho, 1998; Ayettey et al., 1988; Benvenuti et al., 1997; James, 2001; Kafer, 1991; Racker, 1999; Sherf and James, 1979; Thompson, 1983). However, the examined whole mount preparations of the rabbit atria and the RRCV, as well as whole mount preparations of the rabbit interatrial septum (our unpublished observations), did not confirm the occurrence of an internodal pathway in the rabbit atria since the demonstrated cellular "sleeves" positive for HCN4 did not reach the typical region of the atrioventricular node in the rabbit interatrial septum. Our findings demonstrate that these cellular "sleeves" positive for HCN4 are simply the peripheral extensions of SAN cells that proceed outwardly along the RA wall. Noteworthy, analogous cellular "sleeves" positive for HCN4 were previously identified in the mouse heart (Pauza et al., 2013). Therefore, it may be summarized that the distribution of SAN cells in some mammalian hearts, including the rabbit, encompasses the lateral, anterior and posterior sides of the RRCV, extending behind the terminal groove on the lateral side of the RA, but does not reach the typical region of the atrioventricular node in the interatrial septum (Fig. 7). Certainly, these extensions of HCN4-positive pacemaker cells contribute to better propagation of electrical impulses between the SA nodal pacemaker cells and working cardiomyocytes in the rabbit RA.

Both the access and the pathways of nerves that supply the rabbit SAN region and the density of NFs in this region which were identified in the present study are similar to those that were ascertained previously in whole-mount atrial preparations of the rabbit and mouse (Pauza et al., 2014a,b; Richardson et al., 2003; Rysevaite et al., 2011; Roberts, 1991a,b; Roberts et al., 1989; Saburkina et al., 2014). Based on this fact, it may be concluded that innervation of the mammalian SAN region is extensively developed and extremely complex compared with other cardiac regions, including the atrioventricular nodal innervation.

Contrary to earlier investigations (Chow et al., 2001; Crick et al., 1999, 1996, 1994), the present observations identified evident predominance of adrenergic NFs between the rabbit SAN cells positive for HCN4. Most probably, this difference to earlier data may be explained by the use of the histochemical AChE method in former studies, in which all structures stained histochemically for AChE were claimed to be cholinergic (Anderson, 1972; Chow et al., 2001; Crick et al., 1994, 1996, 1999). As our previous studies demonstrate, many neural structures stainable by the AChE histochemical method were not cholinergic if they were simultaneously immunohistochemically labeled for ChAT (Saburkina et al., 2010; Pauza et al., 2014a,b).

The present observations continue earlier investigations begun by Roberts (Roberts, 1991a; Roberts et al., 1989) who demonstrated ganglionic cells in the typical region of the rabbit SA node. As was shown in this study, neuronal somata, distributed extensively in the rabbit SAN region almost over the whole RRCV, were positive both for nNOS and ChAT, and were even simultaneously positive for nNOS and ChAT. It is worth mentioning that purely nitrergic intrinsic cardiac neuronal somata were identified for the first time in the mammalian heart as it has previously been considered that cardiac nitrergic nerve cells are exclusively biphenotypic ones; i.e. they are simultaneously positive for ChAT as well (Mawe et al., 1996; Richardson et al., 2003; Yasuhara et al., 2007). Presumably, this novel finding of the present study is determined by the particular postnatal development of cardiac ganglia discovered in several mammalian species, in which intrinsic cardiac nerve cells may shift their chemical characteristics during the postnatal period (Horackova et al., 2000; Brack, 2014).

Based on morphometric data of this study, it may be considered that neuronal somata distributed on the rabbit RRCV and positive for distinct neuronal markers are different in their size similarly as intrinsic cardiac ganglionic cells in the mouse (Rysevaite et al., 2011). For instance, neuronal somata positive for TH are significantly larger compared with those that were positive for ChAT or were biphenotypic; i.e. were simultaneously positive for ChAT and TH (Rysevaite et al., 2011). Although the detected relationship of the neuronal somata size with its chemical phenotype needs further investigations in the hearts of other species; it is promising that the measurements of neuronal somata may support a reliable identification of functionally different nerve cells in transmission electron microscopy which is exceptionally important in the examination of synaptic connections within intrinsic cardiac ganglia, but which is methodologically challenging when it requires a combination with immunohistochemistry.

Lastly, it is worth noticing that the typical intrinsic cardiac biphenotypic neuronal somata in many mammalian species and human were exceptionally positive for ChAT and TH (Brack, 2014; Mawe et al., 1996; Weihe et al., 2005). In the rabbit SAN region, biphenotypic neuronal somata were determined as well. However, the biphenotypic nerve cells in the rabbit were simultaneously positive for ChAT and nNOS. The ChAT/nNOS coexistence in the same neuronal somata supports the concept that parasympathetic control of the SAN in some mammalian species is presumably implemented by both cholinergic and nitrergic inputs.

Conflicts of interest

All authors have reported that they have nothing to disclose.

Acknowledgements

Authors wish to express thanks to Ruta Godliauskaite, Jurgita Vismantaite and Nida Rutkauskiene for technical assistance throughout the study and to Paulius Alaburda for his editorial assistance. Funding for this study was partly allocated from Grant MIP-13037 provided by Research Council of Lithuania (RCL). H.I. was encouraged by Grant DOK-14568 from RCL.

Appendix A. Supplementary data

Supplementary data associated with this article can be found, in the online version, at http://dx.doi.org/10.1016/j.aanat.2016.03.007.

References

Anderson, R.H., 1972. The disposition, morphology and innervation of cardiac specialized tissue in the guinea-pig. J. Anat. 111, 453–468.
Anderson, R.H., Ho, S.Y., 1998. The architecture of the sinus node, the atrioventricular conduction axis, and the internodal atrial myocardium. J. Cardiovasc. Electrophysiol. 9, 1233–1248.
Arvidsson, U., Riedl, M., Elde, R., Meister, B., 1997. Vesicular acetylcholine transporter (VAChT) protein: a novel and unique marker for cholinergic neurons in the central and peripheral nervous systems. J. Comp. Neurol. 378, 454–467, doi:9034903.
Atkinson, A.J., Logantha, S.J.R.J., Hao, G., Yanni, J., Fedorenko, O., Sinha, A., Gilbert, S.H., Benson, A.P., Buckley, D.L., Anderson, R.H., Boyett, M.R., Dobrzynski, H., 2013. Functional, anatomical, and molecular investigation of the cardiac conduction system and arrhythmogenic atrioventricular ring tissue in the rat heart. J. Am. Heart Assoc. 2, 1–25, http://dx.doi.org/10.1161/JAHA.113.000246.
Ayettey, A.S., Navaratnam, V., Yates, R.D., 1988. Ultrastructure of the internodal myocardium in the rat. J. Anat. 158, 77–90.
Batulevicius, D., Pauziene, N., Pauza, D.H., 2003. Topographic morphology and age-related analysis of the neuronal number of the rat intracardiac nerve plexus. Ann. Anat. 185, 449–459, http://dx.doi.org/10.1016/S0940-9602(03)80105-X.
Batulevicius, D., Pauziene, N., Pauza, D.H., 2005. Architecture and age-related analysis of the neuronal number of the guinea pig intrinsic cardiac nerve plexus. Ann. Anat. 187, 225–243, http://dx.doi.org/10.1016/j.aanat.2005.01.004.
Benvenuti, L.A., Aiello, V.D., Higuchi, M.de L., Palomino, S.A., 1997. Immunohistochemical expression of atrial natriuretic peptide (ANP) in the conducting system and internodal atrial myocardium of human hearts. Acta Histochem. 99, 187–193.

Bharati, S., Levine, M., 1991. The conduction system of the swine heart. Chest, 207–212.
Brack, K.E., 2014. The heart s "little brain" controlling cardiac function in the rabbit. Exp. Physiol., 1–6, http://dx.doi.org/10.1113/expphysiol.2014.080168.
Chow, L.T., Chow, S.S., Anderson, R.H., Gosling, J.A., 2001. Autonomic innervation of the human cardiac conduction system: changes from infancy to senility – an immunohistochemical and histochemical analysis. Anat. Rec. 264, 169–182.
Christoffels, V.M., Moorman, A.F.M., 2009. Development of the cardiac conduction system: why are some regions of the heart more arrhythmogenic than others? Circ. Arrhythm. Electrophysiol. 2, 195–207, http://dx.doi.org/10.1161/CIRCEP.108.829341.
Crick, S.J., Sheppard, M.N., Anderson, R.H., Polak, J.M., Wharton, J., 1996. A quantitative assessment of innervation in the conduction system of the calf heart. Anat. Rec. 245, 685–698, http://dx.doi.org/10.1002/(SICI)1097-0185(199608)245:4<685::AID-AR8>3.0.CO;2-N.
Crick, S.J., Sheppard, M.N., Ho, S.Y., Anderson, R.H., 1999. Localisation and quantitation of autonomic innervation in the porcine heart I: conduction system. J. Anat. 195 (Pt 3), 341–357.
Crick, S.J., Wharton, J., Sheppard, M.N., Royston, D., Yacoub, M.H., Anderson, R.H., Polak, J.M., 1994. Innervation of the human cardiac conduction system. A quantitative immunohistochemical and histochemical study. Circulation 89, 1697–1708, http://dx.doi.org/10.1161/01.CIR.89.4.1697.
Dickie, R., Bachoo, R.M., Rupnick, M.A., Dallabrida, S.M., DeLoid, G.M., Lai, J., DePinho, R.A., Rogers, R.A., 2006. Three-dimensional visualization of microvessel architecture of whole-mount tissue by confocal microscopy. Microvasc. Res. 72, 20–26, http://dx.doi.org/10.1016/j.mvr.2006.05.003.
Dobrzynski, H., Li, J., Tellez, J., Greener, I.D., Nikolski, V.P., Wright, S.E., Parson, S.H., Jones, S.A., Lancaster, M.K., Yamamoto, M., Honjo, H., Takagishi, Y., Kodama, I., Efimov, I.R., Billeter, R., Boyett, M.R., 2005. Computer three-dimensional reconstruction of the sinoatrial node. Circulation 111, 846–854, http://dx.doi.org/10.1161/01.CIR.0000152100.04087.DB.
Fedorov, V.V., Hucker, W.J., Dobrzynski, H., Rosenshtraukh, L.V., Efimov, I.R., 2006. Postganglionic nerve stimulation induces temporal inhibition of excitability in rabbit sinoatrial node. Am. J. Physiol. Heart Circ. Physiol. 291, H612–H623, http://dx.doi.org/10.1152/ajpheart.00022.2006.
Hoover, D.B., Ganote, C.E., Ferguson, S.M., Blakely, R.D., Parsons, R.L., 2004. Localization of cholinergic innervation in guinea pig heart by immunohistochemistry for high-affinity choline transporters. Cardiovasc. Res. 62, 112–121, http://dx.doi.org/10.1016/j.cardiores.2004.01.012.
Horackova, M., Slavikova, J., Byczko, Z., 2000. Postnatal development of the rat intrinsic cardiac nervous system: a confocal laser scanning microscopy study in whole-mount atria. Tissue Cell 32, 377–388, http://dx.doi.org/10.1054/tice.2000.0126.
James, T.N., 2001. The internodal pathways of the human heart. Prog. Cardiovasc. Dis. 43, 495–535, http://dx.doi.org/10.1053/pcad.2001.24598.
Kafer, C.J., 1991. Internodal pathways in the human atria: a model study. Comput. Biomed. Res. 24, 549–563.
Koelle, G.B., 1955. The histochemical identification of acetylcholinesterase in cholinergic, adrenergic and sensory neurons. J. Pharmacol. Exp. Ther. 114, 167–184.
Liu, J., Dobrzynski, H., Yanni, J., Boyett, M.R., Lei, M., 2007. Organisation of the mouse sinoatrial node: structure and expression of HCN channels. Cardiovasc. Res. 73, 729–738, http://dx.doi.org/10.1016/j.cardiores.2006.11.016.
Mawe, G.M., Talmage, E.K., Lee, K.P., Parsons, R.L., 1996. Expression of choline acetyltransferase immunoreactivity in guinea pig cardiac ganglia. Cell Tissue Res. 285, 281–286, http://dx.doi.org/10.1007/s004410050645.
Nachmansohn, D., John, H.M., Berman, M., 1946. Studies on choline acetylase; the formation of acetylcholine in the nerve axon. J. Biol. Chem. 163, 475–480.
Pauza, D.H., Rysevaite, K., Inokaitis, H., Jokubauskas, M., Pauza, A.G., Brack, K.E., Pauziene, N., 2014a. Innervation of sinoatrial nodal cardiomyocytes in mouse. A combined approach using immunofluorescent and electron microscopy. J. Mol. Cell. Cardiol. 75C, 188–197, http://dx.doi.org/10.1016/j.yjmcc.2014.07.016.
Pauza, D.H., Rysevaite-Kyguoliene, K., Vismantaite, J., Brack, K.E., Inokaitis, H., Pauza, A.G., Rimasauskaite-Petraitienė, V., Pauzaite, J.I., Pauziene, N., 2014b. A combined acetylcholinesterase and immunohistochemical method for precise anatomical analysis of intrinsic cardiac neural structures. Ann. Anat. 196, 430–440, http://dx.doi.org/10.1016/j.aanat.2014.08.004.
Pauza, D.H., Saburkina, I., Rysevaite, K., Inokaitis, H., Jokubauskas, M., Jalife, J., Pauziene, N., 2013. Neuroanatomy of the murine cardiac conduction system: a combined stereomicroscopic and fluorescence immunohistochemical study. Auton. Neurosci. 176, 32–47, http://dx.doi.org/10.1016/j.autneu.2013.01.006.
Pauza, D.H., Skripka, V., Pauziene, N., Stropus, R., 1999. Anatomical study of the neural ganglionated plexus in the canine right atrium: implications for selective denervation and electrophysiology of the sinoatrial node in dog. Anat. Rec. 255, 271–294.
Pauza, D.H., Skripka, V., Pauziene, N., Stropus, R., 2000. Morphology, distribution, and variability of the epicardiac neural ganglionated subplexuses in the human heart. Anat. Rec. 259, 353–382.
Racker, D.K., 1999. The AV junction region of the heart: a comprehensive study correlating gross anatomy and direct three-dimensional analysis. Part I. Architecture and topography. Anat. Rec. 256, 49–63, http://dx.doi.org/10.1002/(SICI)1097-0185(19990901)256:1<49::AID-AR7>3.0.CO;2-L.
Richardson, R.J., Grkovic, I., Anderson, C.R., 2003. Immunohistochemical analysis of intracardiac ganglia of the rat heart. Cell Tissue Res. 314, 337–350, http://dx.doi.org/10.1007/s00441-003-0805-2.
Roberts, L.A., 1991a. The sinoatrial ring bundle: a cardiac neural communication system? Am. J. Anat. 191, 250–260, http://dx.doi.org/10.1002/aja.1001910305.
Roberts, L.A., 1991b. Morphological innervation pattern of the developing rabbit heart. Am. J. Anat. 190, 370–384, http://dx.doi.org/10.1002/aja.1001900405.
Roberts, L.A., Slocum, G.R., Riley, D.A., 1989. Morphological study of the innervation pattern of the rabbit sinoatrial node. Am. J. Anat. 185, 74–88, http://dx.doi.org/10.1002/aja.1001850108.
Rysevaite, K., Saburkina, I., Pauziene, N., Vaitkevicius, R., Noujaim, S.F., Jalife, J., Pauza, D.H., 2011. Immunohistochemical characterization of the intrinsic cardiac neural plexus in whole-mount mouse heart preparations. Heart Rhythm 8, 731–738, http://dx.doi.org/10.1016/j.hrthm.2011.01.013.
Saburkina, I., Gukauskiene, I., Rysevaite, K., Brack, K.E., Pauza, A.G., Pauziene, N., Pauza, D.H., 2014. Morphological pattern of intrinsic nerve plexus distributed on the rabbit heart and interatrial septum. J. Anat. 224, 583–593, http://dx.doi.org/10.1111/joa.12166.
Saburkina, I., Rysevaite, K., Pauziene, N., Mischke, K., Schauerte, P., Jalife, J., Pauza, D.H., 2010. Epicardial neural ganglionated plexus of ovine heart: anatomic basis for experimental cardiac electrophysiology and nerve protective cardiac surgery. Heart Rhythm 7, 942–950, http://dx.doi.org/10.1016/j.hrthm.2010.02.036.
Sherf, L., James, T.N., 1979. Fine structure of cells and their histologic organization within internodal pathways of the heart: clinical and electrocardiographic implications. Am. J. Cardiol. 44, 345–369.
Tellez, J.O., Dobrzynski, H., Greener, I.D., Graham, G.M., Laing, E., Honjo, H., Hubbard, S.J., Boyett, M.R., Billeter, R., 2006. Differential expression of ion channel transcripts in atrial muscle and sinoatrial node in rabbit. Circ. Res. 99, 1384–1393, http://dx.doi.org/10.1161/01.RES.0000251717.98379.69.
Thompson, D.R., 1983. Specialized internodal pathways. Int. J. Cardiol. 4, 393–396.
Verkerk, A.O., Geuzebroek, G.S.C., Veldkamp, M.W., Wilders, R., 2012. Effects of acetylcholine and noradrenalin on action potentials of isolated rabbit sinoatrial and atrial myocytes. Front. Physiol. 3 (May), 1–9, http://dx.doi.org/10.3389/fphys.2012.00174.
Weihe, E., Schütz, B., Hartschuh, W., Anlauf, M., Schäfer, M.K., Eiden, L.E., 2005. Coexpression of cholinergic and noradrenergic phenotypes in human and nonhuman autonomic nervous system. J. Comp. Neurol. 492, 370–379, http://dx.doi.org/10.1002/cne.20745.
Yamamoto, M., Dobrzynski, H., Tellez, J., Niwa, R., Billeter, R., Honjo, H., Kodama, I., Boyett, M.R., 2006. Extended atrial conduction system characterised by the expression of the HCN4 channel and connexin45. Cardiovasc. Res. 72, 271–281, http://dx.doi.org/10.1016/j.cardiores.2006.07.026.
Yasuhara, O., Matsuo, A., Bellier, J.-P., Aimi, Y., 2007. Demonstration of choline acetyltransferase of a peripheral type in the rat heart. J. Histochem. Cytochem. 55, 287–299, http://dx.doi.org/10.1369/jhc.6A7092.2006.

Journal of Molecular and Cellular Cardiology 75 (2014) 188–197

Contents lists available at ScienceDirect

Journal of Molecular and Cellular Cardiology

journal homepage: www.elsevier.com/locate/yjmcc

Original article

Innervation of sinoatrial nodal cardiomyocytes in mouse. A combined approach using immunofluorescent and electron microscopy☆

Dainius H. Pauza [a,*], Kristina Rysevaite [a], Hermanas Inokaitis [a], Marius Jokubauskas [a], Audrys G. Pauza [a], Kieran E. Brack [b], Neringa Pauziene [a]

[a] Institute of Anatomy, Faculty of Medicine, Lithuanian University of Health Sciences, Kaunas, Lithuania
[b] Department of Cardiovascular Sciences and NIHR Leicester Cardiovascular Biomedical Research Unit, University of Leicester, Leicester, UK

ARTICLE INFO

Article history:
Received 7 June 2014
Received in revised form 10 July 2014
Accepted 28 July 2014
Available online 4 August 2014

Keywords:
Sinoatrial node
Innervation choline acetyltransferase
Tyrosine hydroxylase
HCN4
Mouse
Electron microscopy

ABSTRACT

Fluorescent immunohistochemistry on the cardiac conduction system in whole mount mouse heart preparations demonstrates a particularly dense and complex network of nerve fibres and cardiomyocytes which are positive to the hyperpolarization activated cyclic nucleotide-gated potassium channel 4 (HCN4-positive cardiomyocytes) in the sinoatrial node region and adjacent areas around the root of right cranial vein. The present study was designed to investigate the morphologic and histochemical pattern of nerve fibres and HCN4-positive cardiomyocytes using fluorescent techniques and/or electron microscopy. Adrenergic and cholinergic nerve fibres together with HCN4-positive cardiomyocytes were identified using primary antibodies for tyrosine hydroxylase (TH), choline acetyltransferase (ChAT), and the HCN4 channel respectively. Amid HCN4-positive cardiomyocytes, fluorescence and electron microscopy data demonstrated a dense distribution of nerve fibres immunoreactive for ChAT and TH. In addition, novel electron microscopy data revealed that the mouse sinoatrial node contained exclusively unmyelinated nerve fibres, in which the majority of axons possess varicosities with clear mediatory vesicles that can be classified as cholinergic. Synapses occurred without any clear terminal connection with the effector cell, i.e. these synapes were of "en passant" type. In general, the morphologic pattern of innervation of mouse HCN4-positive cardiomyocytes identified using electron microscopy corresponds well to the dense network of nerve fibres demonstrated by fluorescent immunohistochemistry in mouse sinoatrial node and adjacent areas. The complex and extraordinarily dense innervation of HCN4-positive cardiomyocytes in mouse sinoatrial node underpins the importance of neural regulation for the cardiac conduction system. Based on the present observations, it is concluded that the occurrence of numerous nerve fibres nearby atrial cardiomyocytes serves as a novel reliable extracellular criterion for discrimination of SA nodal cardiomyocytes using electron microscopy.

1. Introduction

Previous studies have shown that atrioventricular conduction is preferentially sensitive to sympathetic activity, whereas sinoatrial (SA) automaticity is especially responsive to parasympathetic influence [1,2]. Despite this, the anatomical evidence suggests that cholinergic innervation is dense throughout the cardiac conduction system of many mammalian species, including human [3–9]. Contradictions between the physiological effects of autonomic stimulation and the neurochemical phenotype of nodal innervation were enhanced by our recent findings from whole mount mouse heart preparations [10,11]. In these studies, double labelling fluorescent immunohistochemistry demonstrated a dense, widespread and complex network of cholinergic and adrenergic nerve fibres in and around the SA and atrioventricular nodal areas. This was similar in neighbouring areas around the root of right cranial vein, below the orifice of the coronary sinus and along the atrioventricular ring. Whilst the morphology of HCN4-positive or SA nodal cardiomyocytes has been investigated previously [12–20], the reported network of nerve fibres was so unusual with respect to other cardiac regions, that these areas were considered worthy of further examination.

To do this, it is necessary to perform immunohistochemistry for HCN4-positive cardiomyocytes, cholinergic and adrenergic nerve fibres. However, fluorescent microscopy is spatially limited and does not allow for the structural relationships of distinct nerve fibres with cardiac myocytes to be visualized. Therefore, electron microscopy is necessary to facilitate discrimination of cells immunohistochemically labelled for distinct antigens and the correct identification of myocyte/neuronal morphology. Therefore, the present study was designed to examine the morphology and innervation of HCN4-positive or SA nodal cardiomyocytes using two distinct imaging methods—fluorescent immunohistochemistry

☆ Conflicts of interest: All authors have reported that they have nothing to disclose.

* Corresponding author at: Institute of Anatomy, Faculty of Medicine, Lithuanian University of Health Sciences, A. Mickevičiaus Street 9, Kaunas LT-44307, Lithuania. Tel.: +370 37 327313, +370 682 39366(Mobile); fax: +370 37 220733.
E-mail address: dainius.pauza@lsmuni.lt (D.H. Pauza).

http://dx.doi.org/10.1016/j.yjmcc.2014.07.016
0022-2828/

and transmission electron microscopy. The aims of this study are to determine (1) the distribution of HCN4-positive cardiomyocytes in relation to network of nerve fibres on the sinuses of right cranial and caudal veins, (2) the density of nerve fibres within the neural network of the SA nodal area, and (3) how autonomic nerve fibres are related to HCN4-positive cardiomyocytes in the mouse SA nodal area using electron microscope method.

2. Materials and methods

Thirty two 2–4 month-old C57BL/6J-linear mice of either sex were used for this study. Animals were deeply anesthetized with ether and euthanized by cervical dislocation in accordance with local and state guidelines for the care and use of laboratory animals (Permission No. 0206), which also conform to the European Union directive on the protection of animals for scientific research (2010/63/EU).

2.1. Whole mount fluorescent immunohistochemistry

Five mice were used for whole mount preparations to immunohistochemically identify intrinsic cardiac nerve fibres and HCN4-positive cardiomyocytes as previously described [10]. In brief, following euthanasia and a medial thoracotomy, a metal catheter was inserted transmyocardially into left ventricular cavity, where hearts were perfused in situ with phosphate buffered saline (PBS, 0.01 M) at room temperature via the coronary arteries by the aid of special gear that allowed perfusion using constant pressure (100–110 mm Hg). Once cardiac perfusion was confirmed and coronary blood was washed through, hearts were removed from the chest and placed into a dissecting dish containing cold 0.01 M PBS. The left and right atrial walls, appendages and interatrial septum were separated and pinned on a silicone pad in a dissecting dish, for fixation for 25 min at 4 °C in 4% paraformaldehyde (PFA) solution in 0.01 M phosphate buffer (PB, pH 7.4).

To decrease tissue autofluorescence, the flattened tissues were cleared using an ethanol with dimethylsulfoxide (20%, DMSO), hydrogen peroxide in ethanol (6%, H_2O_2) and dehydrated through a graded ethanol series as reported by Dickie et al. [21]. The whole-mount preparations were then rehydrated with 10-minute successive washes through a graded ethanol series, washed, and permeabilized in 3 × 10-minute changes of 0.01 M PBS containing 0.5% Triton X-100 (Carl Roth, Karlsruhe, Germany). Nonspecific binding was blocked for 2 h in PBS containing 5% normal donkey serum (Jackson ImmunoResearch Laboratories, West Grove, PA, USA) and 0.5% Triton X-100. Preparations were subsequently washed (3 × 10 min) in 0.01 M PBS and incubated in a mixture of two primary polyclonal antibodies to identify sympathetic and cholinergic nerve fibres and SA nodal cardiomyocytes for 24–48 h in a dark humid chamber at 4 °C (Table 1). After three 10 min-washes in 0.01 M PBS, the whole-mount preparations were incubated in an appropriate combination of secondary antibodies for 4 h in a dark humid chamber on a shaker stage at room temperature (Table 1). All antibodies were diluted in 0.01 M PBS. Finally, the specimens were washed in 0.01 M PBS, incubated for 2 h in a DMSO and PBS mixture, 1:4 (*v*:*v*) ratio, and mounted in Vectashield Mounting Medium (Vector Laboratories, California, USA). A cover slip was placed on the tissue and then sealed with clear nail polish. Positive and negative controls [omission of primary and or secondary antibodies] were used.

Table 1
Primary and secondary antisera used in the study.

Antigen	Host	Dilution	Supplier	Catalogue number
Primary				
ChAT	Goat	1:100	Chemicon[a]	AB144P
TH	Rabbit	1:500	Chemicon[a]	AB152
TH	Sheep	1:800	Chemicon[a]	AB1542
PGP 9.5	Rabbit	1:500	AbD Serotec[b]	7869-0504
HCN4	Rabbit	1:100	Chemicon[a]	AB5808
Secondary				
Goat^{Cy3}	Donkey	1:300	Chemicon[a]	AP180C
Rabbit^{Cy3}	Donkey	1:300	Chemicon[a]	AP182C
Rabbit^{FITC}	Donkey	1:100	Chemicon[a]	AP182F
Sheep^{FITC}	Donkey	1:100	Chemicon[a]	AP184F
Rabbit^{Biotin}	Donkey	1:100	Chemicon[a]	AP182B

[a] Chemicon International, Temecula, California, USA.
[b] AbD Serotec, Kidlington, UK.

The stained preparations were analysed utilizing an AxioImager Z1 fluorescence microscope equipped with filters to observe the isothiocyanate (FITC) and cyanine (Cy3) tagged secondary antibodies along with an Apotome2 and digital monochrome camera AxioCam MRm using AxioVision software (version 4.8.1., Zeiss, Gottingen, Germany). When necessary, the same whole-mount preparations were additionally analysed and photographed employing a laser-scanning microscope (LSM 700 with ZEN 2010 software, Zeiss, Jena, Germany).

2.2. Heart sections fluorescent immunohistochemistry

In order to verify the presence of SA nodal cardiomyocytes in remote sites from typical regions, two hearts were fixed for 4 days at 4 °C in 4% PFA in 0.01 M PB (pH 7.4). Hearts were embedded in paraffin and sectioned into 4–5 μm thick slices employing a rotatory microtome (HS 355S, Microm, Walldorf, Germany) and applied onto Superfrost Ultra Plus microscope slides (Thermo Scientific, Braunschweig, Germany) and dried for up to 12 h at 50 °C. Sections were rehydrated and subjected to antigen retrieval in Tris–EDTA buffer (pH 9) at 90 °C for 20–40 min in a microwave oven (HistosPro, Milestone, Sorisole, Italy). Double labelling immunohistochemistry for HCN4 along with sympathetic and cholinergic neuronal markers was followed according to protocol described above and cover-slipped for analysis. A standard Masson's trichrome staining procedure was used to differentiate connective tissue, working myocardium and conduction system. In addition, a Periodic acid–Schiff reaction was used to detect higher level of glycogen in SA nodal cardiomyocytes.

2.3. Transmission electron microscopy (TEM)

For TEM examination, 13 mice of either sex were used. Animals were prepared according to the procedures used for whole mount tissue preparation described above. However, when the hearts were washed out from the blood, perfusion was switched to a solution containing 2% PFA and 0.25% glutaraldehyde in 0.1 M PB (pH 7.4). After fixation, hearts were excised from the chest and tissue samples of 1–2 × 2–3 mm from three defined sites (Fig. 1), were extirpated using a dissecting microscope, fine scissors and tweezers in a Petri dish containing 0.1 M PBS. Tissue samples were postfixed in the original fixative solution for at least 4 h at room temperature or overnight at 4 °C. Subsequently, tissue samples were treated with the electron microscopy fixative osmium tetroxide (1%) in 0.1 M PB (pH 7.4) for 2 h, dehydrated through a graded ethanol series and embedded in a mixture of resins Epon 812 and Araldite (Sigma-Aldrich, Steinheim, Germany) using an automated tissue processor (Lynx II, EMS, Hatfield, PA, USA). Before the final resin polymerization at 60 °C, tissue samples were carefully orientated for their transverse sectioning in flat embedding moulds under a stereoscopic microscope (Stemi 2000CS, Zeiss, Gottingen, Germany).

2.4. Electron microscopy immunohistochemistry

For EM immunohistochemistry, hearts of 12 mice were prepared, perfused and fixed as described above avoiding glutaraldehyde in the fixative, due to its strong inhibitory effect on tissue immunogenicity. Tissue samples were harvested from the same cardiac sites as for routine TEM (Fig. 1). The immunohistochemical reactions were performed on tissue samples in accordance with protocol suggested by Goehler

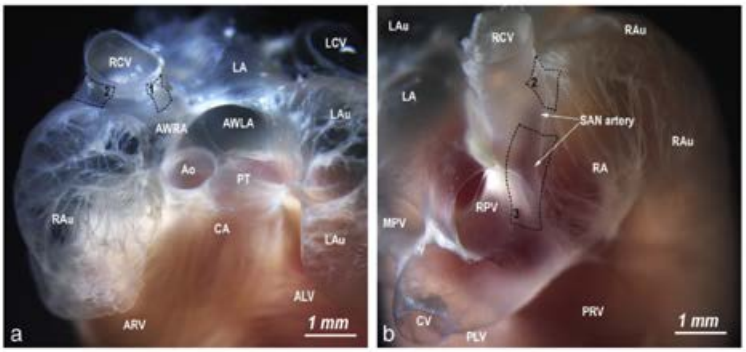

Fig. 1. Macrophotographs of the ventral (a) and right dorsolateral (b) views of the pressure-inflated by 20% gelatin mouse heart to illustrate the three main locations of the tissue pieces sampled for the electron microscopic study described in this manuscript: 1, the anteromedial side of the root of the right cranial vein (RCV); 2, the lateral side of the root of the RCV, including the right atrial wall along the terminal groove; 3, the posterolateral side of the root of the RCV, including the dorsal part of the root of the caudal vein (CV). Other abbreviations: Ao—ascending aorta; ALV—anterior left ventricle; ARV—anterior right ventricle; AWRA—anterior wall of the right atrium; AWLA—anterior wall of the left atrium; LAu—left auricle; LCV—left cranial vein; LPV—left pulmonary vein; LA—left atrium, LV—left ventricle; MPV—middle pulmonary vein; PT—pulmonary trunk; PLV—posterior left ventricle; PRV—posterior right ventricle; RA—right atrium, RAu—right auricle; RPV—right pulmonary vein; RV—right ventricle; SAN—sinoatrial node.

et al. [22]. In brief, tissue samples were incubated with 1% H_2O_2 in methanol for 10 min. After blocking of unspecific protein binding sites for 2 h in PBS containing 5% normal donkey serum (Jackson ImmunoResearch Laboratories, West Grove, PA, USA) and 0.5% Triton X-100, samples were incubated with the primary polyclonal antibodies for either sympathetic, cholinergic nerve fibres or SA nodal cardiomyocytes (see Table 1) for at least 18 h. Samples were washed in 0.1 M PB before incubation with the secondary antibody (see Table 1) for at least 4 h. After additional washes, visualization of the immunoreaction was performed by the 3,3′-diaminobenzidine (DAB) reaction enhanced by 1.5% nickel ammonium sulphate. Following visualization, tissue samples were washed 3 × 10 min in 0.1 M PB, dehydrated, embedded into a mixture of Epon 812 and Araldite resins, and orientated as described above.

From the resin embedded tissue blocks, semi-thin sections were cut (1 μm) and stained with methylene blue according to Rigdway (1986). Ultra-thin sections (50- to 70-nm thick) were cut with a Leica ultramicrotome (model UC7, Leica Mikrosysteme Handelsges m.b.H., Viena, Austria), mounted on 600 mesh thin-bar support nickel grids (Agar scientific, Essex, UK). Tissue sections were stained with uranyl acetate and lead citrate with an automated TEM stainer (model QG-3000SC, RMC, Tucson, Arizona, USA). Finally, ultrathin sections were investigated with a Tecnai BioTwin Spirit G2 transmission electron microscope (FEI, Eindhoven, The Netherlands) at 80–120 kV. Electron microscope images were taken with a bottom mounted 16 Mega pixel TEM CCD camera using TIA software (Eagle 4k, FEI, Eindhoven, the Netherlands).

2.5. Quantification of nerve fibres

To assess the density of nerve fibres, stacks of confocal microscope images were oriented so that nerve fibres could be visualized as sectioned transversally. Using ZEN 2010 software (Zeiss, Germany), the dimensions of each image stack were converted, i.e. z dimensions were converted to y or to x dimensions according to orientation of nerve fibres in areas of interest. Following this conversion, we reduced the number of images in each z-stack, averaging every fifth or tenth image compiling the overall z-stack of 200 images. Background of images was removed and images were binarized adjusting threshold value level from 45 to 65. Finally, the number of nerve fibres was automatically calculated in every image from the whole stack using the FIJI feature from the software module "Analyse particles". To determine the density of nerve fibres in electron microscopy images, every nerve fibre or singular axon was assessed and counted in areas of 1600 square microns, i.e. in one window area of a nickel grid.

2.6. Statistical analysis

Data are expressed as mean ± standard error of the mean (SEM). Statistical analysis for nerve fibre density and the number of nerve fibres related anatomically to CCMs within distinct regions of sinoatrial nodal area were performed using two-sample independent *t*-test by the aid of IBM SPSS software (package 20, IBM). Differences were considered significant when $P < 0.05$.

3. Results

An illustration of HCN4-positive cardiomyocytes and nerve fibres immunoreactive for ChAT is shown in Fig. 2. As shown, HCN4- and ChAT-immunoreactive cells around the mouse SA nodal region were readily identifiable. More importantly, HCN4-immunoreactive SA nodal cardiomyocytes were widely distributed around the root of right cranial vein and formed a well-defined horseshoe-shaped boundary by the side of terminal groove and along the course of SA nodal artery (Fig. 2). Slender and narrow HCN4-immunoreactive myocytes extended from the main mass of the sinoatrial node (SAN) towards the right auricle, the root of right pulmonary vein, and the root of caudal vein (Fig. 2).

An illustration of HCN4-positive cardiomyocytes and nerve fibres at the electron microscope level is shown in Figs. 3 (HCN4) and 4 (ChAT) respectively. Using TEM, HCN4-immunoreactive cardiomyocytes were determined in all sites investigated (Figs. 1 and 2). Electron dense immunoreaction precipitate was well defined on the cell membrane of HCN4-positive cardiomyocytes, thus allowing these cells to be readily discriminated from regular atrial cardiomyocytes (RCMs, Fig. 3), which lacked electron dense immunoreaction precipitate around the cell membrane. In general, qualitative observations demonstrated that the majority of the labelled HCN4-positive cardiomyocytes contained sparse myofibrils and had scanty sarcoplasmic reticulum, and their profiles were smaller in size compared to regular atrial cardiomyocytes (Fig. 3). Whilst the transverse profile of HCN4-positive cardiomyocytes did vary in size and shape, the morphological pattern of the myofibrils in some cardiomyocytes labelled for HCN4 was similar to myofibrils in RCMs. Despite this, in general terms at the electron microscope level,

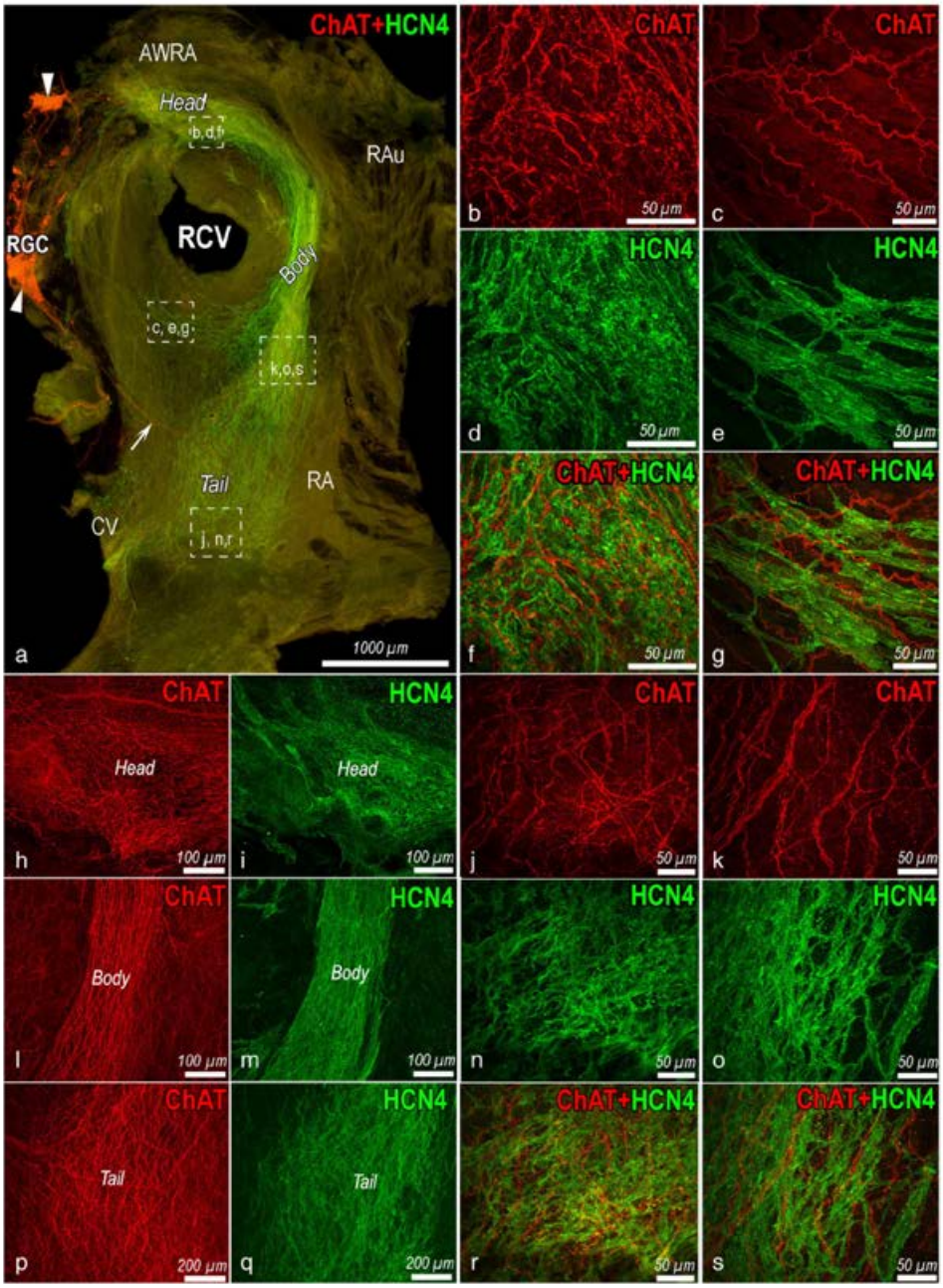
ChAT+HCN4
AWRA
Head
b,d,f
RAu
RCV
RGC
Body
c, e,g
k,o,s
Tail
RA
CV
j, n,r
1000 μm
a
ChAT
50 μm
b
ChAT
50 μm
c
HCN4
50 μm
d
HCN4
50 μm
e
ChAT+HCN4
50 μm
f
ChAT+HCN4
50 μm
g
ChAT
Head
100 μm
h
HCN4
Head
100 μm
i
ChAT
50 μm
j
ChAT
50 μm
k
ChAT
Body
100 μm
l
HCN4
Body
100 μm
m
HCN4
50 μm
n
HCN4
50 μm
o
ChAT
Tail
200 μm
p
HCN4
Tail
200 μm
q
ChAT+HCN4
50 μm
r
ChAT+HCN4
50 μm
s

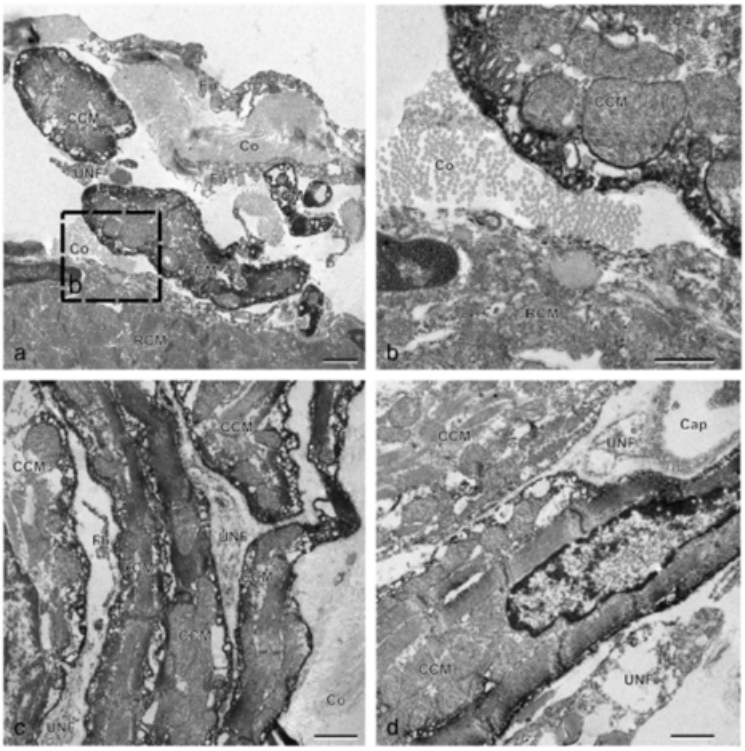

Fig. 3. Electron micrographs demonstrating the SA nodal cardiomyocytes (CCM) labelled with antibody for HCN4 in the mouse SA nodal area. a: Groups of sparse SA nodal cardiomyocytes (CCM), prominent due to electron dense precipitates of the immunoreaction, are located nearby the regular atrial cardiomyocyte (RCM). The labelled cells (CCM) demonstrate the typical features of the SA nodal cardiomyocytes: cells are loosely spread out, they profiles are evidently smaller compared with the regular cardiomyocytes (RCM) and their dense myofibrils oriented in different directions; b: Higher magnification of the boxed area in panel a shows the presence of electron dense precipitates on cardiomyocytes immunoreactive for HCN4 and the unlabelled regular cardiac myocytes (RCM); c: Longitudinal section of cardiomyocytes immunoreactive for HCN4 (CCM) and possessing the typical features of SA nodal cardiomyocytes. Note the numerous unmyelinated nerve fibres (UNF) accompanied the HCN4 immunoreactive nodal cardiomyocytes; d: Two SA nodal cardiomyocytes (CCM) labelled unmistakably for HCN4 possess characteristics of regular cardiomyocytes (RCM)—the regularly oriented dense myofibrils and the plentiful mitochondria interspersed between them. Note the density of UNFs that contain unsheathed axons with synaptic vesicles. Abbreviations: En—endocardial cells, Co—collagen fibres, Fb—fibroblast, Cap—capillary. Scale bar—1 μm for panels a, c, and d, whilst 500 nm for panel b.

HCN4-positive cardiomyocytes could be discriminated from RCMs even in control tissue samples (Figs. 3, 4). In contrast to the electron microscope images, mouse cardiomyocytes immunoreactive for HCN4 using bright field light microscopy were indiscernible from regular atrial cardiomyocytes, as illustrated in the transverse section of the SAN in Fig. 5.

Immunofluorescent microscopy revealed a different pattern of distribution of HCN4-positive cardiomyocytes within the wall of the root of right cranial vein. On the whole mount preparations; the distribution of HCN4-positive cardiomyocytes was fairly superficial and extended 20–30 μm up the wall of RRCV. Both the electron and fluorescent microscope observations of transverse sections through the wall of the root of right cranial vein demonstrated a deeper distribution of HCN4-positive cardiomyocytes as these cells were often identified transmurally (Figs. 2, 5).

Using fluorescence microscopy, all sites in which the HCN4-positive cardiomyocytes were immunoreactive for HCN4, there was a comprehensive and fine meshwork of nerve fibres. As illustrated in the whole mount preparation stained for ChAT and TH (Fig. 6), this network was rich in both cholinergic and adrenergic nerve fibres that possessed axons with a high amount of varicosities (Figs. 2, 6). In the SAN region, ChAT-immunoreactive and TH-immunoreactive nerve fibres were

Fig. 2. Whole-mount fluorescent immunohistochemistry of the mouse right atrium to demonstrate the distribution SA nodal myocytes immunoreactive for HCN4 and cholinergic neural structures (intrinsic nerves, ganglia, and nerve fibres). Atrial appendages, left atrium, interatrial septum and roots of pulmonary veins were dissected in order to flatten the right atrial wall. Myocytes immunoreactive for HCN4 are labelled in green, cholinergic (ChAT) neural structures - in red, the combined immunoreactivity image (ChAT + HCN4) is shown in panels a, f, g, r, and s. Arrowheads indicate the right-sided ganglionic cluster (RGC), from which epicardial nerves (arrow shows one of them) extend towards the SA nodal region. The boxed areas (b though to s) in the left upper panel (a) are enlarged as the corresponding inserted figure panels and do exhibit distribution of cardiac cells immunoreactive for HCN4 with cholinergic nerve meshwork at the roots of right cranial (RCV) and caudal (CV) veins. Other abbreviations: AWRA—anterior wall of right atrium; RCV—orifice of right cranial vein; CV—root of caudal vein; RA—right atrium; RAu—right auricle. (For interpretation of the references to colour in this figure legend, the reader is referred to the web version of this article.)

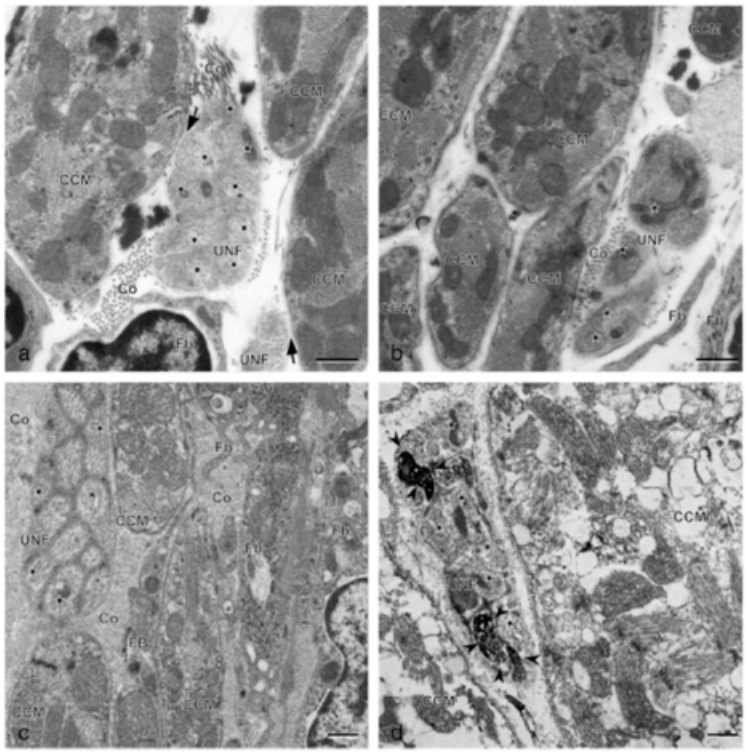

Fig. 4. Electron micrographs demonstrating the profiles of the unmyelinated nerve fibres (UNF) adjacent to the mouse SA nodal cells (CCM) that have typical morphologic pattern of nodal cardiomyocytes, i.e. the sparse, irregularly arranged myofibrils, numerous glycogen granules and mitochondria. a: The UNFs accompanying the SA nodal cardiomyocytes (CCM). Note the numerous axonal varicosities with abundant round, small, clear vesicles (asterisks). All axons are incompletely enveloped by Schwann cell and a fragment of their plasma membrane is in direct contact with the basal lamina surrounding the whole UNF. Some varicosities are located in close contact with SA nodal cardiomyocytes (CCM) and their basal laminas (arrowheads) are coalesced; b: Electron micrographs of low magnification to illustrate the immunoreactive for ChAT nerve fibres UNFs between SA nodal cardiomyocytes (CCM). The boxed area is enlarged as panel c; c: High magnification of the boxed area in panel b shows the presence of electron dense precipitates on three axons immunoreactive for ChAT (arrowheads) and negative (asterisks) within UNF adjacent to SA nodal cardiomyocytes (CCM). Note the differently sized axonal varicosities (asterisks) that are negative for ChAT; d: Unmyelinated nerve fibre (UNF) with varicosities containing small clear vesicles (asterisks) and two axons immunoreactive for TH (arrowheads). Other abbreviations: Fb—fibroblasts, Co—collagen fibres. Scale bars—1 μm.

equally abundant (Fig. 6). Compared with atrial areas adjacent to the root of right cranial vein, the density of nerve fibres amid the HCN4-immunoreactive cells was 3–4 fold higher (Fig. 6; Table 2).

The EM data conclusively demonstrates that all of the nerve fibres identified were composed exclusively of unmyelinated nerve fibres and involved axons with both cholinergic and adrenergic neurotransmitters. This is best illustrated in the fluorescent images (Fig. 6) with supporting evidence in the EM figures (Fig. 4d, black arrowheads). The axons within unmyelinated nerve fibres had varicosities with abundant round, small, clear, and a few dense-cored vesicles (Fig. 4). A number of unmyelinated nerve fibres had axons that were incompletely enveloped by Schwann cells with a fragment of their plasma membrane in direct contact with the basal lamina surrounding the whole unmyelinated nerve fibre (Fig. 4). These unmyelinated nerve fibres had varicosities and were distributed regularly in the vicinity of HCN4-positive cardiomyocytes of the SA nodal region (Figs. 3, 4, 7).

As shown in Table 2, the density of unmyelinated nerve fibres within the distinct zones of the root of right cranial vein with HCN4-positive cardiomyocytes was similar. However, they were significantly higher in respect to neighbouring atrial zones with data corresponding well using both fluorescent and electron microscopy.

Unmyelinated nerve fibres with numerous axonal varicosities were predominantly close to HCN4-positive cardiomyocytes (Figs. 4, 7). The closest unmyelinated nerve fibres were located 0.06 μm from HCN4-positive cardiomyocytes, but occasionally some were 2 μm or more away from HCN4-positive cardiomyocytes. In the mouse SAN, the average distance between HCN4-positive cardiomyocytes and unmyelinated nerve fibres was less than 0.5 μm (Fig. 7). The axons adjacent to HCN4-positive cardiomyocytes HCN4-positive cardiomyocytes of the sinoatrial node region were immunoreactive for all of the neuronal markers examined in this study (Fig. 4). To note, HCN4-positive cardiomyocytes from the SA nodal areas were closely associated by at least one unmyelinated nerve fibre or axon, but the majority of these cells were in close proximity to 2–3 unmyelinated nerve fibres (Fig. 7).

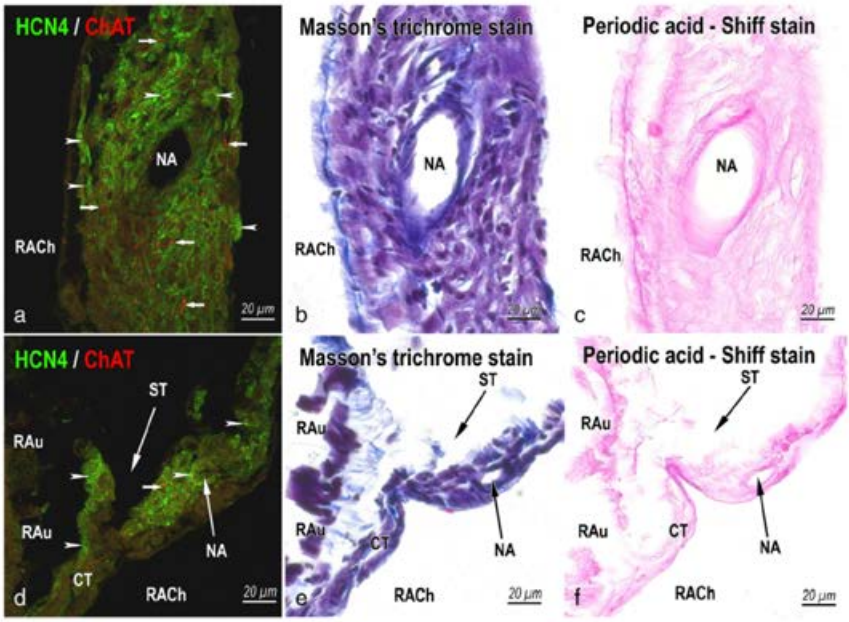

Fig. 5. Transverse sections of the mouse SA nodal area at the anteromedial side of the root of the RCV (a) and at the lateral side of the root of the RCV (d) to demonstrate the transmural distribution of SA nodal cardiomyocytes immunoreactive for HCN4 (in green) and the high density of nerve fibres immunoreactive for ChAT-IR (in red). Panels b and c as well as panels e and f display the subsequent transverse sections of the root of the mouse RCV at the same locations correspondingly as the sections shown in panels a and d, but these subsequent sections were dyed by Masson's trichrome stain (b, e) and histochemically of periodic acid–Shiff reaction (c, f). Notice that Masson's trichrome and periodic acid-Shiff staining does reveal unspecifically the SA nodal cardiomyocytes immunoreactive for HCN4 (arrowheads indicate some these cells). Other abbreviations: NA—SA nodal artery; RACh—right atrial chamber; RAu—right auricle; CT—terminal crest, ST—terminal groove. (For interpretation of the references to colour in this figure legend, the reader is referred to the web version of this article.)

4. Discussion

This study compared neuroanatomical observations from the mouse cardiac conduction system acquired by two distinct imaging methods. To the best of our knowledge, this is the first study to do this and compare immunofluorescent and electron microscope observations in this species. More importantly, novel quantitative data comparing results from fluorescent and electron microscope images demonstrates a dense multi-layered network of nerve fibres in close proximity to HCN4-positive cardiomyocytes in the mouse SA nodal area and adjacent areas around the root of right cranial vein. At the immunofluorescent microscopy level, it was demonstrated that this dense neural network possesses nerve fibres IR for both ChAT and TH. Electron microscope examination has confirmed that the dense neural network undeniably interlaces with HCN4-positive cardiomyocytes and that this network involves only unmyelinated nerve fibres. Applying electron microscopy method, we were successful to show a transmural distribution of HCN4-positive cardiomyocytes. To note, the ultrastructure of many HCN4-positive cardiomyocytes may be distinct from typical SA nodal or pacemaker cells as revealed by immunoelectron histochemistry.

Our data demonstrates that a large amount of axons within unmyelinated nerve fibres are incompletely enveloped by Schwann cells and a certain portion of their plasma membrane is in direct contact with the basal lamina surrounding the whole profile of the unmyelinated nerve fibre. Since these axonal gaps have almost an unimpeded contact with interstitial space between HCN4-positive cardiomyocytes and regular cardiac myocytes (RCMs), it is conceivable that these fibres are involved in autonomic control of cardiac function as alluded to by previous studies [23–25]. More importantly, there is robust evidence that unmyelinated nerve fibres mediate the effects resulting from direct stimulation of efferent cervical vagus nerves controlling heart rate [26], atrioventricular conduction and left ventricular performance [27]. Axons within unmyelinated nerve fibres and free axonal terminals had abundant varicosities with numerous round, small, clear, and a few dense-core vesicles and only one type of synapse that appears to occur "in passing" i.e. "En passant" and without terminal connections, was identified between HCN4-positive cardiomyocytes and axons in the tissue samples studied. In contrast to published observations and common belief, close neuromuscular contacts that are characteristic for cardiac myocytes from the right atrium, ventricles, interatrial and interventricular septum in mouse [13,14], guinea pig [28] and sheep [18] were not determined in the present study.

The discrimination and demonstration of HCN4-positive cardiomyocytes in whole heart preparation became possible following immunohistochemical approach developed by us [10]. The findings of the present study demonstrate that cardiomyocytes immunoreactive for HCN4 were scattered widely beyond the typical SAN area to the roots of right cranial and caudal veins. To note, cardiomyocytes immunoreactive for HCN4 had a distinct ultrastructure that allows the reliable identification of these cells at the electron microscope level, even without any immunohistochemical labelling. Based on these identifiable ultrastructural particularities, these cells may be readily recognizable in

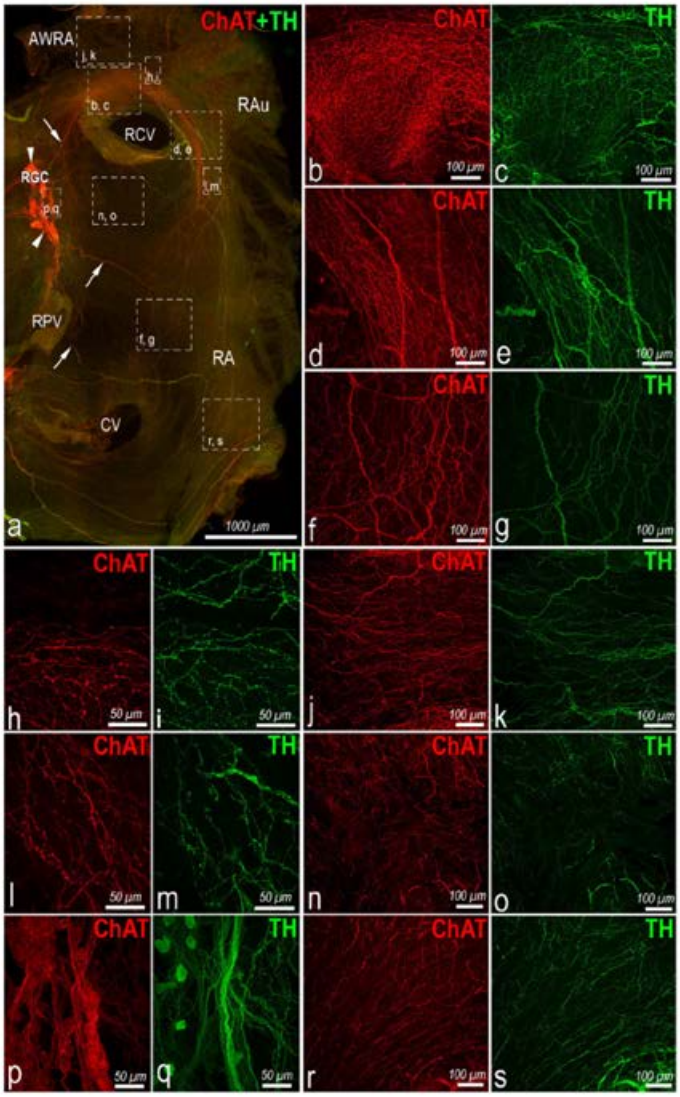

Fig. 6. Whole-mount preparation of the mouse right atrium shows the morphologic pattern of cholinergic (ChAT, in red) and adrenergic (TH, in green) neural meshwork on the root of right cranial vein and right atrial wall. Atrial appendages, interatrial septum, and ventricles were extirpated in order to flatten the atria. Arrows point to epicardial nerves that extend towards the SA nodal area, arrowheads—the right-sided ganglionic cluster (RGC). The boxed areas (b–s) in the left upper panel (a) are enlarged as corresponding figure panels. Note the equal density of meshwork of nerve fibres immunoreactive for ChAT and TH in the diverse areas of the root of cranial vein, including the typical area of SA node (panels b–g, h, i, l, and m), in comparison with the looser network of nerve fibres in the right atrial wall. Of importance, it is equally positive for both neuronal markers TH and ChAT. Panels p and q illustrate a few nerve cells immunoreactive for TH (q) and ChAT (p) from the RGC. Abbreviations: RCV—orifice of right cranial vein; CV—sinus region of the caudal vein; RPV—root of right pulmonary vein; RAu—right auricle; RA—right atrium. (For interpretation of the references to colour in this figure legend, the reader is referred to the web version of this article.)

Table 2
Densities of nerve fibres (NFs) immunoreactive for both ChAT and TH in equal areas (1000 μm^2) of distinct sites of the root of right cranial vein (RRCV) and right atrial regions adjacent to RRCV estimated on electron (TEM) and laser scanning (LSM) microscope images. N represents the number of NFs assessed in tissue samples obtained from the cardiac sites that are shown as the boxed areas in Figs 1, 2a, and 6a.

Site of samples	TEM	*N*	LSM	*N*	*P* value (TEM vs LSM)
Anteromedial side of the RRCV (site 1, Head of SA nodal region)	5.4 ± 0.4	154	4.4 ± 0.14	40,279	0.113
Lateral side of the RRCV (site 2, body of SA nodal region)	3.2 ± 0.4	76	3.9 ± 0.05	34,010	0.067
Dorsolateral side of the RRCV (site 3, tail of SA nodal region)	3.2 ± 0.4	23	3.15 ± 0.08	35,012	0.979
In general (sites 1–3)	4.3 ± 0.3*	253	4.0 ± 0.04*	118,426	0.773
Right atrial regions adjacent to RRCV (in general)	0.9 ± 0.4*	224	1.0 ± 0.02*	11,861	0.095

* The mean densities of NFs in the examined sites of the root of right cranial vein compared to the right atrial ones were significantly different at $p < .05$.

the areas in which HCN4-positive cardiomyocytes were located deep between other cardiac myocytes or amid dense, impenetrable areas for antisera penetration, i.e. in which cardiac myocytes with a typical ultrastructure of SA nodal cardiomyocytes were weakly or even not positive for HCN4. This is particularly important, since our data are not in accord with previous studies [29–31]. One report, demonstrated that the SAN was a highly compact group of cells that forms a comma-shaped transmural structure, which Liu et al. [30] used an ANP-negative/Cx43-negative/HCN4-positive immunolabelled criteria to define the SA node, described as being unique to mouse. At other levels of their sliced preparations, SAN cells do become loosely packed and begun to 'diffuse' with other cells types, which is in accord to the data in the current study. At all times however, the SAN region was reported to be surrounded by connective tissues, which were not labelled in the current study. One limitation of the aforementioned study is that the histological study did not utilize whole atria preparations, but concentrated on transmural analysis. In the current study, we performed a macro immunological investigation using whole atria tissues. Therefore some of the discrepancies in the data could reside in preparation differences. Cryostat sectioned tissue stained for HCN4 and connexin 45 demonstrated that the situation in rats may be more akin to the current study, i.e. there was a more diffuse area populated with SAN cells, which included the surrounding area of the superior vena cava (which corresponded to the right caudal vein in the mouse) [29] and up to the right superior pulmonary vein. These data do accord with the current study that also demonstrated pacemaker cells to be situation in the interatrial groove. However, due to the fact that Yamomoto et al. [29] also used cardiac sections, the true extent of how far HCN4-positive cardiomyocytes are present in atrial tissue was probably underestimated.

4.1. Ultrastructure

The ultrastructure of HCN4-positive cardiomyocytes from the typical sinoatrial nodal region has been previously examined, in which cardiac tissue was sectioned transversely. In these studies, HCN4-positive cardiomyocytes are usually described as small, round cells with electron-lucid cytoplasm containing few myofibrils, poor sarcoplasmic reticulum, and few mitochondria. According to classical report by James et al. [32], the central part of the SAN is composed of typical nodal or P cells, the transverse profiles of which are oval or round in shape and much smaller than regular myocardial cells (RCMs). A population of HCN4-positive cardiomyocytes residing on periphery of SAN represents the all-intermediate stages between the typical HCN4-positive cardiomyocytes and RCMs that have the increasing numbers of myofibrils, large mitochondria, and electron-dense cytoplasm. Interestingly, the atrioventricular node, for instance, has only 5% of typical HCN4-positive cardiomyocytes as the majority of atrio-ventricular nodal cells are "transitional cardiac myocytes" [19]. The immunoelectron microscope investigation in the current study confirmed that the vast majority of cardiomyocytes immunoreactive for HCN4 within sinoatrial node vary in size, shape, and amount of myofibrils. In all examined samples from the sinoatrial nodal area, we observed numerous HCN4-immunoreactive cells that resembled regular cardiac myocytes and could be classified as transitional cardiac myocytes according to their size, shape and amount of myofibrils. Based on our fluorescent and electron microscope observations, we confirm findings by Shimada et al. [20] concerning the dissemination of numerous spindle-shaped HCN4-positive cardiomyocytes with ramifications at their ends within the mouse sinoatrial node. The dense cholinergic innervation of SAN region has been previously demonstrated in a range of mammalian species that have applied histochemical staining for AChE [3–8] as well as by immunohistochemistry for choline transporters [9] and choline acetyltransferase [10]. The data presented with the current study confirm earlier electron microscope observations about distribution of unmyelinated nerve fibres within sinoatrial node area in the mouse [13], rabbit [15] and human [33]. Despite this, we did not confirm previous electron microscope observations concerning the distribution of myelinated nerve fibres that were characteristic for rabbit SAN [15]. Nonetheless, coupled axons containing two distinct enzymes (ChAT and TH) were regularly observed within the neural network of mouse sinoatrial node applying fluorescent double immunolabelling on whole mount preparations.

5. Concluding remarks

Novel data presented within provide information on the density of the TH and ChAT immunoreactive nerve fibres that are associated with the SA nodal cardiomyocytes. These findings were obtained simultaneously by different methods of microscopy (conventional light, LSM and TEM) prove a complex meshwork of TH and ChAT immunoreactive nerve fibres in the SA nodal area and demonstrate close association with HCN4-positive cardiomyocytes. Original quantitative examination of nerve fibre density confirms a high density of innervation that was shown in whole-mount preparations using fluorescent immunohistochemistry. Electron microscope observations show a transmural distribution of HCN4 positive cardiac myocytes in addition to evidence of their ultrastructure, which is distinct from the ordinary SA nodal and atrial myocytes. We therefore provide an updated extracellular criterion for discrimination of SA nodal cardiomyocytes i.e. the adjacency of range (one to a few) unmyelinated nerve fibres to SA nodal cardiomyocytes. Therefore, the presence of unmyelinated nerve fibres adjacent to HCN4-positive cardiomyocytes appears to beneficial, for the reliable discrimination of these cells at the electron microscope level that is not reliant on immunohistochemical labelling that is known to damage cellular ultrastructure and worsen discrimination of labelled cells in this way. This extracellular feature of HCN4-positive cardiomyocytes warrants further investigation in other animal species and for other parts of cardiac conduction system.

Disclosures

None

Acknowledgements

The authors sincerely thank Mrs. Rima Masiene and Mrs. Nida Rutkauskiene for assistance throughout the study. This study was supported by the grants no. MIP-11184 and MIP-13037 (in part) from the

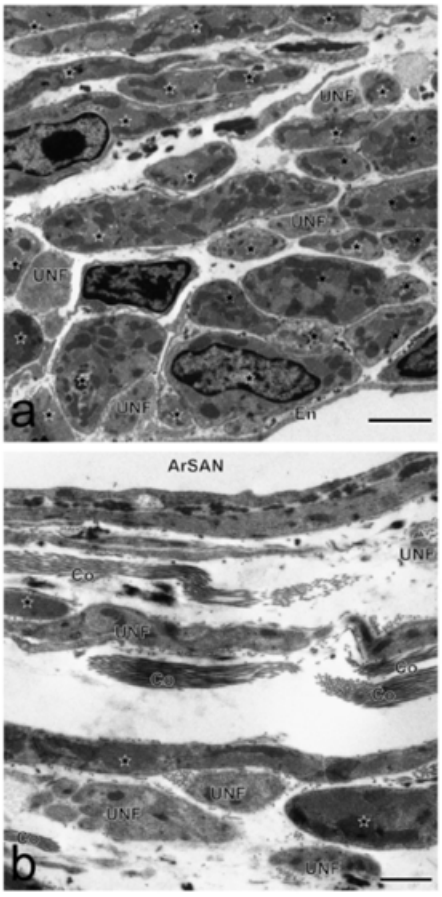

Fig. 7. Electron micrographs of low magnification to illustrate the high density of nerve fibres between the mouse SA nodal cardiomyocytes. a: Numerous unmyelinated nerve fibres (UNF) between SA nodal cardiomyocytes (asterisks) that do vary in size and shape and contain the irregularly arranged myofibrils, numerous glycogen granules and mitochondria. Fibroblasts, collagen and elastic fibres are intervened between SA nodal cardiomyocytes and UNFs. Endocardium (En) borders the lower right corner of the image. b: Solitary slender SA nodal cardiomyocytes (asterisks) intermingled with UNFs located just beneath the epicardial surface (Ep). Note the numerous nerve fibres adjacent to SA nodal cardiomyocytes. Other abbreviations: Co—bundles of collagen fibres. Scale bars—1 μm.

Research Council of Lithuania. KEB is supported by a British Heart Foundation Intermediate Basic Science Research Fellowship (12/2/29300).

References

[1] Wallick DW, Felder D, Levy MN. Autonomic control of pacemaker activity in the atrioventricular junction of the dog. Am J Physiol 1978;235:H308–13.
[2] Randall WC. Efferent sympathetic innervation of the heart. In: Armour JA, Ardell JL, editors. Neurocardiology. New York: Oxford University Press; 1994. p. 77–94.
[3] Bojsen-Moller F, Tranum-Jensen J. Rabbit heart nodal tissue, sinoatrial ring bundle and atrioventricular connexions indentified as a neuromuscular system. J Anat 1972;112:367–82.
[4] Kent KM, Epstein SE, Cooper T, Jacobowitz DM. Cholinergic innervation of the canine and human ventricular conducting system. Anatomic and electrophysiologic correlations. Circulation 1974;50:948–55.
[5] Crick SJ, Sheppard MN, Anderson RH, Polak JM, Wharton J. A quantitative assessment of innervation in the conduction system of the calf heart. Anat Rec 1996;245:685–98.
[6] Crick SJ, Sheppard MN, Ho SY, Anderson RH. Localisation and quantitation of autonomic innervation in the porcine heart I: conduction system. J Anat 1999;195(Pt 3):341–57.
[7] Crick SJ, Wharton J, Sheppard MN, Royston D, Yacoub MH, Anderson RH, et al. Innervation of the human cardiac conduction system. A quantitative immunohistochemical and histochemical study. Circulation 1994;89:1697–708.
[8] Petrecca K, Shrier A. Spatial distribution of nerve processes and beta-adrenoreceptors in the rat atrioventricular node. J Anat 1998;192(Pt 4):517–28.
[9] Hoover DB, Ganote CE, Ferguson SM, Blakely RD, Parsons RL. Localization of cholinergic innervation in guinea pig heart by immunohistochemistry for high-affinity choline transporters. Cardiovasc Res 2004;62:112–21.
[10] Rysevaite K, Saburkina I, Pauziene N, Vaitkevicius R, Noujaim SF, Jalife J, et al. Immunohistochemical characterization of the intrinsic cardiac neural plexus in whole-mount mouse heart preparations. Heart Rhythm 2011;8:731–8.
[11] Pauza DH, Saburkina I, Rysevaite K, Inokaitis H, Jokubauskas M, Jalife J, et al. Neuroanatomy of the murine cardiac conduction system: a combined stereomicroscopic and fluorescence immunohistochemical study. Auton Neurosci 2013;176(1–2):32–47.
[12] Novi AM. An electron microscopic study of the innervation of papillary muscles in the rat. Anat Rec 1968;160:123–41.
[13] Thaemert JC. Fine structure of neuromuscular relationships in mouse heart. Anat Rec 1969;163:575–85.
[14] Thaemert JC. Atrioventricular node innervation in ultrastructural three dimensions. Am J Anat 1970;128:239–63.
[15] Nilsson E, Sporrong B. Electron microscopic investigation of adrenergic and non-adrenergic axons in the rabbit SA-node. Z Zellforsch Mikrosk Anat 1970;111:404–12.
[16] Mochet M, Moravec J, Guillemot H, Hatt PY. The ultrastructure of rat conductive tissue; an electron microscopic study of the atrioventricular node and the bundle of His. J Mol Cell Cardiol 1975;7:879–89.
[17] Marino TA. The atrioventricular node and bundle in the ferret heart: a light and quantitative electron microscopic study. Am J Anat 1979;154:365–92.
[18] Canale E, Fujiwara T, Campbell GR. The demonstration of close nerve-Purkinje fibre contacts in false tendons of sheep heart. Cell Tissue Res 1983;230:105–11.
[19] Sherf L, James TV, Woods WT. Function of the atrioventricular node considered on the basis of observed histology and fine structure. J Am Coll Cardiol 1985;5:770–80.
[20] Shimada T, Noguchi T, Asami I, Campbell GR. Functional morphology of the conduction system and the myocardium in the sheep heart as revealed by scanning and transmission electron microscopic analyses. Arch Histol Jpn 1986;49:283–95.
[21] Dickie R, Bachoo RM, Rupnick MA, Dallabrida SM, Deloid GM, Lai J, et al. Three-dimensional visualization of microvessel architecture of whole-mount tissue by confocal microscopy. Microvasc Res 2006;72:20–6.
[22] Goehler LE, Erisir A, Gaykema RP. Neural–immune interface in the rat area postrema. Neuroscience 2006;140(4):1415–34.
[23] Malliani A, Recordati G, Schwartz PJ. Nervous activity of afferent cardiac sympathetic fibres with atrial and ventricular endings. J Physiol 1973;229(2):457–69.
[24] Arndt JO, Pasch U, Samodelov LF, Wiebe H. Reversible blockade of myelinated and non-myelinated cardiac afferents in cats by instillation of procaine into the pericardium. Cardiovasc Res 1981;15(2):61–7.
[25] Walters GE, Mary DASG. The effect on the efferent vagal nerves to the heart of stimulating atrial receptors in the dog. Q J Exp Physiol 1986;71:549–57.
[26] Jones JFX, Wang Y, Jordan D. Heart rate responses to selective stimulation of cardiac vagal C fibres in anaesthetized cats, rats and rabbits. J Physiol 1995;489(1):203–14.
[27] Garcia Perez M, Jordan D. Effect of stimulating non-myelinated vagal axons on atrioventricular conduction and left ventricular function in anaesthetized rabbits. Auton Neurosci 2001;86(3):183–91.
[28] Hirano H, Ogawa K. Ultrastructural localization of cholinesterase activity in nerve endings in the guinea pig heart. J Electron Microsccbh 1967;16:313–21.
[29] Yamamoto M, Dobrzynski H, Tellez J, Niwa R, Billeter R, Honjo H, et al. Extended atrial conduction system characterised by the expression of the HCN4 channel and connexin45. Cardiovasc Res 2006;72:271–81.
[30] Liu J, Dobrzynski H, Yanni J, Boyett MR, Lei M. Organisation of the mouse sinoatrial node: structure and expression of HCN channels. Cardiovasc Res 2007;73:729–38.
[31] Yanni J, Boyett MR, Anderson RH, Dobrzynski H. The extent of the specialized atrioventricular ring tissues. Heart Rhythm 2009;6:672–80.
[32] James TN, Sherf L, Fine G, Morales AR. Comparative ultrastructure of the sinus node in man and dog. Circulation 1966;34:139–63.
[33] Pauziene N, Pauza DH, Stropus R. Morphology of human intracardiac nerves: an electron microscope study. J Anat 2000;197(Pt 3):437–59.

Autonomic Neuroscience: Basic and Clinical 176 (2013) 32–47

Contents lists available at SciVerse ScienceDirect

Autonomic Neuroscience: Basic and Clinical

journal homepage: www.elsevier.com/locate/autneu

Neuroanatomy of the murine cardiac conduction system
A combined stereomicroscopic and fluorescence immunohistochemical study

Dainius H. Pauza [a,*], Inga Saburkina [a], Kristina Rysevaite [a], Hermanas Inokaitis [a], Marius Jokubauskas [a], José Jalife [b], Neringa Pauziene [a]

[a] Institute of Anatomy, Faculty of Medicine, Lithuanian University of Health Sciences, Kaunas, Lithuania
[b] Center for Arrhythmia Research, University of Michigan, Ann Arbor, USA

ARTICLE INFO

Article history:
Received 14 November 2012
Received in revised form 7 January 2013
Accepted 8 January 2013

Keywords:
Sinuatrial node
Atrioventricular node and rings
Innervation
Cardiac ganglia
Neurons
Conduction system
HCN4
Tyrosine hydroxylase
Choline acetyltransferase
Acetylcholinesterase
Immunohistochemistry
Mouse

ABSTRACT

The mouse heart is a popular model to study the function and autonomic control of the specialized cardiac conduction system (CCS). However, the precise identity and anatomical distribution of the intrinsic cardiac nerves that modulate the function of the mouse CCS have not been adequately studied. We aimed at determining the organization and distribution of the intrinsic cardiac nerves that supply the CCS of the mouse. In whole mouse heart preparations, intrinsic neural structures were revealed by histochemical staining for acetylcholinesterase (AChE). Adrenergic, cholinergic and peptidergic neural components were identified, respectively, by immunohistochemical labeling for tyrosine hydroxylase (TH), choline acetyltransferase (ChAT), calcitonin gene related peptide (CGRP), substance P (SP), and protein gene product 9.5 (PGP 9.5). Myocytes of the CCS were identified by immunolabeling of hyperpolarization activated cyclic nucleotide-gated potassium channel 4 (HCN4). In addition, the presence of CCS myocytes in atypical locations was verified using fluorescent immunohistochemistry performed on routine paraffin sections. The results demonstrate that four microscopic epicardial nerves orientated toward the sinuatrial nodal (SAN) region derive from both the dorsal right atrial and right ventral nerve subplexuses. The atrioventricular nodal (AVN) region is typically supplied by a single intrinsic nerve derived from the left dorsal nerve subplexus at the posterior interatrial groove. SAN myocytes positive for HCN4 were widely distributed both on the medial, anterior, lateral and even posterior sides of the root of the right cranial (superior caval) vein. The distribution of HCN4-positive myocytes in the AVN region was also wider than previously considered. HCN4-positive cells and thin slivers of the AVN extended to the roots of the ascending aorta, posteriorly to the orifice of the coronary sinus, and even along both atrioventricular rings. Notwithstanding the fact that cholinergic nerve fibers and axons clearly predominate in the mouse CCS, adrenergic nerve fibers and axons are abundant therein as well. Altogether, these results provide new insight into the anatomical basis of the neural control of the mouse CCS.

1. Introduction

The morphology of the cardiac conduction system (CCS) and its nerve supply have been studied in whole-mount preparations or histological sections in several animal species, including humans (Bojsen-Moller and Tranum-Jensen, 1971; Anderson, 1972a,b; Bojsen-Moller and Tranum-Jensen, 1972; Roberts et al., 1989; Crick et al., 1996a, 1999; Chow et al., 2001). A number of neuroanatomical studies have shown that all regions of the CCS possess a significantly higher density of nerve fibers than the adjacent working myocardium (Crick et al., 1996b). However, within the CCS, the density of nerve fibers varies between the regions of the sinuatrial node (SAN), atrioventricular node (AVN), atrioventricular bundle, and the components of CCS on the ventricular walls, as well as among species, i.e. humans, pig, guinea pig, calf, etc. Similarly, the density of cholinergic, adrenergic, and peptidergic nerve fibers differs significantly among the CCS components and species (Crick et al., 1996b, 1999).

In the human heart, as well as the hearts of all mammalian species we have examined to date, both the dorsal and ventral right atrial neural subplexuses are the source of the SAN neural network, while the left or middle dorsal neural subplexuses supply the AVN region (Pauza et al., 1999, 2000; Batulevicius et al., 2003, 2005; Saburkina and Pauza, 2006; Saburkina et al., 2010; Rysevaite et al., 2011a). The neural meshwork of the AVN region is usually comprised by minute endocardial nerves extending from epicardial ganglia distributed in the dorsal–posterior interatrial groove. However, in the dog heart there are additional thin endocardial nerves that spread from the ventral and dorsal right atrial subplexuses toward the AVN zone (Pauza et al., 2002). Our investigations on the general distribution, architecture and neurochemistry of

* Corresponding author at: Institute of Anatomy, Faculty of Medicine, Lithuanian University of Health Sciences, A. Mickeviciaus Street 9, Kaunas LT-44307, Lithuania. Tel.: +370 37 327313, +370 682 39366 (mobile); fax: +370 37 220733.
E-mail address: dainius.pauza@lsmuni.lt (D.H. Pauza).

1566-0702/$ – see front matter © 2013 Elsevier B.V. All rights reserved.
http://dx.doi.org/10.1016/j.autneu.2013.01.006

Table 1
Primary and secondary antisera used in the study.

Antigen	Host	Dilution	Supplier	Catalog number
Primary				
ChAT	Goat	1:100	Chemicon[a]	AB144P
TH	Rabbit	1:500	Chemicon[a]	AB152
TH	Sheep	1:800	Chemicon[a]	AB1542
CGRP	Rabbit	1:4000	Chemicon[a]	AB5920
SP	Rabbit	1:800	ImmunoStar[b]	20064
PGP 9.5	Rabbit	1:500	ABD Serotec[c]	7869–0504
HCN4	Rabbit	1:100	Chemicon[a]	AB5808
Secondary				
Goat ^{Cy3}	Donkey	1:300	Chemicon[a]	AP180C
Rabbit ^{Cy3}	Donkey	1:300	Chemicon[a]	AP182C
Rabbit ^{FITC}	Donkey	1:100	Chemicon[a]	AP182F
Sheep ^{FITC}	Donkey	1:100	Chemicon[a]	AP184F

[a] Chemicon International, Temecula, California, USA.
[b] ImmunoStar Incorporation, Wisconsin, USA.
[c] AbD Serotec, Kidlington, UK.

the intrinsic nerve plexus in the mouse heart demonstrated the access of extrinsic cardiac nerves at the right and left cranial veins onto the heart base, where they interblend within the ganglionated nerve plexus of the heart hilum (Rysevaite et al., 2011a,b). The latter studies demonstrated that nerves and neural bundles extend epicardially from the nerve plexus of the heart hilum to the atria and ventricles forming the left dorsal, dorsal right atrial, right ventral, and ventral left atrial neural subplexuses. Abundant cholinergic (positive for choline acetyltransferase, ChAT) and adrenergic (positive for tyrosine hydroxylase, TH) nerve fibers were revealed within nerves accessing the mouse heart, but TH-immunoreactive nerve fibers were clearly predominant within the epicardium of the dorsal and ventral left atrium, whereas the majority of ChAT-positive fibers proceeded onto the heart base toward the intrinsic ganglia and the epicardium of the root of the right cranial vein (Rysevaite et al., 2011b). In the mouse heart, the intrinsic ganglia are concentrated close to the pulmonary veins on the left atrium. Most neuronal somata are ChAT-immunoreactive, while ~4% are TH-immunoreactive, and ~14% of ganglionic neurons are biphenotypic for ChAT and TH. Substance P-positive and calcitonin gene-relative peptide-immunoreactive nerve fibers are abundant in the mouse epicardium and within intrinsic ganglia (Rysevaite et al., 2011b).

The use of immunohistochemistry to identify specific proteins representing the specialized cells of the CCS demonstrated that these cells spread more widely within both the right atrium and the interatrial septum than previously considered (Anderson et al., 2009; Aanhaanen et al., 2010). In rat and rabbit hearts, CCS cells that are positive for HCN4 and connexin 45, but negative for connexin 43, extend downwards from the superior vena cava in the interatrial groove and are capable of independent pacemaker activity (Yamamoto et al., 2006). Additionally, these specific cells are distributed as particular rings alongside both atrioventricular orifices in rats, mice, and guinea pigs (Yamamoto et al., 2006; Yanni et al., 2009). These rings took their origin from an inferior extension of the atrioventricular node, but the right ring runs around the vestibule of the tricuspid valve, whereas the left ring encircles

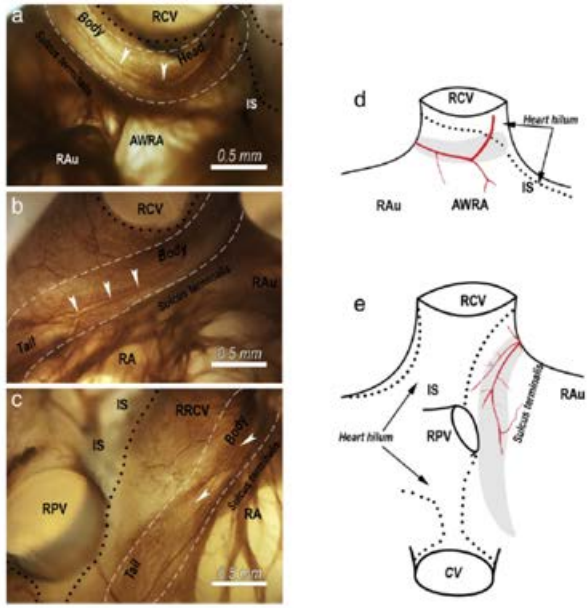

Fig. 1. Macrophotographs of ventral (a), right lateral (b) and dorsal (c) views and schematic drawings of ventral (d) and dorsal (e) surfaces of the root of the right cranial vein (RCV) demonstrate positive immunohistochemical staining for AChE in the sinuatrial nodal area distributed along the course of the sinuatrial nodal artery in the mouse heart. The white dashed line indicates the SAN area with its three portions – head, body and tail; the arrowheads point to the SAN artery; the red curved and branched lines in the drawings represent the course of SAN artery, while the gray area is the SAN region stained in brownish due to AChE histochemical reaction. Abbreviations: AWRA – anterior wall of right atrium; IS – anterior (in a) and dorsal (in c) groove of the interatrial septum; RA – right atrium; RAu – right auricle; RRCV – root of the right cranial vein; RPV – right pulmonary vein.

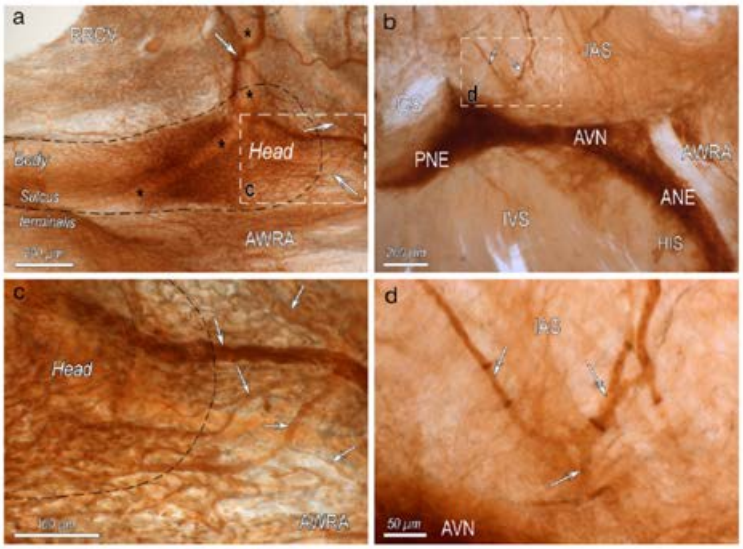

Fig. 2. Microphotographs of the root of the mouse right cranial vein (a and c) and the right lateral surface of the cardiac septa (b and d) stained histochemically for AChE. The boxed areas (c and d) in the upper (a and b) panels are enlarged as lower (c and d) panels to demonstrate the intrinsic nerves (arrows) and nerve bundles stained in brown. Note the dense network of AChE-positive nerve fibers in the outlined area of the SAN (c), as well as the strongly brown area in the region of the AVN and its posterior (PNE) and anterior (ANE) extensions. Asterisks demarcate the course of artery of the SAN that is outlined by the black dashed line and in which its head and body zones are marked. Abbreviations: ANE — anterior extension of atrioventricular node; AVN — atrioventricular nodal area; AWRA — external (in a and c) and internal (in d) surface of the anterior wall of right atrium; CS — internal surface of coronary sinus; HIS — His bundle; IAS — interatrial septum; IVS — interventricular septum anterior; RRCV — root of the right cranial vein; PNE — posterior extension of atrioventricular node.

the mitral valve. On returning toward the atrial septum, the tricuspid ring crosses over the penetrating part of the AVN, reuniting with the mitral ring to form the specific "retroaortic node" (Yanni et al., 2009).

The mouse heart has been widely used to investigate mechanisms of AV conduction (Aanhaanen et al., 2010) and electrophysiology of the sinuatrial node (Verheijck et al., 2001; Liu et al., 2007; Glukhov et al., 2010). This species is also appropriate to investigate molecular mechanisms of sympathetic-parasympathetic imbalance in cardiac arrhythmia and as a novel cardiac ablation model (Bernstein et al., 2011; Lang et al., 2011; Rose et al., 2011). However, to date, the innervation of the mouse CCS has not been investigated in any detail. Therefore, the study presented here was designed to examine precisely the localization, structural organization and immunoreactivity of intrinsic cardiac nerves and ganglia that are anatomically related to the CCS of the mouse.

2. Materials and methods

Forty three 2–4 month-old C57BL/6J-linear mice of either gender were used to examine the intrinsic cardiac neural plexus. Animals were deeply anesthetized with ether and euthanized by cervical dislocation in accordance with local and state guidelines for the care and use of laboratory animals (Permission No. 0206).

2.1. Non-sectioned pressure distended heart preparations

After euthanasia, the mouse chest was opened and the heart was perfused with 0.01 M phosphate-buffered saline (PBS; 0.9% NaCl, pH 7.4), via a cannula inserted into the left ventricular cavity. Eighteen whole (i.e., non-parceled and non-sectioned) hearts were prepared for histochemical acetylcholinesterase (AChE) staining of the nerve plexus, as described previously (Pauza et al., 1999). The flabby atrial walls were pressure inflated in situ by a transmyocardial injection of a 20% warm water solution of gelatin into the atria and ventricles. Once the injected gelatin jelled, the heart was removed from the chest and immersed in a chamber filled with PBS at room temperature. Subsequently, the pericardium, pulmonary arteries, and mediastinal fat were gently separated from the heart base. The prepared hearts were prefixed for 30 min at 4 °C in a 4% paraformaldehyde solution and 0.01 M phosphate buffer (pH 7.4). In order to stain intrinsic neural elements distributed within cardiac septa, eleven pressure-distended hearts were dissected to expose the interatrial and interventricular septa by cutting off the walls of both atria and ventricles. After prefixation, the heart preparations were washed for 12 h at 4 °C in PBS containing hyaluronidase (0.5 mg/100 ml, Carl Roth, Karlsruhe, Germany) and placed for 3 h at 4 °C in Karnovsky–Roots medium, as described previously (Pauza et al., 1999). Finally, heart preparations stained for AChE were fixed and stored in a 4% paraformaldehyde solution and 0.01 M phosphate buffer (pH 7.4).

2.2. Whole-mount preparations

To examine the intrinsic cardiac neural plexus using immunofluorescence, hearts perfused with PBS 25 were removed from the chest and placed into a dissecting dish containing cold 0.01 M PBS as described previously (Rysevaite et al., 2011b). For optimal visualization of both specialized conducting myocytes and neural structures, the

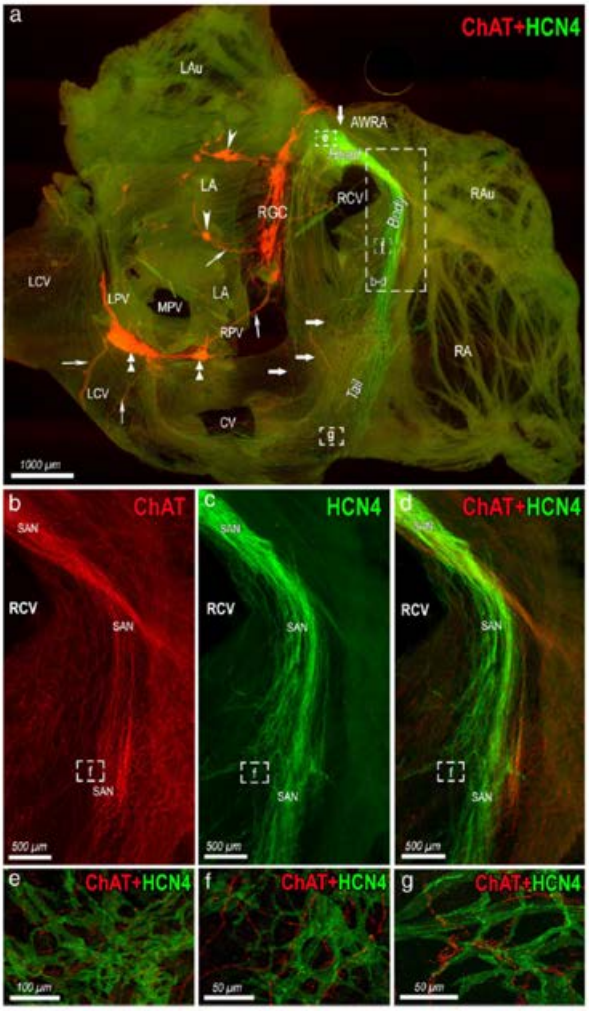

Fig. 3. Whole-mount preparation of the mouse atria demonstrates the distribution of HCN4 immunoreactive (IR) conductive myocytes and ChAT-IR neural structures (intrinsic nerves, ganglia, and nerve fibers). Both the atrial appendages and the roots of the pulmonary veins were dissected to flatten the atria. Cholinergic (ChAT) neural structures (nerves and ganglia) are labeled in red (b), HCN4 cells in green (c), the merged immunoreactivity (ChAT + HCN4) is shown in panels a, d and e–g. Arrows point to the epicardial nerves extending toward the SAN region. Arrowheads indicate some small intrinsic cardiac ganglia in the limits of the heart hilum, double arrowheads — the left ganglionic cluster, RGC means the right-sided ganglionic cluster, from which epicardial nerves (arrows) extend toward the SAN region. The boxed areas (b–d, e, f, and g) in the upper panel (a) are enlarged as the lower panels (b–g) to display the overlapped distribution of the cholinergic nerve meshwork and cells immunoreactive for HCN4 at the roots of the right cranial (RCV) and caudal (CV) veins. The head, body, and tail in the upper panel mean the portions of the mouse SAN region. Abbreviations: AWRA — anterior wall of right atrium; RCV — orifice of right cranial vein; CV — orifice of caudal vein; LA — left atrium; LAu — left auricle; LCV — flattened surface of left cranial vein; LPV — orifice of left pulmonary vein; RA — right atrium; RAu — right auricle; RPV — orifice of right pulmonary vein; MPV — orifice of middle pulmonary vein.

atrial walls and the interatrial septum were separated from the ventricles and then pinned on a silicone pad in a dissecting dish, in which tissues were prefixed for 25 min at 4 °C in a 4% paraformaldehyde solution in 0.01 M phosphate buffer (pH 7.4). To decrease background light during fluorescence microscopy, the tissues were cleared using a dimethylsulfoxide and hydrogen peroxide solution and dehydrated as reported previously (Dickie et al., 2006). After tissue clearing, the whole-mount preparations were rehydrated by successive

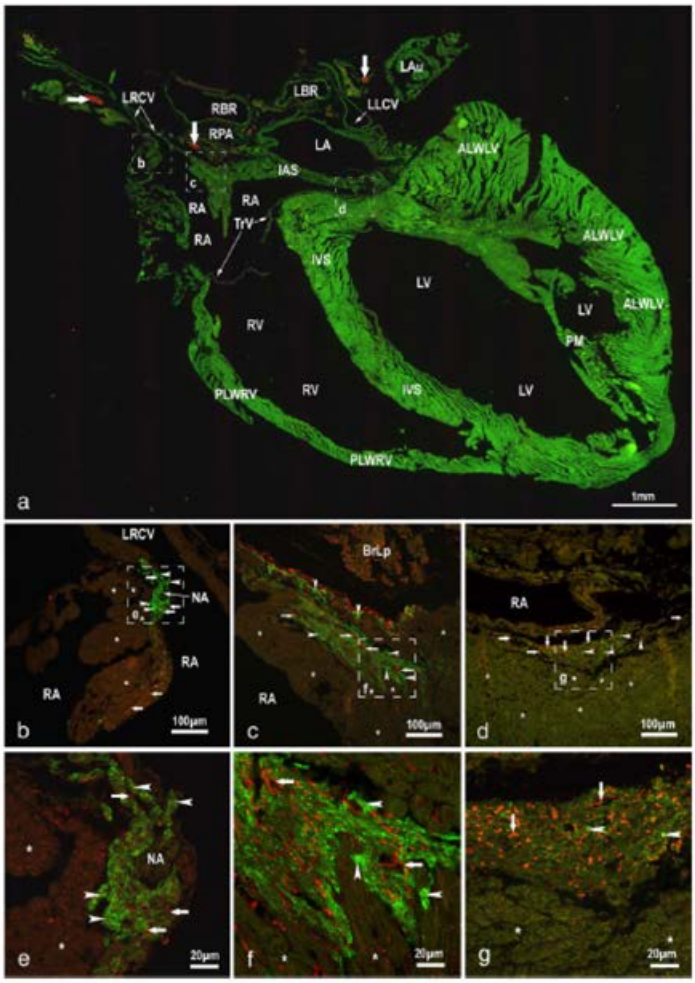

Fig. 4. Microphotographs of the longitudinally diagonal sections of the mouse heart demonstrating the HCN4 immunoreactive (IR) conductive myocytes (in green) accompanied with plenty of ChAT-IR nerve fibers (in red) on the lateral and medial sides of the root of the right cranial vein (RCV). The boxed areas (b) and (c) in the upper (a) panel are enlarged as the middle (b and c) panels and represent correspondingly the body (b) and the head (c) of the SAN. The boxed areas in b, c and d panels are enlarged in the lower (e–f) panels to display clearly the HCN4-IR cardiac myocytes and numerous ChAT-IR nerve fibers accompanied the HCN4-IR cells. Thick arrows in the upper (a) panel point to some mediastinal nerves containing ChAT-IR nerve fibers. Arrows in the lower (b–g) panels show the cholinergic nerve fibers, arrowheads – conductive cells, and asterisks – some working cardiac myocytes. Abbreviations: LBr, RBr – left and right bronchi; LLCV, LRCV – lumens of left and right cranial veins; NA – profile of SA nodal artery; RPA – lumen of right pulmonary artery; RA, LA – right and left atria, LA, RV – left and right ventricles; TrV – tricuspid valve; IAS, IVS – interatrial and interventricular septa; LAu, RAu – left and right auricles; PLWRV – posterior lateral wall of right ventricle; ALWLV – anterior lateral wall of left ventricle.

10-minute washes through a graded ethanol series, then washed, and permeabilized in 3×10-minute changes of 0.01 M PBS containing 0.5% Triton X-100 (Carl Roth, Karlsruhe, Germany). Nonspecific binding was blocked for 2 h in PBS containing 5% normal donkey serum (Jackson ImmunoResearch Laboratories, West Grove, PA, USA) and 0.5% Triton X-100. Next, preparations were washed three times for 10 min in 0.01 M PBS and incubated in a mixture of double primary antibodies for 48 h in a dark humid chamber at +4 °C (Table 1). After

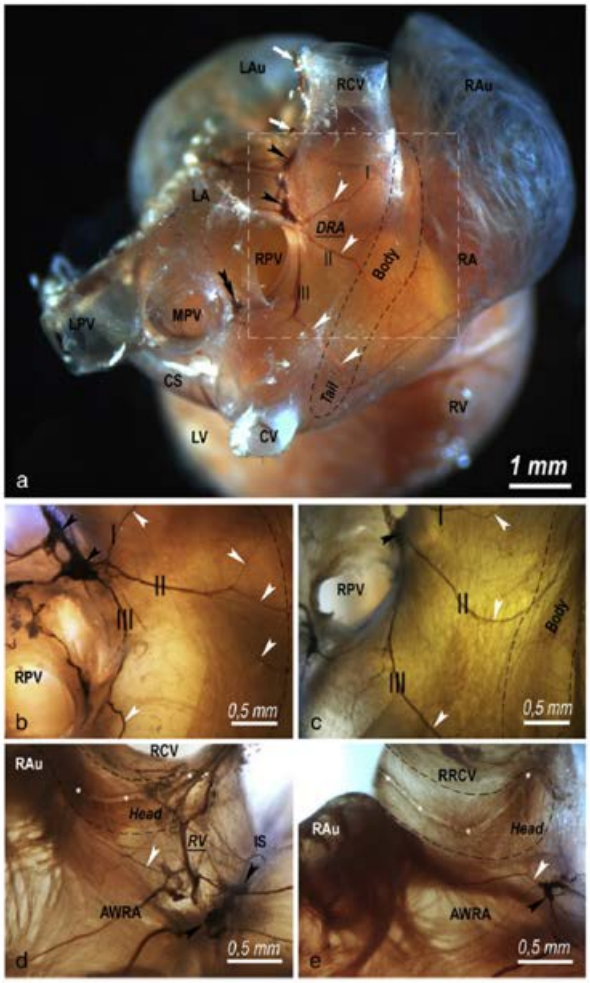

Fig. 5. Macrophotographs of the dorso-cranial (a–c) and ventral (d, e) surfaces of the mouse heart stained histochemically for AChE demonstrating part of intrinsic cardiac nerve plexus, the dorsal right atrial (DRA) and right ventral (RV) nerve subplexuses, associated with the SAN region. The black dashed line indicates the SAN area with its three portions—head, body and tail; the asterisks point to the course of the SAN artery. The boxed area in the upper (a) panel outlines the area on the mouse heart, which is shown in the lower (b, c) panels. The Ib–e panels display the persistent topography and similar appearance of three dorsal right atrial (b, c) and one right ventral (d, e) subplexal nerves (white arrowheads and roman numerals in b and c) extending from the right ganglion cluster to the SAN region in two mouse hearts stained histochemically for AChE. White arrows point to the right-sided preganglionated nerves accessing the right ganglion cluster (black arrowheads), white arrowheads—the DRA and RV subplexal epicardial nerves extending toward the SAN region, double black arrowheads—the left ganglion cluster. Abbreviations: CS — coronary sinus; CV — caudal cava vein; DRA — dorsal right atrial nerve subplexus; IS — groove of interatrial septum; LAu — left auricle; LPV — left pulmonary vein; LA — left atrium, LV — left ventricle; MPV — middle pulmonary vein; RA — right atrium, RAu — right auricle; RCV — right cranial vein; RRCV — root of right cranial vein; RPV — right pulmonary vein; RV — right ventricle; RV — right ventral nerve subplexus.

three 10 min-washes in 0.01 M PBS, the whole-mount heart preparations were incubated in an appropriate combination of secondary antibodies for 4 h in a dark humid chamber on a shaker stage at room temperature (Table 1). All antibodies were diluted in 0.01 M PBS. Thereafter the specimens were again washed in 0.01 M PBS, incubated for 2 h in a dimethylsulfoxide and PBS mixture, 1:4 (v:v) ratio, and mounted in Vectashield Mounting Medium (Vector Laboratories, California, U.S.A.). A cover slip was placed on the tissue and

Table 2
The mean number and the range of intrinsic cardiac neurons in general per one heart, per one ganglion, in the right (RGC) and in the left (LGC) ganglionic clusters from 11 whole-mount mouse heart preparations. The differences between RGC and LGC are insignificant at $p<.05$.

The number of neurons	Mean ± SE	Range
In general	1804 ± 176	1121–2621
Per ganglion	221 ± 28	11–1013
RGC	972 ± 70	621–1229
LGC	860 ± 105	413–1463

oven (Milestone HistosPro, Sorisole, Italy), according to the protocol described above.

2.4. Microscopic examination and quantitative analysis

The neural structures stained histochemically for AChE were examined stereoscopically at 6–50× magnification using a Stemi 200 CS stereomicroscope (Zeiss, Gottingen, Germany) applying transient light from fiber optic illuminators (Zeiss, Gottingen, Germany). The stereoscopically observed ganglia and nerves were photographed

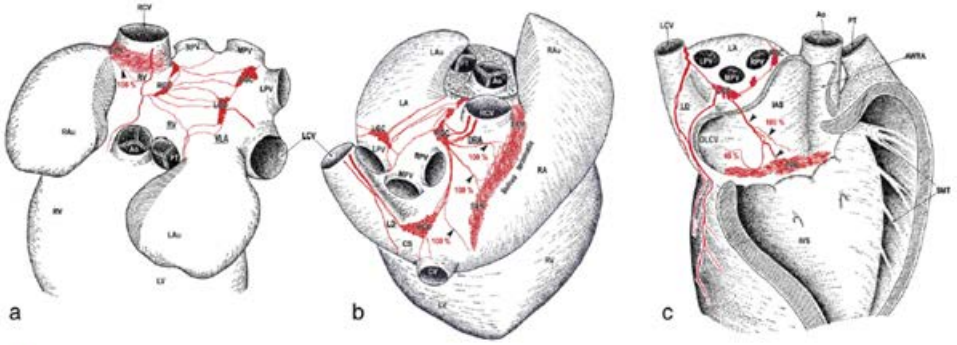

Fig. 6. Drawings of the ventral (a) and dorsal (b) views of the pressure-inflated mouse heart, and of the right side of the interatrial and interventricular septa (c). Here we illustrate the morphologic pattern of the intrinsic cardiac ganglionated plexus associated with the SAN and AVN regions. Large portions of both the right atrium and right ventricle were removed to expose the cardiac septa from the right side (c). The nerve plexus (drawn in red) was outlined from a cardiac preparation stained histochemically for AChE, while the neural meshwork in the SAN and the AVN regions are revealed by immunofluorescence for HCN4, TH and ChAT. Black arrowheads point to the topographically persistent intrinsic cardiac nerves that extend toward the SAN (a and b) and AVN (c) regions. In red, the polygonal bubbled areas depict the intrinsic cardiac ganglia, the thin wiggle and ramifying lines — the intrinsic nerves linked anatomically with the SAN and AVN regions, and the dense tiny network insinuates the comparatively densest neural network distributed at regions adjacent to SAN and AVN. The numbers on the nerves extending toward the SAN and AVN regions indicate the percentage of preparations in which these drawn nerves were identified. Abbreviations: Ao — ascending aorta; AVN — region of typical atrioventricular node; AWRA — anterior wall of the right atrium; CS — coronary sinus; CV — caudal vein; DRA — dorsal right atrial nerve subplexus; IAS — interatrial septum; IVS — interventricular septum; LAu — left auricle; LCV — left cranial cava vein; LGC — left ganglion cluster; LD — left dorsal subplexus; LPV — left pulmonary vein; LV — left ventricle; MPV — middle pulmonary vein; PT — pulmonary trunk; RAu — right auricle; RCV — right cranial cava vein; RGC — right ganglion cluster; RPV — right pulmonary vein; RV — right ventricle; RV — right ventral subplexus; SAN — region of typical sinuatrial node; SMT — septomarginal trabeculae; VLA — ventral left atrial subplexus.

then sealed with clear nail polish. Both positive and negative controls were used.

2.3. Heart sections

To verify the presence of conductive myocytes in atypical cardiac locations, hearts were fixed for 4 days at 4 °C in a 4% paraformaldehyde solution in 0.01 M phosphate buffer (pH 7.4) and routinely embedded in paraffin and sectioned in 4–5 μm thick slices employing a rotatory microtome. Heart tissue sections were stuck on microscope slides by electrostatic attraction (Superfrost Ultra Plius, Thermo Scientific, Braunschweig, Germany) and dried up to 12 h at 50 °C. Double immunostaining for HCN4 and neuronal markers, as well as cover-slipping, was conducted after rehydration and antigen retrieval in Tris-EDTA buffer (pH 9) at 90 °C for 20–40 min in a microwave using a digital camera Axiocam HRc (Zeiss, Gottingen, Germany). Adjustments for final images and measurements of cardiac neural structures were performed using AxioVision 4.8.1 software (Zeiss, Jena, Germany). Whole-mount preparations stained immunohistochemically were analyzed utilizing an Axiolmager Z1 fluorescence microscope (Zeiss, Gottingen, Germany) equipped with a set of filters to observe the fluorescein isothiocyanate (FITC) and cyanine (Cy3) fluorescence, an Apotome (Zeiss, Gottingen, Germany), and a digital monochrome camera AxioCam MRm (Zeiss, Gottingen, Germany). When necessary, the same whole-mount preparations were additionally analyzed and photographed employing a laser scanning microscope LSM 700 (Zeiss, Jena, Germany) with its ZEN 2010 software (Zeiss, Jena, Germany).

The number of neurons inside intrinsic cardiac ganglia was estimated in 0.3–0.5 μm optical sections of the whole-mount

Fig. 7. Whole-mount preparation of the mouse atria shows the morphologic pattern of the cholinergic (ChAT, in red) and adrenergic (TH, in green) neural meshworks in the SAN region. Left and right atrial appendages, interatrial septum, and ventricles were extirpated in order to flatten the atria. The root of the right cranial vein was cut medially with the aim of unbending it. Thick arrows point to the epicardial nerves that extend toward the SAN region; thin arrows point to some epicardial nerves with predominant adrenergic nerve fibers on the wall of the left cranial vein (LCV) and with prevalent cholinergic nerve fibers on the left atrium (LA); RGC means the right-sided ganglionic cluster; double arrowheads point to the left ganglionic cluster. The boxed areas in the left upper (a) panel are enlarged as b–l. In d, e, g, h, j, and k we illustrate the dense neural meshwork of the ChAT immunoreactive (IR) and TH-IR nerve fibers within distinct parts (head, body, and tail) of the SAN region. Asterisks in d and e demarcate the course of the SAN artery. In f, i, and l the epicardial nerves containing a distinct ratio of ChAT and TH immunoreactive nerve fibers are shown by close-up. Abbreviations: RCV — orifice of right cranial vein; CV — orifice of caudal vein; LCV — flattened surface of left cranial vein; RPV, MPV, LPV — roots of right, middle and left pulmonary veins; ST — terminal groove; RAu — right auricle; RA — right atrium, LA — left atrium.

preparations *in silico* by counting exclusively the PGP 9.5 immuno-reactive nerve cells that contained well-visible nuclei. The latter rule was followed to avoid the overestimation of the number of neurons residing in the intrinsic cardiac ganglia, since it was evident that some neuron nuclei appeared in more than one optical section.

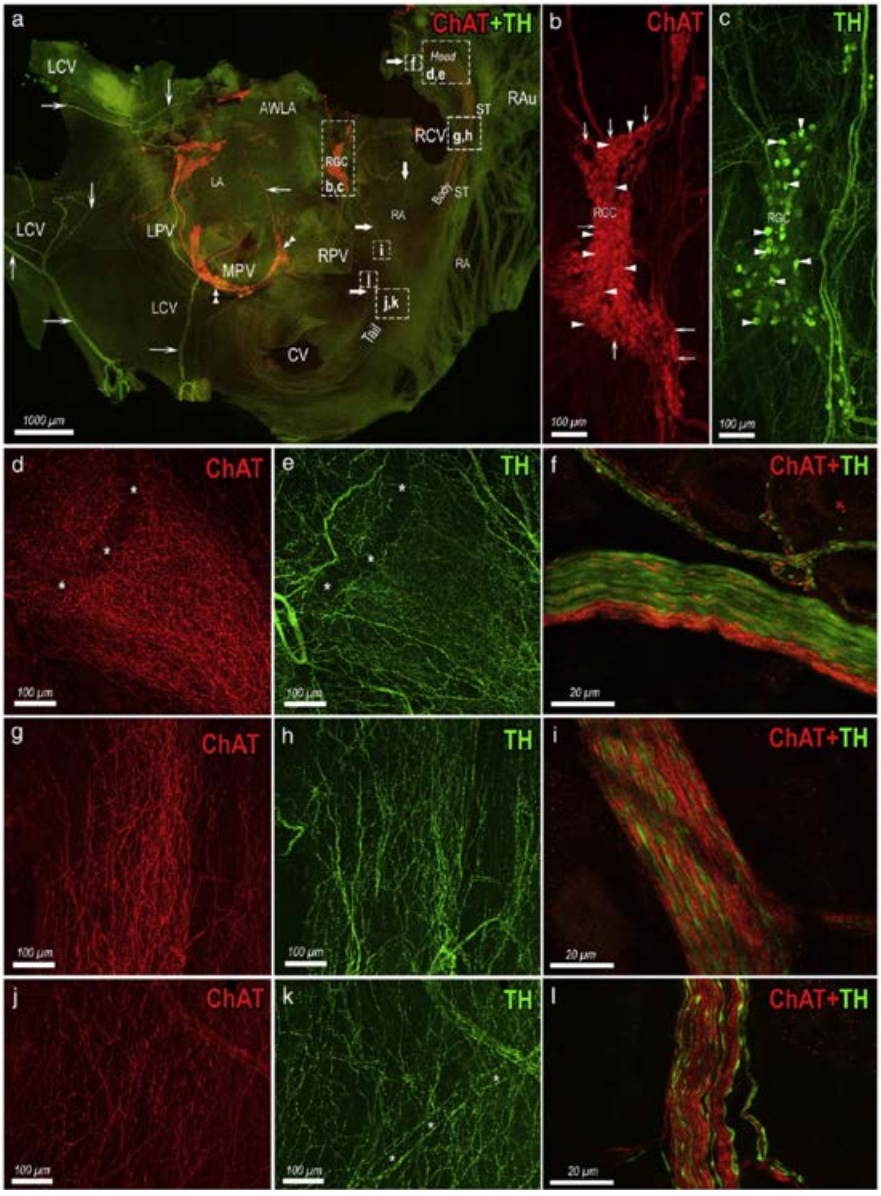

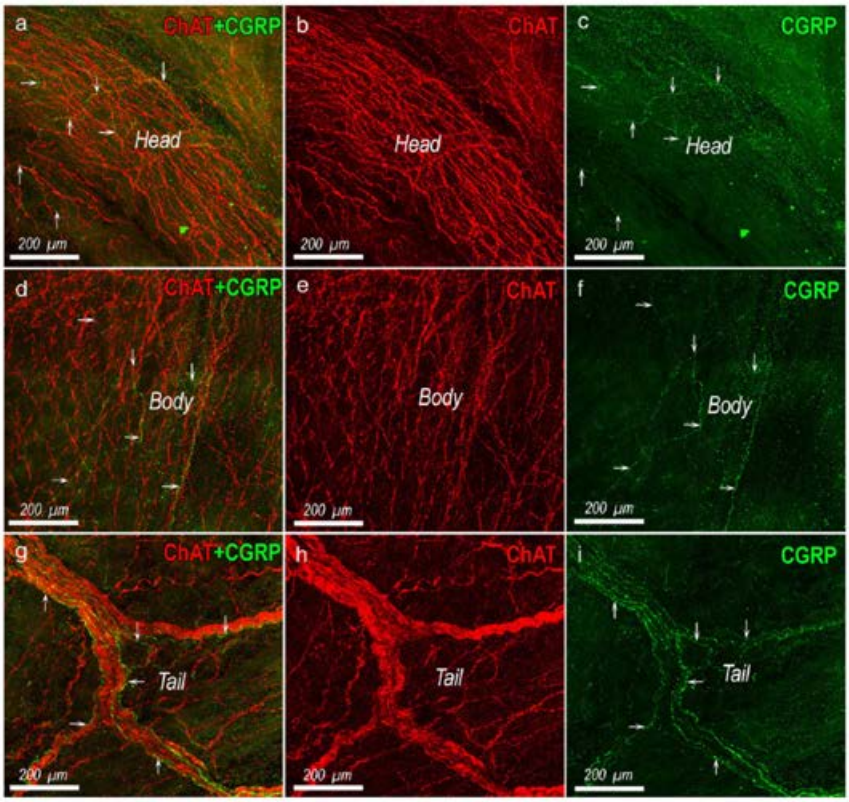

Fig. 8. Microphotographs of the whole mount atrial preparation to demonstrate the CGRP immunoreactive (green, arrows) and ChAT immunoreactive (red) nerve fibers at distinct areas of the SAN region — head (a–c), body (d–f), and tail (g–i). Note the numerous fine varicosities along the CGRP immunoreactive nerves fibers, independently from their location.

2.5. Statistical analysis

Data were processed using the Origin Lab software version 6.1 (OriginLab Corporation, Northampton, Massachusetts, USA). Data are expressed as mean ± standard error of the mean (SEM). Statistical analysis of the number of neurons related anatomically via epicardial nerves to SAN and AVN regions was performed using one-way analysis of variance (ANOVA). Differences were considered significant when $p<0.05$.

3. Results

3.1. Morphologic pattern of the nerve plexus of the SAN region

Upon histochemical staining for AChE, the elongated brownish SAN area appears on one side of the terminal groove and along the course of the SA nodal artery, which corresponds to the intrinsic prolongation of the lateral branch of the right cardiomediastinal artery (Fig. 1; Halpern, 1955, 1957). Bright-field microscopy of the SAN region in combination with AChE histochemistry revealed a dense network of AChE positive nerve fibers (Fig. 2). Fluorescence immunohistochemistry for HCN4 performed on both whole-mount preparations and whole-heart sections confirmed that the brownish area stained histochemically for AChE around the root of the right cranial vein (RRCV) overlaps entirely with the distribution of HCN4-positive SAN myocytes in this area (Figs. 3 and 4). Myocytes positive for HCN4 were mostly concentrated on the medial, ventral, lateral and dorsal sides of the RRCV forming a poorly demarcated horseshoe-shaped collar almost around the whole RRCV, but slivers of HCN4-positive cells extended far away from the main mass of these cells toward the right atrium, right auricle and the root of the caudal vein (Fig. 3). The SAN region comprised by the mass of the HCN4 positive cells around the RRCV was considered as the mouse SAN region, in which the broadest part, *the head*, locates on the medial and ventral sides of the RRCV, the intermediate portion, *the body*, along the terminal groove, and the last part, *the tail*, descends dorsally from the end of the terminal groove toward the root of the caudal vein (Figs. 1 and 3).

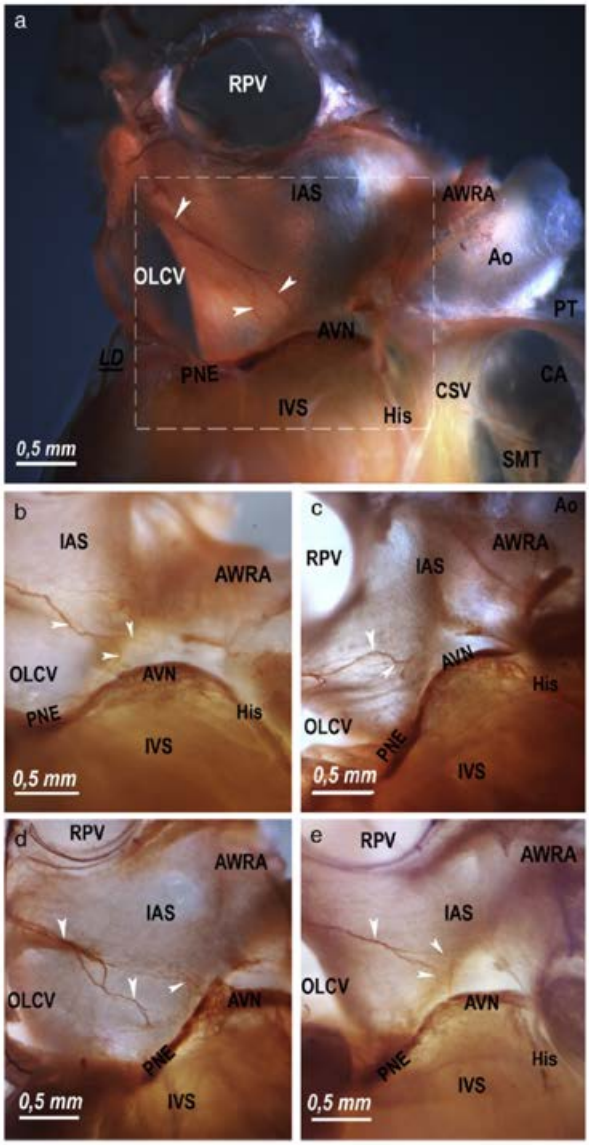

Fig. 9. Macrophotographs of the right side of the cardiac septa in five mice to demonstrate the endocardial pathway of the left dorsal (LD) subplexal nerve and its branches (white arrowheads) extending toward the AVN region (histochemical staining for AChE). The right atrium and right ventricle were cut off to expose the septa from the right side as shown in Fig 6c. Note the persistent topography and lesser morphologic variability of the endocardial septal nerve and its branches (white arrowheads) that expand on the right side of the interatrial septum from the left dorsal subplexus (LD) toward the AVN region. Abbreviations: Ao – ascending aorta; AVN – atrioventricular nodal region; AWRA – reminder of anterior wall of right atrium; CA – canal of conus arteriosus CSV – crista supraventricularis; His – bundle of His; IAS – interatrial septum; IVS – interventricular septum; LD – some nerves of left dorsal subplexus; OLCV – orifice of left cranial vein; PNE – posterior extension of AVN; PT – pulmonary trunk; RPV – orifice of right pulmonary vein; SMT – septomarginal trabeculae.

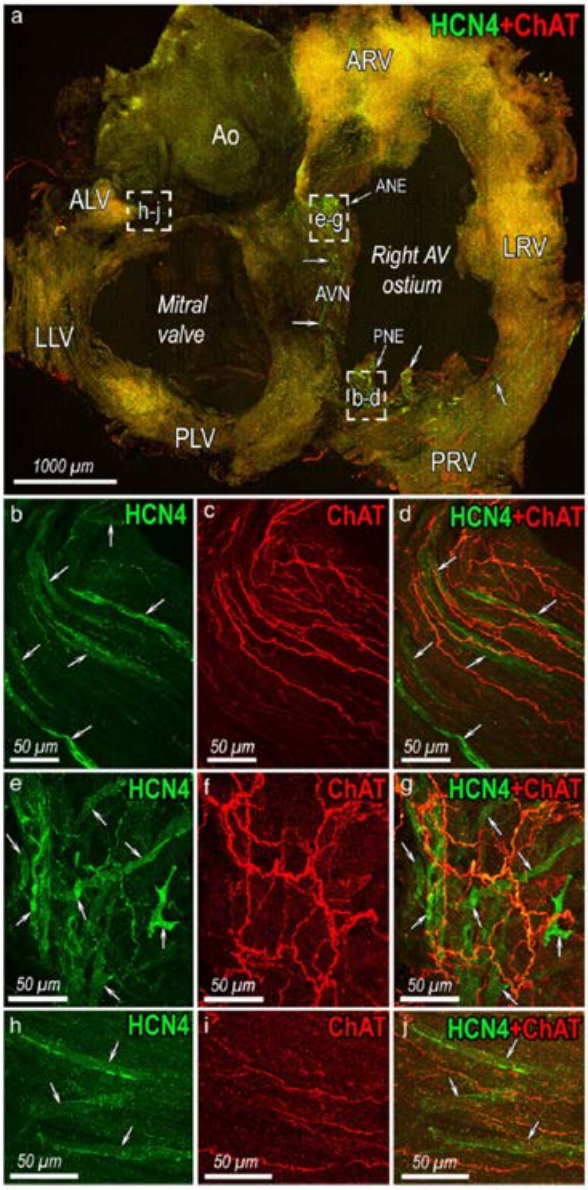

Fig. 10. Whole-mount preparation of the mouse atrioventricular rings demonstrates the extensions of the HCN4-positive cells (arrows) extending alongside both atrioventricular rings and toward the root of ascending aorta (Ao). Both atria and ventricles were cut off to flatten and expose the AV rings from above. The boxed areas in the upper (a) panel are enlarged as b–j. Cholinergic (ChAT) nerve fibers are labeled in red, HCN4 cells — in green, the merged immunoreactivity (ChAT + HCN4) is shown in a, d, g and j. Abbreviations: Ao — root of ascending aorta; AVN — typical atrioventricular nodal region; ALV, LLV, PLV — anterior lateral and posterior sides of left ventricle; ARV, LRV, PRV — anterior, lateral and posterior side of right ventricle.

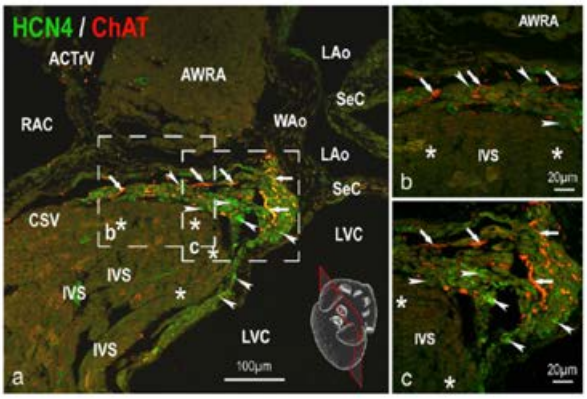

Fig. 11. Microphotographs from a mouse heart section as shown in the right lower part of the left (a) panel to validate the distribution of conductive myocytes immunoreactive for HCN4 (in green) and abundant ChAT-IR nerve fibers (in red) at the root of the ascending aorta (Ao). The boxed areas (b–c) in the left (a) panel are enlarged as the left (b–c) panels to exhibit the conductive myocytes accompanied by numerous cholinergic nerve fibers. Arrows indicate some cholinergic nerve fibers, arrowheads — conductive cardiac myocytes, asterisks — working cardiac myocytes. Abbreviations: RAC — chamber of right atrium; LAo — lumen of ascending aorta; SeC — semilunar cusp; WAo — wall of ascending aorta; ACTrV — anterior cusp of tricuspid valve; AWRA — anterior wall of right atrium; CSV — crista supraventricularis; IVS — interventricular septum; LVC — left ventricular chamber.

The SAN receives the AChE positive tiny epicardial nerves from the ganglionated nerve plexus on the heart base that was earlier defined in detail by us as the nerve plexus of the heart hilum (Rysevaite et al., 2011a). The right-sided cluster of ganglia located within this plexus on the left atrium at the root of the right pulmonary vein is the sole source of epicardial nerves extending toward the SAN region (Figs. 3 and 5). That cluster is comprised mostly by several ganglia containing variable numbers of neurons (Fig. 5, Table 2). The ganglia of the right cluster are comprised by numerous interconnected inter-ganglionic nerve fibers that connect also with the left ganglionic cluster (Fig. 3). From the right ganglia, epicardial nerves reach the SAN both by the ventral and dorsal surfaces of the right atrium (Figs. 5 and 6). The head of the SAN receives the single stereomicroscopically identifiable and persistent epicardial nerve that arises from the right ventral (RV) subplexus (Figs. 5 and 6). In all pressure-distended heart preparations examined, that nerve coursed diagonally to the junction of the RCV and right auricle where it became gradually thinner and penetrated into the myocardium (Fig. 5). Both body and tail of the SAN were supplied by 3 persistent epicardial nerves that originated from the dorsal right atrial (DRA) subplexus (Figs. 5 and 6). In all hearts, two epicardial nerves arose cranially from the right ganglia and coursed directly from the heart hilum to the body of the SAN, while the third one extended more caudally and coursed toward the SAN tail and the root of the caudal vein (Figs. 5 and 6).

Within the mouse SAN region we identified a dense meshwork of fine ChAT-positive fibers that were dispersed around HCN4 immunoreactive myocytes (Fig. 3). Double immunostaining for ChAT and TH revealed that the neural meshwork within the SAN region consisted of numerous nerve bundles, singular nerve fibers and axons with varicosities, but was devoid of any neuronal somata (Fig. 7). Both ChAT and TH immunoreactive nerve structures displayed distinct densities. However, the ChAT positive nerve fibers and axons were more numerous near cardiac myocytes than TH immunoreactive nerve fibers, which were chiefly located around blood vessels (Fig. 7). Finally, we identified only a few CGRP- and/or SP-positive nerve fibers in the whole area around the root of the RCV that was occupied by HCN4-positive cells (Fig. 8).

3.2. Neural routes and morphology of nerve plexus of the AVN region

Similar to the SAN region around the root of the RCV, a remarkably dense network of AChE positive nerve fibers concentrated on the lowest part of the mouse interatrial septum extending from the orifice of the LCV and the aortic root (Figs. 2 and 9). In the whole-mount atrial preparations the positivity to HCN4 of the myocytes within the AVN region was evidently weaker than the SAN region (Figs. 3 and 10). However, cardiac myocytes immunoreactive to HCN4 in the lower portion of the interatrial septum extended beyond the typical AVN region and their distribution coincided with the septal area that stained brown on AChE histochemistry (Figs. 9 and 10). Moreover, thick sleeves containing cells positive for HCN4 expanded toward the root of the ascending aorta and bundle of His, and thin slivers of these cells extended even alongside both atrioventricular rings (Figs. 10 and 11).

AChE-positive nerves enter the AVN mostly from the left ganglion cluster (LGC), which localizes near the roots of the left and middle pulmonary veins (Figs. 3, 6, 7, and 9). The LGC consists of several ganglia of differing size that contain variable numbers of ganglionic cells (Figs. 3, 6 and 7; Table 2). LGC ganglia were interconnected by numerous nerves that also connected them to the ganglia of the right ganglionic cluster (RGC) located near the dorsal interatrial groove, at the root of the right pulmonary vein (Figs. 3, 6, and 7). In general, the AVN region was supplied by a clearly identifiable septal endocardial nerve that arose from the LGC in the middle pulmonary vein (Figs. 6, 9, and 12). In all examined pressure-distended heart preparations, that nerve extended dorsoventrally on the right side of the interatrial septum, where it gradually became thinner, ramified and penetrated into the septal myocardium (Fig. 9).

Numerous ChAT and TH positive nerve bundles and fibers spread endocardially toward the AVN region (Fig. 12). At the ventral edge of the interatrial septum, the endocardial nerves branched out from the LGC and merged with a network of ChAT-positive and TH-positive nerve fibers that spread from the side of the ventral interatrial groove and aortic root (Fig. 12).

The typical AVN region contains a fine neural meshwork of cholinergic nerve fibers whose density is greater than the surrounding tissues.

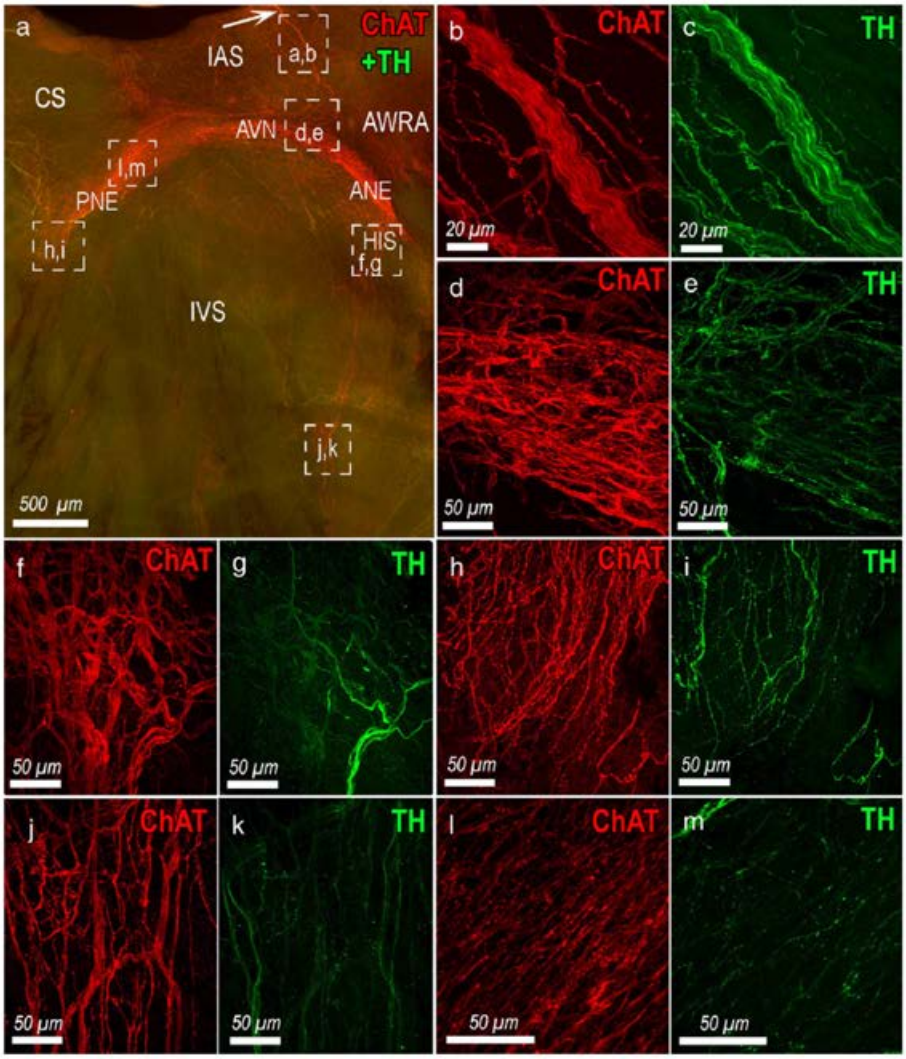

Fig. 12. Whole-mount preparation of the mouse interatrial and interventricular septa illustrating the intrinsic nerves proceeding on the right septal side toward the AVN region and the meshwork of cholinergic (ChAT, in red) and adrenergic (TH, in green) nerve fibers located in different areas of the cardiac septa. In order to expose the cardiac septa from the right side, the atrial and ventricular walls were removed and septa flattened as much as possible. The boxed areas in the left upper (a) panel are enlarged as b–m. Note the evident predominance of ChAT-IR fibers within the neural meshwork of the AVN and probable His bundle regions compared with TH-IR nerve fibers. White arrows point to the endocardial nerve and its branches that extend toward the AVN region. Abbreviations: ANE — anterior extension of AVN; AWRA — internal surface of anterior wall of right atrium; CS — internal surface of coronary sinus; AVN — atrioventricular nodal region; IAS — interatrial septum; IVS — interventricular septum; HIS — bundle of HIS; PNE — posterior extension of atrioventricular node.

Fig. 13. Whole-mount preparation of the mouse atrioventricular rings demonstrates the morphologic pattern of the neural meshwork of the AVN region and along the atrioventricular rings. The atria and ventricles were cut off to expose the AV rings from above. The boxed areas in the upper (a) panel are enlarged as b–m to illustrate the variable density of ChAT-IR and TH-IR neural networks in different areas of AVN region and AV rings. Cholinergic (ChAT-IR) nerve fibers are labeled in red, adrenergic (TH-IR) cells — in green, the merge immunoreactivity (ChAT + TH) is shown in a, d, g, j and m. Arrows indicate the epicardial nerves on the ventricles that are comprised mainly by adrenergic (TH-IR) nerve fibers. Abbreviations: ANE — anterior extension of atrioventricular node; AO — orifice of ascending aorta; AVN — atrioventricular node region; ALV, LLV, PLV — anterior lateral and posterior sides of left ventricle; ARV, LRV, PRV — anterior, lateral and posterior sides of right ventricle; PNE — posterior extension of atrioventricular node; PT — orifice of pulmonary trunk.

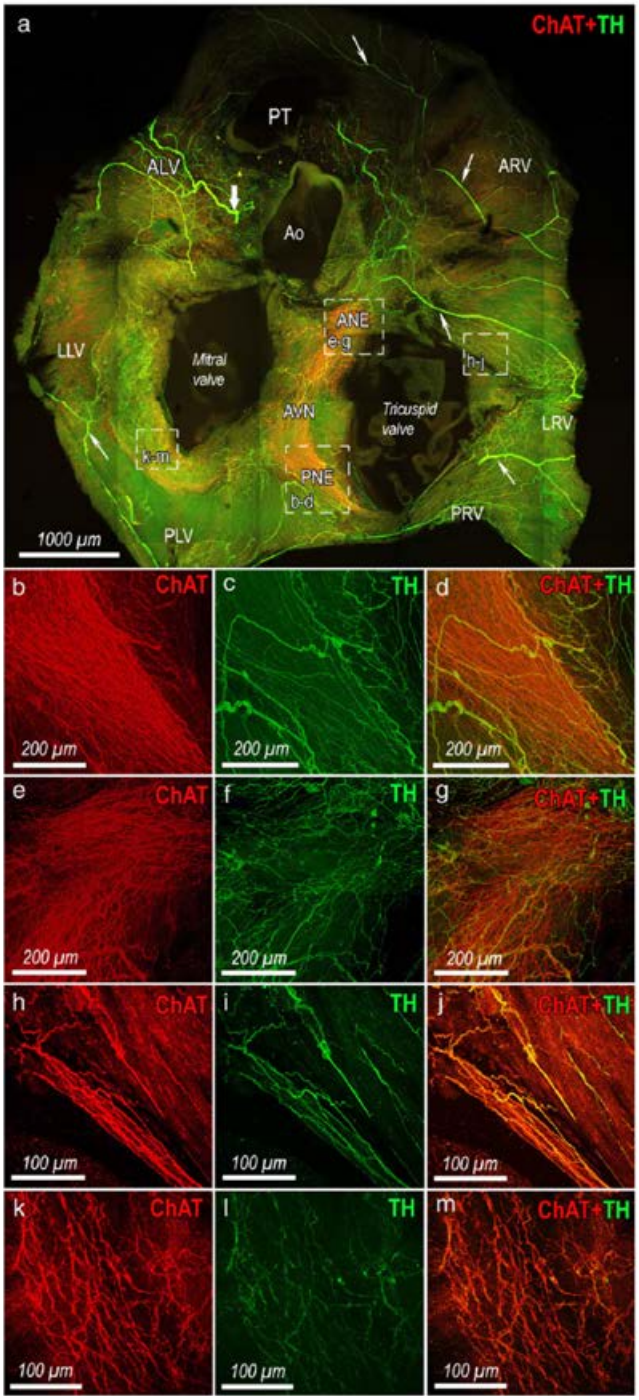
a
ChAT+TH
PT
ALV
ARV
Ao
ANE
e-g
h-j
LLV
Mitral valve
AVN
Tricuspid valve
LRV
k-m
PNE
b-d
PRV
1000 µm
PLV
b
ChAT
200 µm
c
TH
200 µm
d
ChAT+TH
200 µm
e
ChAT
200 µm
f
TH
200 µm
g
ChAT+TH
200 µm
h
ChAT
100 µm
i
TH
100 µm
j
ChAT+TH
100 µm
k
ChAT
100 µm
l
TH
100 µm
m
ChAT+TH
100 µm

Such a network occupies the entire lower portion of the interatrial septum (Figs. 12 and 13). Similar to the SAN region, in the AVN region cholinergic nerve fibers predominate over adrenergic fibers (Fig. 13).

In sharp contrast to either node, cells of the His bundle are weakly positive to HCN4 and accompanied by sparser cholinergic and adrenergic nerve fibers (Fig. 12). On the other hand, neither AVN nor His bundle seems to contain CGRP- or SP-positive nerve fibers.

3.3. The number of intrinsic nerve cells supplying the mouse SAN and AVN regions

The number, appearance and size of neural ganglia supplying the mouse SAN and AVN regions, as well as the number of neurons in these ganglia varied substantially from heart to heart, as summarized in Table 2. Nevertheless, quantitative confocal microscopy of ganglionic cells immunoreactive to PGP 9.5 suggests that approximately 1000 intrinsic cardiac neurons residing within the RGC may influence the function of the mouse SAN, whereas for the AVN, the number of such neurons inside the LGC is slightly lower (Table 2). However, the difference is not statistically significant.

4. Discussion

This neuroanatomical examination focuses on the intrinsic cardiac nerves and ganglia that are anatomically related to the mouse CCS. The morphologic pattern of the intrinsic CCS nerve plexus was revealed in non-sectioned, pressure-inflated hearts by histochemical AChE staining. The technique is particularly suitable for the purposes of investigating the topography and architecture of the fine intrinsic nerve plexuses in the mouse heart, and differs substantially from earlier neuroanatomical approaches of the mammalian CCS that relied on histological sections or flattened whole mounts. In addition, combined immunohistochemistry for TH, ChAT, and HCN4 allowed us to reveal the subtle dense intramural nerve meshwork in the CCS regions, as well as the functionally distinct nerve fibers proceeding via epicardial nerves from the ganglionated neural plexus of the heart hilum toward the various CCS regions. Based on stereomicroscopy, we demonstrate that the SAN is supplied only by 4 tiny but topographically persistent epicardial nerves derived from both the dorsal right atrial (3 nerves) and the right ventral (1 nerve) nerve subplexuses. Surprisingly, the AVN receives only 1 interatrial nerve originated from the left dorsal nerve subplexus. Immunohistochemically, all epicardial nerves entering the SAN region include both cholinergic and the adrenergic nerve fibers, but the cholinergic fibers predominate inside the interatrial nerve coursing toward the AVN region. The fine neural meshworks are appreciably denser in the SAN and AVN than the surrounding cardiac tissues. While in the mouse CCS cholinergic nerve fibers predominate, adrenergic nerve fibers constitute a particularly dense network as well.

The morphology of the CCS and its nerve supply have been studied in several animal species, including humans (Bojsen-Moller and Tranum-Jensen, 1971; Anderson, 1972a,b; Bojsen-Moller and Tranum-Jensen, 1972; Roberts et al., 1989; Crick et al., 1996b, 1999; Chow et al., 2001). In the above studies, the specialized tissues of the CCS were typically revealed using unspecific staining methods, i.e. histochemistry for AChE, Masson's trichrome, hematoxylin and eosin, methylene blue and toluidine blue stains. Employing immunohistochemistry for specific CCS markers like HCN4 (Baruscotti et al., 2005; Liu et al., 2007; Yanni et al., 2009), we managed to demonstrate clearly the distribution of the SAN and AVN in whole-mount preparations of the mouse heart.

The murine SAN has been described as a ~1.5 mm structure that extends parallel to the crista terminalis and is separated from atrial muscle by connective tissue at the border both with the crista terminalis and the atrial septum (Liu et al., 2007). Here we demonstrate that the mouse SAN is a poorly demarcated horseshoe-shaped collar around the root of the right cranial vein. The limits of distribution of the SAN cells in the right atrium are rather obscure; numerous slivers of SAN cells extend substantially in space from the main mass of the node toward the right atrial wall, the appendage, and the right cranial and caudal veins. Presumably, the demonstrated extensions of the SAN cells may impact action potential conduction from the SAN into the surrounding more hyperpolarized atrial muscle (Oosthoek et al., 1993; Verheijck et al., 1998; Boyett et al., 2000).

Here we demonstrate HCN4-positive cells within the typical AVN region and along both atrioventricular rings. This is only partly consistent with an earlier study in the rat heart that showed expression of HCN4 in the atrioventricular ring bundle (including the atrioventricular node) encircling the tricuspid valve, but not in the atrioventricular ring bundle encircling the mitral valve (Yamamoto et al., 2006). We show also that HCN4 positive myocytes outspread as a ventral extension of the AVN toward the root of the ascending aorta. Contrary to the AVN and atrioventricular (His) bundle, whose well-known roles are, respectively, to delay the electrical impulse from the atria and to relay that impulse from the AVN to the ventricular myocardium (Rozanski and Jalife, 1986; Anumonwo et al., 1990; McGuire et al., 1996), the functional value of the atrioventricular rings and the ventral AVN extension toward the root of the ascending aorta remains unclear. It is possible that in the mouse heart the expansive distribution of sleeves and thin slivers of HCN4-positive AV nodal cells may somehow relate to the weakly developed His bundle and its fascicles in the mouse cardiac ventricles as was demonstrated in the present study employing immunohistochemistry for HCN4 on whole-mount preparations.

Histochemical AChE staining of the intrinsic nerve plexus in the pressure-inflated hearts and subsequent stereomicroscopic examination enabled us to display both the precise topography and 3-dimensional architecture of the nerves coursing in the direction of the mouse CCS. In general, the neuroanatomy of the mouse CCS is comparable to the rat, guinea pig, and dog and even humans, but there are significant topographical species-dependent differences regarding SAN and AVN innervation. In dogs (Pauza et al., 1999, 2002), humans (Pauza et al., 2000), guinea pigs (Batulevicius et al., 2005), rats (Batulevicius et al., 2003), and sheep (Saburkina et al., 2010) the nerves supplying the SAN and AVN regions branch off from the ganglia located in the vicinity of the nodes; i.e., the root of the right cranial vein, the dorsal interatrial groove, the interatrial septum and the coronary sinus. In contrast, in the mouse heart such ganglia reside at comparatively larger distances from either node; i.e. the heart base of the left atrium, near the limits of the heart hilum.

We estimate that ~1000 intrinsic neurons residing within the right cluster at the interatrial groove of the left atrium are involved in the neural regulation of the mouse SAN. On the other hand, the mouse AVN receives neural input from ~860 intrinsic nerve cells laying in the left ganglion cluster beneath the opening of the middle pulmonary vein on the left atrium. Unfortunately, there is no direct evidence that all neurons located in ganglia innervate the mouse CCS regions and control cardiac impulse generation and conduction. Further functional studies will be necessary to prove this definitely, as was done in the rat heart, in which it was clearly shown that electrical stimulation of the right and the left neuronal clusters resulted in negative chronotropic and dromotropic effects in the SAN and AVN, respectively (Sampaio et al., 2003).

In this study, we demonstrated that there are abundant ChAT and TH-immunoreactive nerve fibers within all epicardial nerves entering the SAN and AVN regions, as well as in the fine dense nerve meshwork within each node. Previously, a dense and complex cholinergic innervation of the SAN and AVN regions was demonstrated based on histochemistry for AChE in mouse, rat, rabbit, dog, pig, calf and humans (Bojsen-Moller and Tranum-Jensen, 1972; Kent et al., 1974; Crick et al., 1994, 1996a; Petrecca and Shrier, 1998; Crick et al., 1999), as well as by immunohistochemistry to ChAT in the mouse (Rysevaite et al., 2011b) and to choline transporters in guinea pig (Hoover et al., 2004). However, we were unable to confirm the rank order in relative nerve density in the SAN, AVN and His bundle, as was reported by

Such a network occupies the entire lower portion of the interatrial septum (Figs. 12 and 13). Similar to the SAN region, in the AVN region cholinergic nerve fibers predominate over adrenergic fibers (Fig. 13).

In sharp contrast to either node, cells of the His bundle are weakly positive to HCN4 and accompanied by sparser cholinergic and adrenergic nerve fibers (Fig. 12). On the other hand, neither AVN nor His bundle seems to contain CGRP- or SP-positive nerve fibers.

3.3. The number of intrinsic nerve cells supplying the mouse SAN and AVN regions

The number, appearance and size of neural ganglia supplying the mouse SAN and AVN regions, as well as the number of neurons in these ganglia varied substantially from heart to heart, as summarized in Table 2. Nevertheless, quantitative confocal microscopy of ganglionic cells immunoreactive to PGP 9.5 suggests that approximately 1000 intrinsic cardiac neurons residing within the RGC may influence the function of the mouse SAN, whereas for the AVN, the number of such neurons inside the LGC is slightly lower (Table 2). However, the difference is not statistically significant.

4. Discussion

This neuroanatomical examination focuses on the intrinsic cardiac nerves and ganglia that are anatomically related to the mouse CCS. The morphologic pattern of the intrinsic CCS nerve plexus was revealed in non-sectioned, pressure-inflated hearts by histochemical AChE staining. The technique is particularly suitable for the purposes of investigating the topography and architecture of the fine intrinsic nerve plexuses in the mouse heart, and differs substantially from earlier neuroanatomical approaches of the mammalian CCS that relied on histological sections or flattened whole mounts. In addition, combined immunohistochemistry for TH, ChAT, and HCN4 allowed us to reveal the subtle dense intramural nerve meshwork in the CCS regions, as well as the functionally distinct nerve fibers proceeding via epicardial nerves from the ganglionated neural plexus of the heart hilum toward the various CCS regions. Based on stereomicroscopy, we demonstrate that the SAN is supplied only by 4 tiny but topographically persistent epicardial nerves derived from both the dorsal right atrial (3 nerves) and the right ventral (1 nerve) nerve subplexuses. Surprisingly, the AVN receives only 1 interatrial nerve originated from the left dorsal nerve subplexus. Immunohistochemically, all epicardial nerves entering the SAN region include both cholinergic and the adrenergic nerve fibers, but the cholinergic fibers predominate inside the interatrial nerve coursing toward the AVN region. The fine neural meshworks are appreciably denser in the SAN and AVN than the surrounding cardiac tissues. While in the mouse CCS cholinergic nerve fibers predominate, adrenergic nerve fibers constitute a particularly dense network as well.

The morphology of the CCS and its nerve supply have been studied in several animal species, including humans (Bojsen-Moller and Tranum-Jensen, 1971; Anderson, 1972a,b; Bojsen-Moller and Tranum-Jensen, 1972; Roberts et al., 1989; Crick et al., 1996b, 1999; Chow et al., 2001). In the above studies, the specialized tissues of the CCS were typically revealed using unspecific staining methods, i.e. histochemistry for AChE, Masson's trichrome, hematoxylin and eosin, methylene blue and toluidine blue stains. Employing immunohistochemistry for specific CCS markers like HCN4 (Baruscotti et al., 2005; Liu et al., 2007; Yanni et al., 2009), we managed to demonstrate clearly the distribution of the SAN and AVN in whole-mount preparations of the mouse heart.

The murine SAN has been described as a ~1.5 mm structure that extends parallel to the crista terminalis and is separated from atrial muscle by connective tissue at the border both with the crista terminalis and the atrial septum (Liu et al., 2007). Here we demonstrate that the mouse SAN is a poorly demarcated horseshoe-shaped collar around the root of the right cranial vein. The limits of distribution of the SAN cells in the right atrium are rather obscure; numerous slivers of SAN cells extend substantially in space from the main mass of the node toward the right atrial wall, the appendage, and the right cranial and caudal veins. Presumably, the demonstrated extensions of the SAN cells may impact action potential conduction from the SAN into the surrounding more hyperpolarized atrial muscle (Oosthoek et al., 1993; Verheijck et al., 1998; Boyett et al., 2000).

Here we demonstrate HCN4-positive cells within the typical AVN region and along both atrioventricular rings. This is only partly consistent with an earlier study in the rat heart that showed expression of HCN4 in the atrioventricular ring bundle (including the atrioventricular node) encircling the tricuspid valve, but not in the atrioventricular ring bundle encircling the mitral valve (Yamamoto et al., 2006). We show also that HCN4 positive myocytes outspread as a ventral extension of the AVN toward the root of the ascending aorta. Contrary to the AVN and atrioventricular (His) bundle, whose well-known roles are, respectively, to delay the electrical impulse from the atria and to relay that impulse from the AVN to the ventricular myocardium (Rozanski and Jalife, 1986; Anumonwo et al., 1990; McGuire et al., 1996), the functional value of the atrioventricular rings and the ventral AVN extension toward the root of the ascending aorta remains unclear. It is possible that in the mouse heart the expansive distribution of sleeves and thin slivers of HCN4-positive AV nodal cells may somehow relate to the weakly developed His bundle and its fascicles in the mouse cardiac ventricles as was demonstrated in the present study employing immunohistochemistry for HCN4 on whole-mount preparations.

Histochemical AChE staining of the intrinsic nerve plexus in the pressure-inflated hearts and subsequent stereomicroscopic examination enabled us to display both the precise topography and 3-dimensional architecture of the nerves coursing in the direction of the mouse CCS. In general, the neuroanatomy of the mouse CCS is comparable to the rat, guinea pig, and dog and even humans, but there are significant topographical species-dependent differences regarding SAN and AVN innervation. In dogs (Pauza et al., 1999, 2002), humans (Pauza et al., 2000), guinea pigs (Batulevicius et al., 2005), rats (Batulevicius et al., 2003), and sheep (Saburkina et al., 2010) the nerves supplying the SAN and AVN regions branch off from the ganglia located in the vicinity of the nodes; i.e., the root of the right cranial vein, the dorsal interatrial groove, the interatrial septum and the coronary sinus. In contrast, in the mouse heart such ganglia reside at comparatively larger distances from either node; i.e. the heart base of the left atrium, near the limits of the heart hilum.

We estimate that ~1000 intrinsic neurons residing within the right cluster at the interatrial groove of the left atrium are involved in the neural regulation of the mouse SAN. On the other hand, the mouse AVN receives neural input from ~860 intrinsic nerve cells laying in the left ganglion cluster beneath the opening of the middle pulmonary vein on the left atrium. Unfortunately, there is no direct evidence that all neurons located in ganglia innervate the mouse CCS regions and control cardiac impulse generation and conduction. Further functional studies will be necessary to prove this definitely, as was done in the rat heart, in which it was clearly shown that electrical stimulation of the right and the left neuronal clusters resulted in negative chronotropic and dromotropic effects in the SAN and AVN, respectively (Sampaio et al., 2003).

In this study, we demonstrated that there are abundant ChAT and TH-immunoreactive nerve fibers within all epicardial nerves entering the SAN and AVN regions, as well as in the fine dense nerve meshwork within each node. Previously, a dense and complex cholinergic innervation of the SAN and AVN regions was demonstrated based on histochemistry for AChE in mouse, rat, rabbit, dog, pig, calf and humans (Bojsen-Moller and Tranum-Jensen, 1972; Kent et al., 1974; Crick et al., 1994, 1996a; Petrecca and Shrier, 1998; Crick et al., 1999), as well as by immunohistochemistry to ChAT in the mouse (Rysevaite et al., 2011b) and to choline transporters in guinea pig (Hoover et al., 2004). However, we were unable to confirm the rank order in relative nerve density in the SAN, AVN and His bundle, as was reported by

Crick et al. in calf and guinea pig hearts (Crick et al., 1996a, 1999). The whole-mount preparations used in our study revealed a homogeneous dense network of ChAT nerve fibers within both SAN and AVN regions, and a comparatively sparser network along the His bundle. Nevertheless, the presence of abundant adrenergic nerve fibers in both nodes of the mouse CCS suggests that apparently both are under significant adrenergic influence as well. Therefore, our observations in the mouse contrast with earlier reports in other mammalian species, including humans, in which cholinergic nerve fibers and muscarinic receptors represent the predominant population within the nodes and reflect the superiority of the inhibitory cholinergic system in cardiac conductivity (Crick et al., 1994). As such, the present findings provide a novel anatomical basis for further physiological experiments, especially those aimed at improving the treatment of cardiac arrhythmia by experimental ablation of distinct atrial areas (Bernstein et al., 2011).

Acknowledgments

The authors sincerely thank Mrs. Rima Masiene and Mrs. Nida Rutkauskiene for technical assistance throughout the study. This study was supported by the Grant No. MIP-11184 from the Research Council of Lithuania.

References

Aanhaanen, W.T., Mommersteeg, M.T., Norden, J., Wakker, V., de Gier-de, Vries C., Anderson, R.H., Kispert, A., Moorman, A.F., Christoffels, V.M., 2010. Developmental origin, growth, and three-dimensional architecture of the atrioventricular conduction axis of the mouse heart. Circ. Res. 107, 728–736.

Anderson, R.H., 1972a. The disposition and innervation of atrioventricular ring specialized tissue in rats and rabbits. J. Anat. 113, 197–211.

Anderson, R.H., 1972b. The disposition, morphology and innervation of cardiac specialized tissue in the guinea-pig. J. Anat. 111, 453–468.

Anderson, R.H., Yanni, J., Boyett, M.R., Chandler, N.J., Dobrzynski, H., 2009. The anatomy of the cardiac conduction system. Clin. Anat. 22, 99–113.

Anumonwo, J.M., Delmar, M., Jalife, J., 1990. Electrophysiology of single heart cells from the rabbit tricuspid valve. J. Physiol. 425, 145–167.

Baruscotti, M., Bucchi, A., Difrancesco, D., 2005. Physiology and pharmacology of the cardiac pacemaker ("funny") current. Pharmacol. Ther. 107, 59–79.

Batulevicius, D., Pauziene, N., Pauza, D.H., 2003. Topographic morphology and age-related analysis of the neuronal number of the rat intracardiac nerve plexus. Ann. Anat. 185, 449–459.

Batulevicius, D., Pauziene, N., Pauza, D.H., 2005. Architecture and age-related analysis of the neuronal number of the guinea pig intrinsic cardiac nerve plexus. Ann. Anat. 187, 225–243.

Bernstein, S.A., Duggirala, S., Floberg, M., Elfvendal, P., Kuznekoff, L.M., Lader, J.M., Vasquez, C., Morley, G.E., 2011. Spatiotemporal electrophysiological changes in a murine ablation model. Europace 13, 1494–1500.

Bojsen-Moller, F., Tranum-Jensen, J., 1971. Whole-mount demonstration of cholinesterase-containing nerves in the right atrial wall, nodal tissue, and atrioventricular bundle of the pig heart. J. Anat. 108, 375–386.

Bojsen-Moller, F., Tranum-Jensen, J., 1972. Rabbit heart nodal tissue, sinuatrial ring bundle and atrioventricular connexions indentified as a neuromuscular system. J. Anat. 112, 367–382.

Boyett, M.R., Honjo, H., Kodama, I., 2000. The sinoatrial node, a heterogeneous pacemaker structure. Cardiovasc. Res. 47, 658–687.

Chow, L.T., Chow, S.S., Anderson, R.H., Gosling, J.A., 2001. Autonomic innervation of the human cardiac conduction system: changes from infancy to senility—an immunohistochemical and histochemical analysis. Anat. Rec. 264, 169–182.

Crick, S.J., Wharton, J., Sheppard, M.N., Royston, D., Yacoub, M.H., Anderson, R.H., Polak, J.M., 1994. Innervation of the human cardiac conduction system. A quantitative immunohistochemical and histochemical study. Circulation 89, 1697–1708.

Crick, S.J., Sheppard, M.N., Anderson, R.H., Polak, J.M., Wharton, J., 1996a. A quantitative assessment of innervation in the conduction system of the calf heart. Anat. Rec. 245, 685–698.

Crick, S.J., Sheppard, M.N., Anderson, R.H., Polak, J.M., Wharton, J., 1996b. A quantitative study of nerve distribution in the conduction system of the guinea pig heart. J. Anat. 188 (Pt 2), 403–416.

Crick, S.J., Sheppard, M.N., Ho, S.Y., Anderson, R.H., 1999. Localisation and quantitation of autonomic innervation in the porcine heart I: conduction system. J. Anat. 195, 341–357.

Dickie, R., Bachoo, R.M., Rupnick, M.A., Dallabrida, S.M., Deloid, G.M., Lai, J., Depinho, R.A., Rogers, R.A., 2006. Three-dimensional visualization of microvessel architecture of whole-mount tissue by confocal microscopy. Microvasc. Res. 72, 20–26.

Glukhov, A.V., Fedorov, V.V., Anderson, M.E., Mohler, P.J., Efimov, I.R., 2010. Functional anatomy of the murine sinus node: high-resolution optical mapping of ankyrin-B heterozygous mice. Am. J. Physiol. Heart Circ. Physiol. 299, H482–H491.

Halpern, M.H., 1955. The sino-atrial node of the rat heart. Anat. Rec. 123, 425–435.

Halpern, M.H., 1957. The dual blood supply of the rat heart. Am. J. Anat. 101, 1–16.

Hoover, D.B., Ganote, C.E., Ferguson, S.M., Blakely, R.D., Parsons, R.L., 2004. Localization of cholinergic innervation in guinea pig heart by immunohistochemistry for high-affinity choline transporters. Cardiovasc. Res. 62, 112–121.

Kent, K.M., Epstein, S.E., Cooper, T., Jacobowitz, D.M., 1974. Cholinergic innervation of the canine and human ventricular conducting system. Anatomic and electrophysiologic correlations. Circulation 50, 948–955.

Lang, D., Glukhov, A.V., Efimova, T., Efimov, I.R., 2011. Role of Pyk2 in cardiac arrhythmogenesis. Am. J. Physiol. Heart Circ. Physiol. 301, H975–H983.

Liu, J., Dobrzynski, H., Yanni, J., Boyett, M.R., Lei, M., 2007. Organisation of the mouse sinoatrial node: structure and expression of HCN channels. Cardiovasc. Res. 73, 729–738.

McGuire, M.A., de Bakker, J.M., Vermeulen, J.T., Moorman, A.F., Loh, P., Thibault, B., Vermeulen, J.L., Becker, A.E., Janse, M.J., 1996. Atrioventricular junctional tissue. Discrepancy between histological and electrophysiological characteristics. Circulation 94, 571–577.

Oosthoek, P.W., Viragh, S., Mayen, A.E., van Kempen, M.J., Lamers, W.H., Moorman, A.F., 1993. Immunohistochemical delineation of the conduction system. I: The sinoatrial node. Cardiovasc. Res. 73, 473–481.

Pauza, D.H., Skripka, V., Pauziene, N., Stropus, R., 1999. Anatomical study of the neural ganglionated plexus in the canine right atrium: implications for selective denervation and electrophysiology of the sinoatrial node in dog. Anat. Rec. 255, 271–294.

Pauza, D.H., Skripka, V., Pauziene, N., Stropus, R., 2000. Morphology, distribution, and variability of the epicardiac neural ganglionated subplexuses in the human heart. Anat. Rec. 259, 353–382.

Pauza, D.H., Skripka, V., Pauziene, N., 2002. Morphology of the intrinsic cardiac nervous system in the dog: a whole-mount study employing histochemical staining with acetylcholinesterase. Cells Tissues Organs 172, 297–320.

Petrecca, K., Shrier, A., 1998. Spatial distribution of nerve processes and beta-adrenoreceptors in the rat atrioventricular node. J. Anat. 192, 517–528.

Roberts, L.A., Slocum, G.R., Riley, D.A., 1989. Morphological study of the innervation pattern of the rabbit sinoatrial node. Am. J. Anat. 185, 74–88.

Rose, R.A., Sellan, M., Simpson, J.A., Izaddoustdar, F., Cifelli, C., Panama, B.K., Davis, M., Zhao, D., Markhani, M., Murphy, G.G., Striessnig, J., Liu, P.P., Heximer, S.P., Backx, P.H., 2011. Iron overload decreases CaV1.3-dependent L-type Ca2 + currents leading to bradycardia, altered electrical conduction, and atrial fibrillation. Circulation 4, 733–742.

Rozanski, G.J., Jalife, J., 1986. Automaticity in atrioventricular valve leaflets of rabbit heart. Am. J. Physiol. 250, H397–H406.

Rysevaite, K., Saburkina, I., Pauziene, N., Noujaim, S.F., Jalife, J., Pauza, D.H., 2011a. Morphologic pattern of the intrinsic ganglionated nerve plexus in mouse heart. Heart Rhythm 8, 448–454.

Rysevaite, K., Saburkina, I., Pauziene, N., Vaitkevicius, R., Noujaim, S.F., Jalife, J., Pauza, D.H., 2011b. Immunohistochemical characterization of the intrinsic cardiac neural plexus in whole-mount mouse heart preparations. Heart Rhythm 8, 731–738.

Saburkina, I., Pauza, D.H., 2006. Location and variability of epicardiac ganglia in human fetuses. Anat. Embryol. (Berl) 6, 585–594.

Saburkina, I., Rysevaite, K., Pauziene, N., Mischke, K., Schauerte, P., Jalife, J., Pauza, D.H., 2010. The epicardial neural ganglionated plexus of the ovine heart: anatomical basis for experimental cardiac electrophysiology and nerve protective cardiac surgery. Heart Rhythm 7, 942–950.

Sampaio, K.N., Mauad, H., Spyer, K.M., Ford, T.W., 2003. Differential chronotropic and dromotropic responses to focal stimulation of cardiac vagal ganglia in the rat. Exp. Physiol. 88, 315–327.

Verheijck, E.E., Wessels, A., van Ginneken, A.C., Bourier, J., Markman, M.W., Vermeulen, J.L., de Bakker, J.M., Lamers, W.H., Opthof, T., Bouman, L.N., 1998. Distribution of atrial and nodal cells within the rabbit sinoatrial node: models of sinoatrial transition. Circulation 97, 1623–1631.

Verheijck, E.E., van Kempen, M.J., Veereschild, M., Lurvink, J., Jongsma, H.J., Bouman, L.N., 2001. Electrophysiological features of the mouse sinoatrial node in relation to connexin distribution. Cardiovasc. Res. 52, 40–50.

Yamamoto, M., Dobrzynski, H., Tellez, J., Niwa, R., Billeter, R., Honjo, H., Kodama, I., Boyett, M.R., 2006. Extended atrial conduction system characterised by the expression of the HCN4 channel and connexin45. Cardiovasc. Res. 72, 271–281.

Yanni, J., Boyett, M.R., Anderson, R.H., Dobrzynski, H., 2009. The extent of the specialized atrioventricular ring tissues. Heart Rhythm 6, 672–680.

SUMMARY

ABBREVATIONS

AChE – acetylcholinesterase
ANS – autonomic nervous system
CCS – cardiac conductive system
ChAT – choline acetyltransferase
CV – caudal vein
HCN4 – hyperpolarization activated cyclic nucleotide-gated potassium channel 4
MPV – middle pulmonary vein
NA – nodal artery
NFs – nerve fibers
nNOS – neuronal nitric oxide synthase
PGP9.5 – protein gene product 9.5
RA – right atrium
RCV – right cranial vein
RPV – right pulmonary vein
RRCV – root of the right cranial vein
SAN – sinoatrial node
SP – substance P
TH – tyrosine hydroxylase

BACKGRUOND AND NOVELTY OF THE STUDY

Autonomic nervous system (ANS) modulates cardiac conductive system (CCS) activity and its abnormal activity may lead to arrhythmias or even sudden death [1]. The sinoatrial node (SAN) is the primary pacemaking component that generates the electric impulse in heart [2]. Morphology, neuromorphology and physiology of SAN are an object of interest since it was discovered [3, 4].

To date morphological studies of SAN usually focused either on its myocardial anatomy or innervation [4–6]. Earlier neuroanatomical studies were performed only on cross section preparations and only a few used whole mounts [6–8]. Neuroanatomical studies that performed a quantitative analysis of SAN neural components were based on histochemical acetylcholinesterase (AChE) method as cholinergic marker, combining it with histochemical methods to detect adrenergic and sensory neural components. These studies revealed that cholinergic neural components are dominant ones in all parts of the CCS [8, 9]. However, AChE is criticized as non-selective method by many investigators [10–12]. Since acetylcholine is synthesized by the choline acetyltransferase (ChAT) in cholinergic neurons [13], this enzyme is suggested as a reliable marker of cholinergic neural components [10–12]. There is a lack of studies that used this marker in general cardiac innervation [14–16], not to mention the neuroanatomy of CCS.

Hearts of mouse, rabbit and pig are a widely used in cardio physiological experiments. To date, there are only few studies that analyzed both, the distribution of pacemaker cells and their innervation. Besides there are no studies that examined interspecific differences of these structures in the aforementioned cardio physiological models. This is the first study that simultaneously analyzed both innervation and structure of SAN in whole mount and cross section preparations, by using a multiple imunohistochemical staining for pacemaker cells and neural components.

Results of this study showed that the distribution of pacemaker cells is much wider and the innervation of SAN cells is more complex than it was considered before. It also revealed the distribution of nerve fibers of distinct chemical phenotype in different zones within the sinoatrial node. In addition to this, the immunohistochemical analysis of neurons within sinoatrial node was conducted for the first time. Finally, a novel finding, nitrergic neurons that were purely positive for neuronal nitric oxide synthase (nNOS), was observed in this study.

AIM OF AND OBJECTIVES OF THE STUDY

The aim of the study: to identify limits and innervation of the sinoatrial node in hearts of mice, rabbits and pigs.

Objectives:

1. To examine the distribution of pacemaker cells within the right atrium.
2. To examine the density of innervation within the sinoatrial node.
3. To examine the distribution of neuronal somata within the sinoatrial node.
4. To examine neurochemical properties of neurons within the sinoatrial node.
5. To compare the morphology of neurons within the sinoatrial node.

MATERIAL AND METHODS

25 mice, 22 rabbits and 21 piglets and 3 young adult pigs' hearts were used in this study. A multiple immunohistochemical staining for HCN4 (pacemaker cells), ChAT (cholinergic neurons), TH (adrenergic neurons), nNOS (nitrergic neurons) and SP (sensory neurons) markers, were applied on whole mount and cross section preparations.

Whole-mount preparations

Following animal euthanasia, hearts were dissected from the chest, washed out from the blood with 0.01M phosphate buffer saline (PBS) and coronary vessels were retrogradely perfused with PBS. Afterwards, the atria were dissected from the ventricles and the interatrial septum. Then, the atria was flattened and pinned in a Petri dish with a silicone bottom. The flattened specimen was fixed for 40 min at 4° C in 4% paraformaldehyde solution in 0.01 M phosphate buffer (pH=7.4). In order to decrease background light for laser scanning microscopic examination, tissues were bleached using a dimethyl sulfoxide and hydrogen peroxide solution. Subsequently, whole-mount preparations were rehydrated through a graded ethanol series (in each for 10 min), washed 3×10 min in 0.01 M PBS containing 0.5% Triton X–100. Non–specific binding was blocked for 2 hours in PBS containing 5% normal donkey serum. Afterwards, the specimens were incubated with an appropriate combination of primary antisera for 48–72 hours at 4° C (Table 1). After that, whole-mounts were washed 3 times for 10 min in 0.01 M PBS and incubated with an appropriate combination of secondary antisera for 4 hours at room temperature. During

the last stage, specimens were washed 3 times for 10 min in 0.01 M PBS, mounted with mounting medium, cover slipped and sealed with clear nail polish.

Sectioned tissue preparations

In order to obtain transverse sections of walls of the right atrium (RA) and root of the right cranial vein (RRCV), hearts were dissected, perfused and prefixed as described above. In order to compare the densities of NFs distributed between cardiac cells positive for HNC4 distinct localities on RRCV, specimens were taken from 3 specific zones in SAN region: (1) from frontal part of RCV, (2) lateral part of RCV, (3) between dorsal part of RCV and CV. Following 40 min fixation at 4° C in 4% paraformaldehyde solution in 0.01 M phosphate buffer (pH=7.4), tissues were washed 3x10 min in PBS and cryoprotected by immersion in PBS containing 20–25% sucrose until their complete sinking (4° C, 24 h). Then, following cryoprotection, the tissues were frozen for sectioning. The pieces of the sampled tissues were orientated on a cryomicrotome stage so that the slice cutting plane would be perpendicular to the interatrial septum, the right atrial wall and the terminal groove and all layers (epicardium, myocardium and endocardium) could be well discernible in the slice. Tissues were sectioned into 20 μm slices using a cryomicrotome at –22° C and sections were mounted onto microscope slides. Afterwards, immunohistochemical procedures were performed as earlier described by applying an appropriate combination of primary and secondary antisera (Table 1). Finally, specimens were washed 3 times for 5 min in 0.01 M PBS and mounted with mounting medium and cover slipped.

Quantitative and statistical analysis

Both whole-mount preparations and RA wall transverse sections, in which immunohistochemical reactions were the most contrast and sharp, were used for quantitative analysis. The size of clearly visible neuronal somata was measured on digital images and expressed as the mean of their long and short axes. The densities of NFs within distinct portions of the SAN area were evaluated in transverse sections. The density of NFs was expressed in percentage of the area occupied by NFs.

Ganglia and neurons were calculated in whole mount preparations. Ganglia size was evaluated by the number of neurons within. Long and short axes of neurons were measured. Diameter of somata was expressed by the mean of short and long axis.

Table 1. *Primary and secondary antisera used in the study*

Antigen	Host	Dilution	Company	Catalog number.
Primary:				
ChAT	Goat	1:100	Chemicon[1]	AB144P
TH	Rabbit	1:500	Chemicon[1]	AB152
TH	Mouse	1:200	Chemicon[1]	MAB-318
TH	Sheep	1:800	Chemicon[1]	AB1542
SP	Guinea pig	1:1000	Abcam[2]	AB1053
SP	Rabbit	1:800	ImmunoStar[3]	20064
PGP 9.5	Mouse	1:200	ABD Serotec[4]	7863-1004
PGP 9.5	Rabbit	1:500	ABD Serotec[4]	7869-0504
HCN4	Mouse	1:200	StressMarq Biosciences[5]	SMC-320D
HCN4	Rabbit	1:100	Chemicon[1]	AB5808
nNOS	Mouse	1:500	Santa Cruz Biotechonology[6]	SC-5302
Secondary:				
Goat ^{Cy3}	Donkey	1:300	Chemicon[1]	AP180C
Mouse ^{Cy3}	Donkey	1:300	Chemicon[1]	AP192C
Mouse $^{DyLight\ ®488}$	Donkey	1:300	Abcam[3]	AB96875
Mouse ^{FITC}	Donkey	1:100	Jackson Immunoresearch[7]	715-095-151
Sheep ^{FITC}	Donkey	1:100	Chemicon[1]	AP184F
Guinea pig ^{FITC}	Donkey	1:100	Chemicon[1]	AP193F
Rabbit ^{Cy3}	Donkey	1:300	Chemicon[1]	AP182C
Rabbit ^{FITC}	Donkey	1:100	Chemicon[1]	AP182F

[1]Chemicon International, Temecula, California, USA.
[2]Abcam, Cambridge, UK.
[3]ImmunoStar Incorporation, Wisconsin, USA.
[4]AbD Serotec, Kidlington, UK.
[5]StressMarq Biosciences Incorporation, Cadboro Bay, Victoria, Canada.
[6]Santa Cruz Biotechnology, Dallas, TX, USA.
[7]Jackson Immunoresearch, West Grove, PA, USA.

RESULTS

Distribution of HCN4 cells in SAN area

HCN4 positive cells were similarly distributed around RCV in all investigated species (Fig. 1). The main mass of cells formed a "hook" shape figure around RCV, which started in the frontal part of RCV and extended downward to CV and almost reached its orifice. HCN4 cells occupied 3.1±0.1 mm^2 in mouse, 18.0±2.4 mm^2 rabbit and 52.2±5.2 mm^2 pig area of RA. Some minor interspecific differences were also observed. HCN4 cells formed thin bundle in the medial side of RCV in mouse SAN different than in rabbit and pig. In the medial side of RCV of rabbit and pig HCN4 cells were not observed.

Due to a wide distribution of HCN4 positive cells, SAN was divided into 3 parts (Fig. 1): "head" (at frontal part of RCV), "body" (at lateral part of RCV) and "tail" (rest of the area to caudal vein).

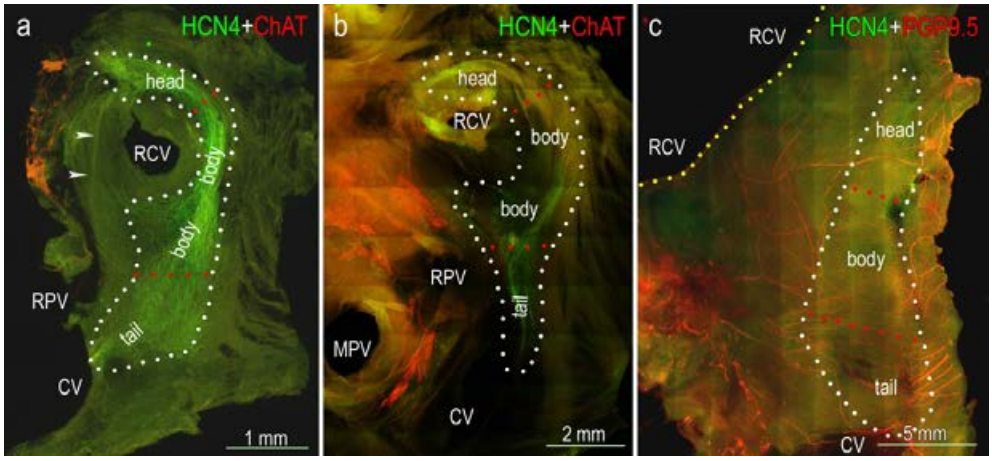

Fig. 1. *The distribution of HCN4 cells around RCV in mouse (a), rabbit (b) and pig (c) whole mount preparations.*

White dotted line demarks the area of HCN4 cells. Red dotted line demarks the limits of zones (head, body and tail). Yellow dotted line demarks the orifice of RCV (box c). Arrowheads in box (a) indicate some HCN4 cells in the medial side of RCV. CV – caudal; vein; MPV – middle pulmonary vein; RPV – right pulmonary vein; RVC – right cranial vein.

Whole mount preparations revealed that SAN is uninterrupted structure. However, it was possible to distinguish central and peripheral parts of the node in both whole mount and cross section preparations. The central part of the node was formed by the main mass of HCN4 positive cells. In this

region HCN4 cells were densely distributed and clustered in several layers. Peripheral part of SAN consisted of HCN4 cells "sleeves" that extended far the main mass node to the right atria myocardium (Fig. 2). In frontal part of the node these structures almost reached the roots of aorta and atrioventricular groove in lateral. These "sleeves" looked like a solitary HCN4 positive cells in cross section preparations.

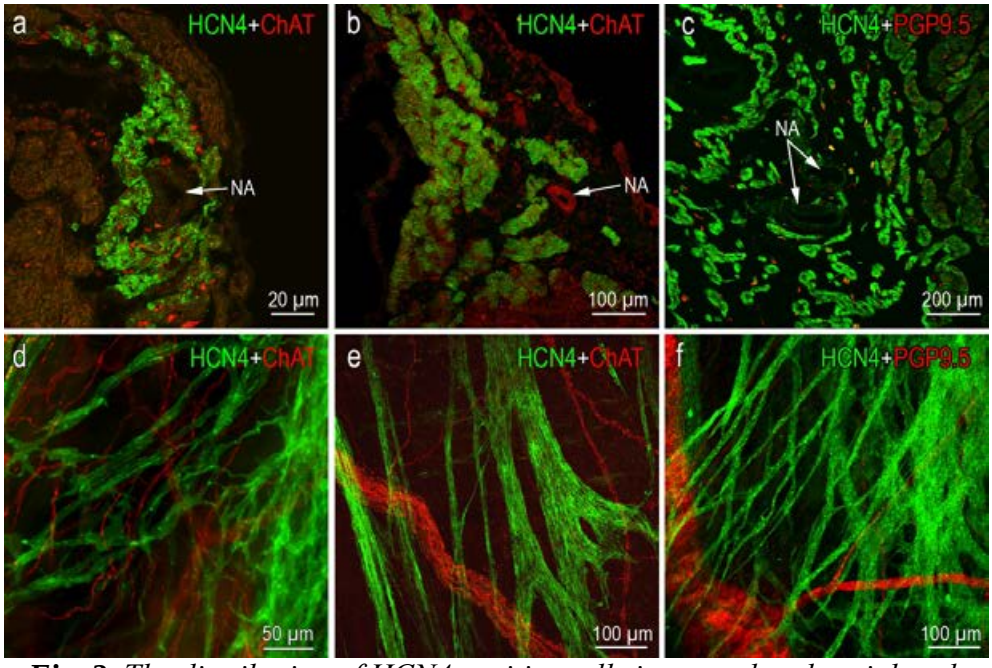

Fig. 2. *The distribution of HCN4 positive cells in central and peripheral parts of SAN.*

HCN4 cells around SAN artery in (a) mouse, (b) rabbit and (c) pig SAN center in cross section preparations. HCN4 peripheral "sleeves" in whole mount preparations of (d) mouse, (e) rabbit and (f) pig SAN. NA – nodal artery.

Various distributions of HCN4 cells were observed within atria wall in different zones of the node. In the head of SAN they formed a thin plate widely spread right under epicardium. In body of SAN these cells were distributed throughout the whole myocardial wall around the nodal artery or its branches and in the tail of the node cells formed a thin bundle close to endocardium.

Innervation of SAN

SAN contained a dense meshwork of NFs that corresponded to the area of HCN4 cells in all investigated species. The density of NFs in SAN area was ~4 times higher than in working myocardium in all investigated species. The highest density of nerve fibres in mouse and rabbit SAN was observed within head and the lowest in tail. The highest density of NFs in pig SAN was observed in body and the lowest in tail.

NFs densities of distinct neurochemical phenotype were analysed more detailed in rabbit and pig SAN. TH NFs were dominant in both species. Another big group of NFs were ChAT positive. SP and nNOS NFs took the minority. SP NFs were distributed equally in all areas of SAN in both species.

Neurons and ganglia within the sinoatrial node

No neuronal somata were found in mouse SAN. Neurons and ganglia were present in the area of rabbit and pig SAN. Most of neurons and nerves in rabbit SAN were found within epicardial layer. Ganglia and nerves in pig SAN were also found descended into myocardium (Fig. 3). Such ganglia were observed interrupted between the clusters of HCN4 cells.

Solitary neurons and small ganglia (3.6±0.3 neurons in each) were typical for rabbit SAN. In general rabbit SAN contained 57.7±10 neurons. 78.6±6.0 % of neurons were clustered in small ganglia. The biggest number of ganglia consisted of 2–4 neurons, and only few, 5 or more neuronal somata. 21.4±6.0 % of all observed nerve cells were scattered solitary (Fig. 4).

Pigs SAN contained 97.5±10.1 that consisted of 21.3±2.4 neurons (~2000 neurons per SAN). Solitary neurons were also observed, but number of these cells were insignificant (<10 neurons per SAN). Based on size, ganglia were divided into groups as follows: small (≤10 neurons); medium (11–50 neurons); big (51–100); very big (>100 neurons).

Small and medium sized ganglia took the majority. The biggest number of neurons was observed in medium sized and the lowest in small ganglia (Fig. 4).

Size of neurons varied between species. Pig's SAN neurons were bigger (19.2±0.3 μm) than rabbit's (16.5±0.2 μm). Solitary neurons in rabbit SAN were bigger (17.2±0.6 μm) than those observed in SAN ganglia (16.2±0.3 μm).

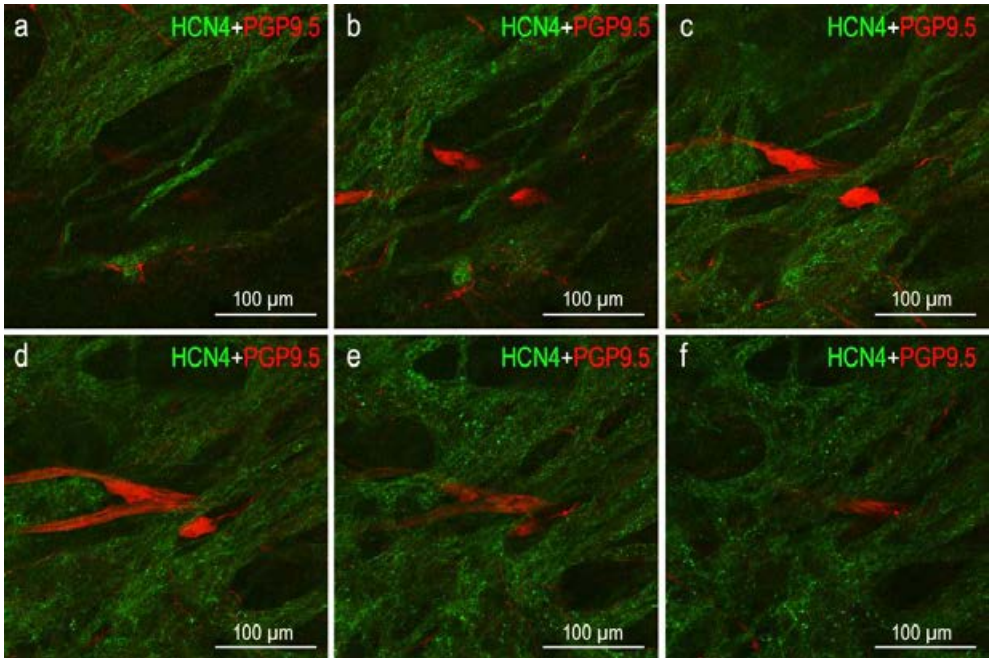

Fig. 3. *Nerves and neurons interrupted between the clusters of HCN4 positive cells.*

a – f optical sections in different depth, from the epicardium (a) down to endocardium (f).

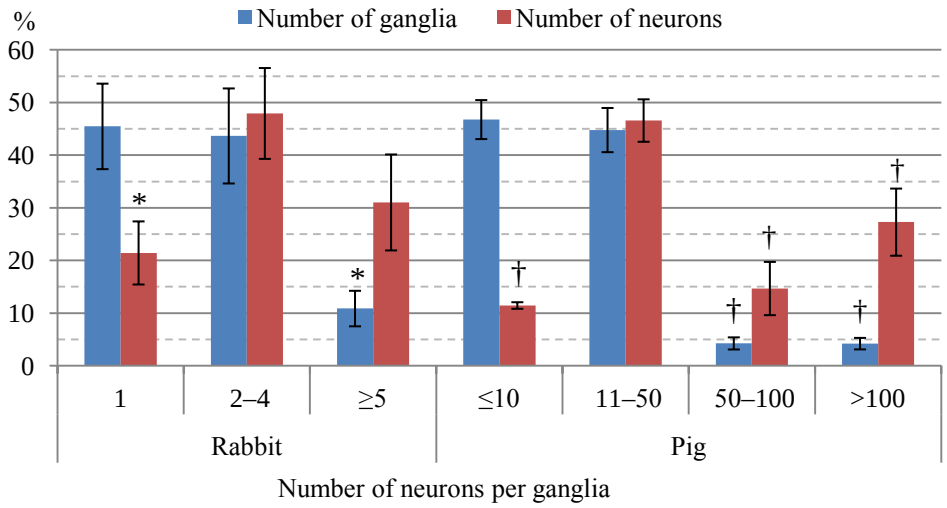

Fig. 4. *The distribution of various size ganglia and neurons within ganglia in rabbit and pig SAN.*

*Significantly different from ganglia that consisted of 2–4 neuros in rabbit's SAN ($p<0.05$).
†Significantly different from ganglia that consisted of 11–50 neurons in pig's SAN ($p<0.05$).

The variety of neurons within sinoatrial node

3 phenotypes of neurons were observed in rabbit SAN that were positive for ChAT, nNOS and biphenotypic – ChAT+nNOS (Fig. 5). In general, ChAT neurons were dominant ones and contained 50.3±4.9 % of all observed neural cells (Fig. 6). 35.5±4.2 % neurons were biphenotypic and 14.2±1.7 % nNOS positive.

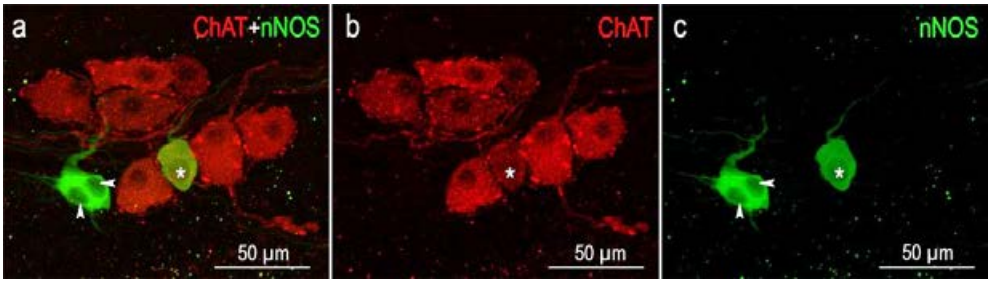

Fig. 5. *Several neuronal somata positive for ChAT (in red), nNOS (in green), and simultaneously for both neuronal markers.*
Biphenotypic neuronal soma is marked with asterisk (boxes a–c). Arrowheads points to purely nNOS positive neurons (boxes a, c).

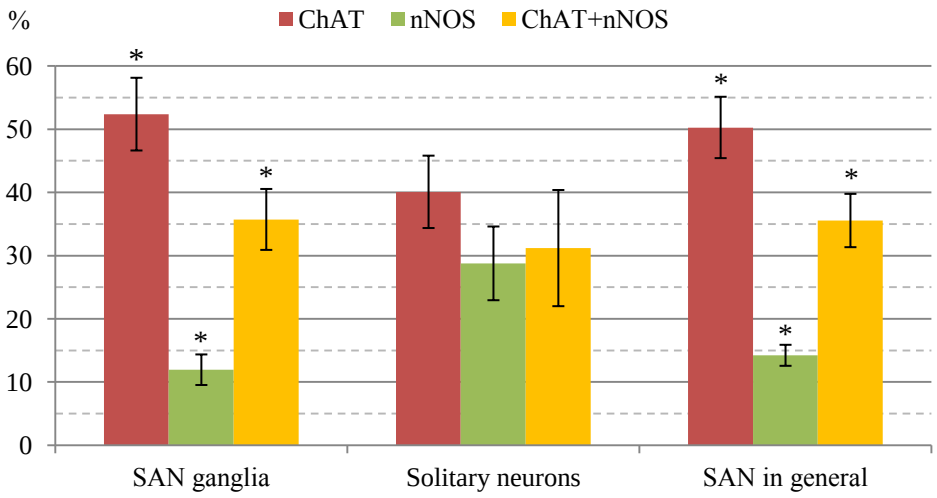

Fig. 6. *The distribution of neurons of distinct phenotype in rabbit SAN.*
*Statistically different between the groups of cells of distinct chemical phenotype.

Some differences of distributions were observed between solitary and SAN ganglia neurons groups. Solitary neurons of distinct neurochemical

type were distributed equally. In SAN ganglia ChAT positive neurons were dominant and the smallest group was purely nNOS positive cells.

5 chemical phenotypes of neural cells were observed in pig's SAN. These neurons were purely positive for ChAT, nNOS, TH and biphenotypic – positive for ChAT+nNOS and TH+ChAT. SIF cells were also observed in this area (Fig. 7).

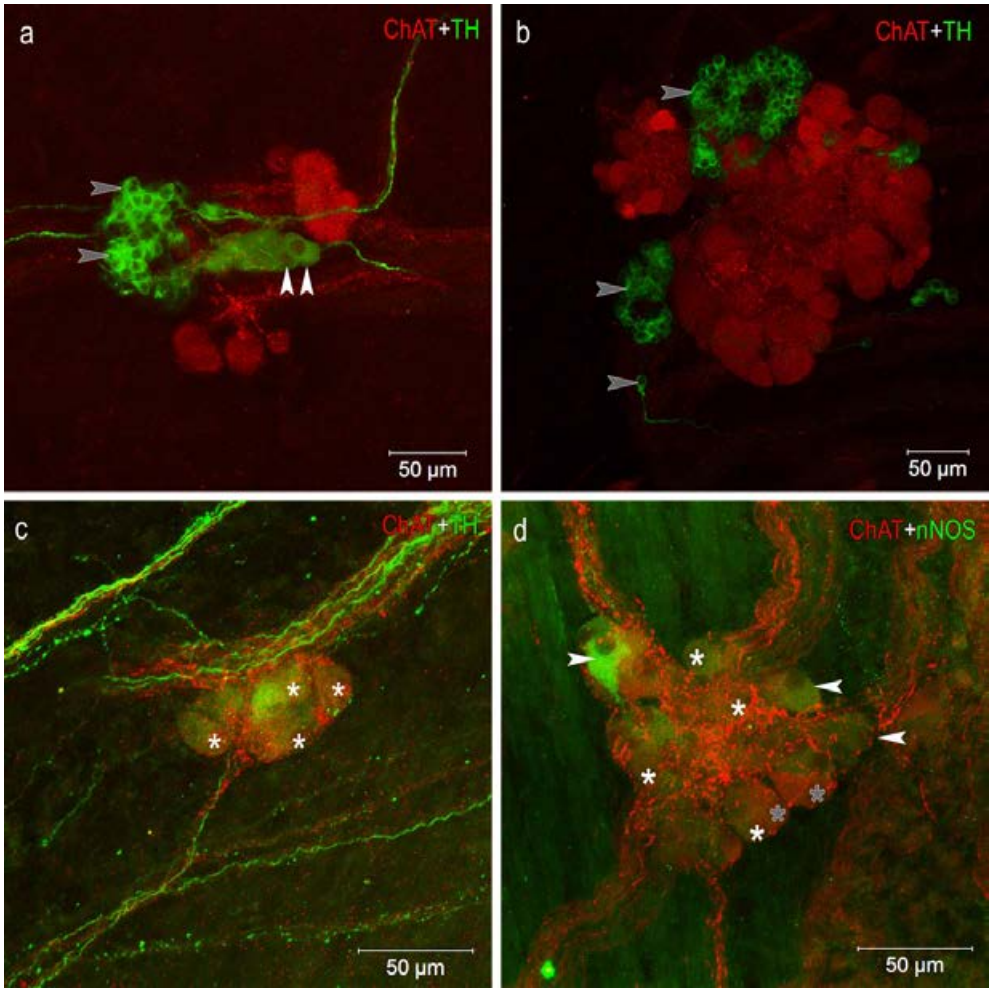

Fig. 7. *Neurochemical variety of neurons within pig's SAN.*
a – white arrowheads point to TH positive neurons. a–b grey arrowheads point to SIF cells. c – asterisks point to biphenotypic ChAT+TH neurons. In panel d, white arrowheads point to purely nNOS positive neurons, white asterisks – biphenotypic ChAT+nNOS neurons and grey asterisks – purely ChAT positive neurons.

Since it was technically possible to make only double immunohistochemical labelling, ganglia and neurons in pig SAN were evaluated in preparations double labelled for ChAT+TH or ChAT+nNOS. The measurements of distinct neuronal somata were also performed in these two groups.

In the preparations double labelled for ChAT+nNOS, ChAT positive neurons were the dominant ones (figure 8). This group formed 65.5±4.4 % of all observed neurons, and the smallest group 12.9±2.6 % was purely nNOS positive cells. 21.6±3.5 % of neural cells were biphenotypic (ChAT+nNOS).

In preparations double labelled for ChAT+TH, purely ChAT positive and biphenotypic neurons were dominant. These two groups of neural cells were equal in size. 47.6±7.1 % of neurons were biphenotypic and 45.5±7.3 % ChAT positive. Purely TH positive cells formed the smallest group. Only 6.9±3.3 % of neurons were of this type (Fig. 8).

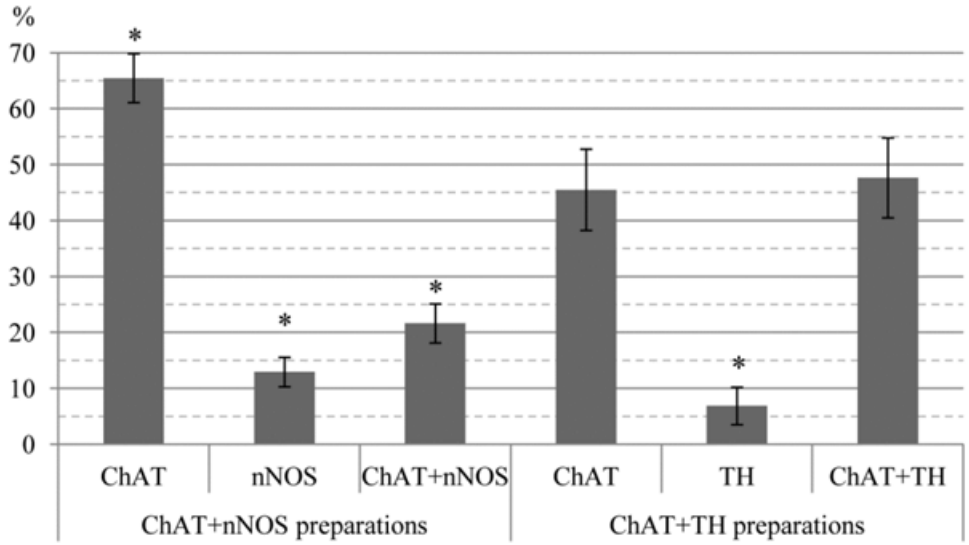

Fig. 8. *The distribution of neurons of distinct phenotype in pig SAN.*
*Statistically different between the groups of cells of distinct chemical phenotype.

Correlation between neurons size and neurochemical phenotype was observed. In rabbit SAN ChAT positive neurons were the smallest and the biggest were biphenotypic (ChAT+nNOS) neurons. In SAN of pig the biggest were ChAT and the smallest nNOS positive neurons.

CONCLUSIONS

1. Pacemaker cells were similarly distributed in the right atria of mouse, rabbit and pig hearts. Pacemaker cells:
   a) occupied 1/3 of right atria;
   b) formed a compact and central parts of node;
   c) formed extensions that descendent far from the main mass of node.
2. SAN were denser innervated compared to working myocardium independently from the area of node and nerve fibers type. TH positive nerve fibers were dominant. Less frequent were ChAT positive nerve fibers. SP and nNOS nerve fibers took the minority.
3. No ganglia or solitary neurons were observed in mouse SAN. Sparse of solitary neurons and small ganglia were found in rabbit SAN. Plentiful of various size ganglia were common for pig SAN.
4. Neurons of various chemical phenotypes were found in SAN area:
   a) 3 types of neurons were found in rabbit SAN that were positive for ChAT, nNOS and biphenotypic – positive for ChAT+nNOS.
   b) 5 types of neurons were typical within pig SAN that were positive for ChAT, TH, nNOS and biphenotypic positive for ChAT+TH and ChAT+nNOS.
5. Neurons sizes correlated with cells chemical phenotype and animal species.

REFERENCES

[1] Armour JA. Potential clinical relevance of the “little brain” on the mammalian heart. Experimental Physiology 2008;93:165–76.
[2] Christoffels VM, Moorman AFM. Development of the cardiac conduction system: why are some regions of the heart more arrhythmogenic than others? Circulation Arrhythmia and Electrophysiology 2009; 2:195–207.
[3] Silverman ME, Grove D, Upshaw CB. Why does the heart beat? The discovery of the electrical system of the heart. Circulation 2006;113: 2775–81.
[4] Monfredi O, Dobrzynski H, Mondal T, Boyett MR, Morris GM. The anatomy and physiology of the sinoatrial node. A contemporary review. Pacing and Clinical Electrophysiology 2010;33:1392–406.
[5] Hasan W. Autonomic cardiac innervation: development and adult plasticity. Organogenesis 2013;9:176–93.

[6] Roberts LA, Slocum GR, Riley DA. Morphological study of the innervation pattern of the rabbit sinoatrial node. The American Journal of Anatomy 1989;185:74–88.
[7] Roberts LA. The sinoatrial ring bundle: a cardiac neural communication system? The American Journal of Anatomy 1991;191:250–60.
[8] Crick SJ, Wharton J, Sheppard MN, Royston D, Yacoub MH, Anderson RH, et al. Innervation of the human cardiac conduction system. A quantitative immunohistochemical and histochemical study. Circulation 1994;89:1697–708.
[9] Crick SJ, Sheppard MN, Ho SY, Anderson RH. Localisation and quantitation of autonomic innervation in the porcine heart I: conduction system. Journal of Anatomy 1999;195 (Pt3):341–57.
[10] Hoover DB, Ganote CE, Ferguson SM, Blakely RD, Parsons RL. Localization of cholinergic innervation in guinea pig heart by immunohistochemistry for high affinity choline transporters. Cardiovascular Research 2004;62:112–21.
[11] Yasuhara O, Matsuo A, Bellier JP, Aimi Y. Demonstration of choline acetyltransferase of a peripheral type in the rat heart. The Journal of Histochemistry and Cytochemistry 2007;55:287–99.
[12] Arvidsson U, Riedl M, Elde R, Meister B. Vesicular acetylcholine transporter (VAChT) protein: a novel and unique marker for cholinergic neurons in the central and peripheral nervous systems. The Journal of Comparative Neurology 1997;378:454–67.
[13] Nachmansohn D, John HM, Berman M. Studies on choline acetylase; the formation of acetylcholine in the nerve axon. The Journal of Biological Chemistry 1946;163:475–80.
[14] Rysevaite K, Saburkina I, Pauziene N, Vaitkevicius R, Noujaim SF, Jalife J, et al. Immunohistochemical characterization of the intrinsic cardiac neural plexus in whole-mount mouse heart preparations. Heart Rhythm 2011;8:731–8.
[15] Richardson RJ, Grkovic I, Anderson CR. Immunohistochemical analysis of intracardiac ganglia of the rat heart. Cell and Tissue Research 2003;314:337–50.
[16] Leger J, Croll RP, Smith FM. Regional distribution and extrinsic innervation of intrinsic cardiac neurons in the guinea pig. The Journal of Comparative Neurology 1999;407:303–17.

CURRICULUM VITAE

Name, Surname	Hermanas Inokaitis
Date of birth:	1983.04.07
Education	
Year:	**Institution:**
2011–2015	PhD studies of Biology, Biomedicine at Lithuanian University of Health Sciences, Medical Academy, Faculty of Medicine, Institute of Anatomy
2006–2008	Masters qualification degree of Rehabilitation, Professional Qualification of Physiotherapist at Lithuanian Academy of Physical Education, Faculty of Sport Biomedicine
2002–2006	Bachelors qualification degree of Rehabilitation, Professional Qualification of Physiotherapist at Kaunas University of Medicine, Faculty of Nursing
2000–2002	Kaunas Jesuit Gymnasium
1990–2000	Kaunas Jonas Basanavičius Secondary School
Work expierence	
Year:	**Institution:**
2013 02–present	Assistant at Lithuanian University of Health Sciences, Medical Academy, Faculty of Medicine, Institute of Anatomy
2013 12–2015 10	Researcher at Lithuanian University of Health Sciences, Medical Academy, Faculty of Medicine, Institute of Anatomy
2011 06–2015 09	Labor at Lithuanian University of Health Sciences, Medical Academy, Faculty of Medicine, Institute of Anatomy, Museum of Human Anatomy
2011 02–2011 06	Physical Therapist at Sanatorium “Tulpės”
2010 09–2013 02	Physical Therapist, Administrator at UAB “Natura Munda”
2009 04–present	Ind. Act. “Assurance of physical health”
2008 08–2010 09	Special Educator at “Kaunas Swimming School”

2007 11–2008 08	Physical Therapist at AB Birstonas Sanatorium "Versmė"
2006 07–2006 12	Manager at UAB "Litfas"
2005 07–2007 11	Driver UAB "Farmahelis"
1999 07–2002 09	Worker at ind. comp. "Inos Inokaitienės Vaistinė"

Publications:

- Inokaitis H, Pauziene N, Rysevaite-Kyguoliene K, Pauza DH. *Innervation of sinoatrial nodal cells in the rabbit.* Annals of Anatomy 2016; 205:113–21.
- Paužienė N, Alaburda P, Rysevaitė-Kyguolienė K, Pauža AG, Inokaitis H, Masaitytė A, Rudokaitė G, Saburkina I, Plisienė J, Pauža DH. *Innervation of the rabbit cardiac ventricles.* Journal of Anatomy 2016; vol. 228, no. 1.
- Pauza DH, Rysevaite-Kyguoliene K, Vismantaite J, Brack KE, Inokaitis H, Pauza AG, Rimasauskaite-Petraitiene V, Pauzaite JI, Pauziene N. *A combined acetylcholinesterase and immunohistochemical method for precise anatomical analysis of intrinsic cardiac neural structures.* Annals of Anatomy 2014;196, 430–440.
- Pauza DH, Saburkina I, Rysevaite K, Inokaitis H, Jokubauskas M, Jalife J, Pauziene N. 2013. *Neuroanatomy of the murine cardiac conduction system: A combined stereomicroscopic and fluorescence immunohistochemical study.* Autonomic Neuroscience: Basic & Clinical 2013;176, 32–47.
- Pauza DH, Rysevaite K, Inokaitis H, Jokubauskas M, Pauza AG, Brack KE, Pauziene N. *Innervation of sinoatrial nodal cardiomyocytes in mouse. A combined approach using immunofluorescent and electron microscopy.* Journal of molecular and cellular cardiology 2014;75C, 188–197.
- Kliziene I, Sipaviciene S, Imbrasiene D, Klizas S, Inokaitis H. *Effect of core stability exercise on cross-sectional area of lumbar multifidus muscle and physical capacity*. Education Physical Training Sport 2011; 3, 9–16

During my PhD candidature I have also presented my research in a number of international (12) and national (1) conferences. For seven of these publications I was a lead author.

PADĖKA

Dėkoju visiems prisidėjusiems prie šio darbo.

Labiausiai norėčiau padėkoti savo darbo vadovei prof. dr. Neringai Paužienei už patarimus ir suteiktas žinias, pagalbą vykdant tyrimus ir palaikymą visus doktorantūros studijų metus.

Taip pat esu labai dėkingas Lietuvos sveikatos mokslų universiteto Medicinos akademijos Anatomijos instituto vadovui prof. dr. Dainiui H. Paužai už palaikymą, patarimus ir pagalbą vykdant tyrimus bei rengiant publikacijas.

Lietuvos sveikatos mokslų universiteto Medicinos akademijos Anatomijos instituto elektroninės mikroskopijos laboratorijos vedėjai dr. Kristinai Rysevaitei-Kyguolienei noriu padėkoti už pagalbą įsisavinant tyrimui reikalingus metodus; Lietuvos sveikatos mokslų universiteto Medicinos akademijos Anatomijos instituto kolegoms – už pagalbą, paramą bei gerus žodžius.

Esu dėkingas šeimai ir draugams už supratimą, padrąsinimus ir buvimą kartu sunkiu metu.